Genome-Scale Analysis of Transcriptional Regulation by the Fbw7 Ubiquitin Ligase

Heshani Nayanga Thirimanne

A dissertation

submitted in partial fulfillment of the

requirements for the degree of

Doctor of Philosophy

University of Washington

2021

Reading Committee:

Bruce E. Clurman, Chair

Steven Henikoff

Jason Bielas

Program Authorized to Offer Degree:

Molecular Medicine and Mechanisms of Disease

University of Washington

Abstract

Genome-Scale Analysis of Transcriptional Regulation by the Fbw7 Ubiquitin Ligase

Heshani Nayanga Thirimanne

Chair of the Supervisory Committee:
Bruce E. Clurman, MD PhD
Executive Vice President and Deputy Director
Professor, Divisions of Clinical Research and Human Biology
Fred Hutchinson Cancer Research Center
Professor, Department of Medicine, University of Washington

Protein turnover is tightly regulated by the ubiquitin proteasome system (UPS). Dysregulated UPS components lead to many diseases, including cancer. Fbw7 is the substrate receptor of the SCF^{Fbw7} E3 ubiquitin ligase and is one of the most commonly mutated tumor suppressor genes. Fbw7 is mutated in a wide array of cancers, including T-cell leukemia, colorectal and endometrial cancers. Fbw7 targets more than two dozen proteins for degradation and the majority of them are transcription factors (TFs). Therefore, Fbw7 exerts a widespread influence on transcription and cellular mechanisms. A holistic molecular level overview of how Fbw7 regulates multiple TFs and global transcription is needed to unravel the complex regulatory network of Fbw7. Heterozygous arginine missense mutations ($Fbw7^{Arg/+)}$ that impair Fbw7's function is favored by human cancers over complete loss of Fbw7. However, the tumorigenic mechanisms led by $Fbw7^{Arg/+}$ are as of yet poorly understood. Therefore, I initiated an integrative study where I employed RNA-Seq and chromatin profiling tools (CUT&RUN) to understand

context-specific transcriptional regulation in Fbw7 wild-type and mutant cells. I investigated the deregulation of two well-studied oncogenic Fbw7 substrates (cMyc, cJun) in colorectal cancer cell lines and neural stem cells. This work revealed that Fbw7 regulates substrates at specific genomic sites which may not always be reflected by analysis of mRNA. Fbw7 preferentially regulates TF occupancy at distal regulatory genomic regions; however, the specific targeted genes and genomic loci differ in a cell-type and mutation-type specific manner. Fbw7 also coordinately co-regulates both Jun and Myc at some genomic sites. I discovered that loss of Fbw7 upregulates class II HLA genes by controlling cMyc and cJun occupancy at one of the co-regulated sites, which is within the *CIITA* upstream regulatory region. Together, this body of work improves our understanding of context-specific transcriptional regulation by Fbw7 that may be useful in developing better targeted therapies. The identification of class II HLA regulation by Fbw7 may be incorporated in developing prognostic and diagnostic methods.

Table of Contents

LIST OF FIGURES

LIST OF TABLES

ACKNOWLEDGEMENTS

I am extremely thankful to my thesis advisor, Bruce Clurman, for accepting me as his graduate student. Despite his busy schedule, Bruce always made sure to reserve time for his students. I am so grateful for all the support and guidance he provided to design and implement my dissertation work, and to improve myself as a scientist. It is rare to find a mentor who is both a great scientist and humble human being with good values. During the past five years, Bruce was consistently supportive of not only my scientific work, also to help me thrive graduate school while maintaining a healthy work-life balance. I feel fortunate to have had a mentor like Bruce.

I feel honored to have been mentored by Steve Henikoff who served as my co-mentor. It is safe to say Steve is one of the humblest, yet highly renowned and brilliant scientists. Steve's support, guidance and encouragements indeed helped me thrive and preserver. I could not be more grateful for the opportunity to work with Steve and his lab members.

All Clurman lab members provided tremendous support for my research work. I am so grateful to Markus Welcker for teaching me many scientific skills that I would certainly value for the rest of my career, and for encouraging me to persevere through many inconclusive steps in the dissertation project. Thanks to Jherek Swanger for helping me with experiments, to improve my writing skills, and above all for keeping our lab well organized. Thanks to Shlomo Handeli, Ryan Davis and Hakan Gem for being kind and helpful, and most importantly for being amazing lab peers while creating an enjoyable work culture. I cannot thank Ahmed Diab enough for great feedback and valuable discussions that helped my project take major turns towards success. My heartfelt gratitude to all other lab members including Yong, Yasser, Stuart, Will, Bonnie and Kristine for the many favors extended to make my time in lab enjoyable and productive.

I am grateful to all the Henikoff lab members for sharing their resources, knowledge and time with me all of which made a major positive impact on my dissertation work. Thanks to Derek Janssense, Jay Sarthy, Mike Meers and Steven Wu for taking time off of their busy schedules to provide scientific insights and answer many questions I had on data analysis. Thanks to Christine Codomo for library preparation, sequencing and for helping me to learn and execute protocols starting from ground zero. Thanks to Terri for all the many favors with reagents and instruments. Many thanks to Pete Skene for bearing with me as I struggled to learn and troubleshoot CUT&RUN as a fresh graduate student, and most importantly for encouraging and inspiring me to learn computational tools.

I am beyond grateful for my thesis advisory committee members for guiding me with great feedback to improve and navigate my project to the final stage. Thanks to Jonathan Cooper, for very helpful scientific insight on my work, and for serving as a true Graduate Student Representative and checking up on me. Many thanks to Ryan Cassaday for serving as the clinical mentor and providing me with opportunities to shadow him at the clinic and for always emphasizing the clinical significance of my work. A special thanks to Jason Bielas and Steve Henikoff for reading and providing page to page suggestions to improve the dissertation.

I would not be here today if not for the M3D program and its directors who recruited me to this highly renowned PhD program. My heartfelt gratitude to Bill (William Mahoney) for always checking up on the students' graduate school journey, not only in terms of the scientific growth but overall wellbeing and future goals.

I thank Patrick Paddison's lab and Jason Bielas's lab for sharing reagents and work force to generate NSC knockouts and perform scRNA-Seq experiments, respectively. Thanks to the Genomics and Bioinformatics Center at the Fred Hutch for library preparation, sequencing and data analysis. Special thanks to Phil Corrin, Alyssa Dawson, Feinan Wu, Matt Fitzigibbon and Jeff Delrow. My utmost gratitude to the funding sources; NIH NCI T32CA080416 grant and Fred Hutch.

I would not have survived this half a decade of roller coaster ride if not for the unwavering support and encouragement from my husband, Heshan. Many thanks to him for believing in me and reminding me of my strengths when I got easily lost among negativities. Honestly, I do not have enough words to appreciate how supportive he has been and how much he sacrificed to simply see me succeed. Minuk, my now two-year-old son, has been unknowingly sacrificing so much since his days *in utero* to let me work on my passion and reach the end goal.

Ammi and Thaththi, my dear parents are the sole reason for my existence here today. If they had not been open minded and supportive of their daughter's dreams, I would not be here on the other side of the world, thousands of miles away from their nest, doing what I have been wanting to do despite peer pressure to pursue alternative careers. I owe you both so much more than I can ever payback. I find two best friends in my sister and brother who I could run to for anything and everything. They both are inspiring role models to me in many ways in life.

I appreciate the sincere efforts by all my teachers that shaped me into the person I am today. Last but not least, my deepest gratitude to my dear friends; the kind and compassionate souls that surround me through thick and thin.

DEDICATION

To my better half, my pillar of strength - Heshan
To the unwavering joy in my life - my son, Minuk

Chapter 1. Introduction

1.1 The Ubiquitin Proteasome System

The ubiquitin proteasome system (UPS) is a tightly regulated protein degradation pathway in eukaryotes (**Figure 1.1**) (Hershko, A., and Ciechanover, 1998). It is the primary destruction mechanism of proteins, thus a major mediator of cellular homeostasis. It has major implications on important cellular processes such as cell proliferation, apoptosis, metabolism, immune response and cell differentiation. UPS components are often deregulated leading to various diseases including cancer, and now it is being exploited as a target for diagnostics and therapeutic strategies (Hoeller & Dikic, 2009; Lecker et al., 2006).

The UPS labels proteins by attaching small ubiquitin molecules, in a process called ubiquitylation (Hershko, A., and Ciechanover, 1998; Weissman, 2001). It consists mainly of three enzymes; E1 ubiquitin activating enzymes, E2 ubiquitin conjugating enzymes, and E3 ubiquitin ligases. The E1 enzyme activates the ubiquitin molecule and transfers it to E2. The E2 enzyme transfers the activated ubiquitin molecule on to the protein of interest (hereafter also named as the substrate) that is properly positioned by the E3 ligase. A covalent bond is formed between the carboxy-terminus of ubiquitin and the ε-amino group of a lysine residue on the targeted substrate. Substrates can be monoubiquitylated, multi-monoubiquitylated or polyubiquitylated. Ubiquitin molecules have seven lysines, which are utilized to generate diverse polyubiquitin chains, which signal different cellular processes. Ubiquitin chains that extend from lysine 48 are targeted by the proteasome complex while chains that extend from lysine 63 are involved in translation and DNA repair (Weissman, 2001).

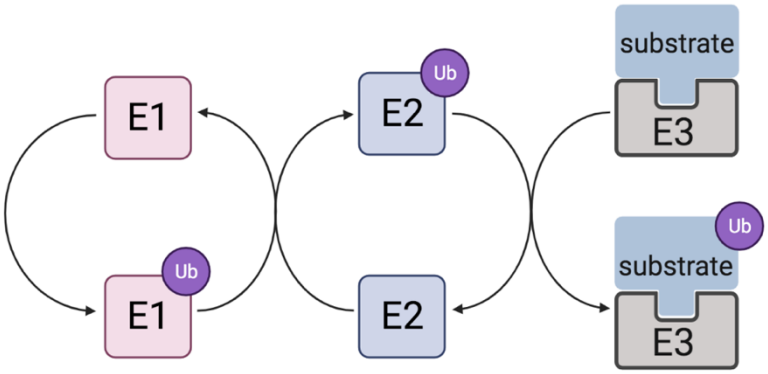

Figure 1.1 Overview of the ubiquitin proteasome system

The UPS consists of three enzymes to link ubiquitin molecules to the substrates. The first step of UPS is mediated by E1 ubiquitin activating enzymes that forms the E1-ubiquitin thiol ester bond. Next the ubiquitin molecule is transferred to an E2 ubiquitin conjugating enzyme. After E3 ubiquitin ligase secures the substrate, E2 enzyme covalently attaches the ubiquitin to the substrate. Substrate specificity is mediated by E3 enzymes. Human genome encodes for two E1 enzymes, approximately 30 E2 and more than 700 E3 enzymes.

1.2 E3 ubiquitin ligases

E3 ubiquitin ligases determine the substrate specificity, recognize and bind to protein substrates to facilitate their ubiquitylation. There are two major classes of E3 ligases: the HECT (homologous to E6AP C-terminus) domain and the RING-finger domain containing ligases (Weissman, 2001). RING-finger proteins are single or multi-subunit E3s. Mdm2 is a well-studied example for a single-subunit E3. Cullin-RING ligases (CRLs) and anaphase promoting complex/cyclosome (APC) are examples for multi-subunit E3.

CRLs are the largest family of E3 ubiquitin ligases which consists of four components: cullins, RINGs, adaptor proteins and substrate receptors (Zhao & Sun, 2013). In humans there are two RING components (RBX1 and RBX2), eight Cullin proteins (Cul 1-3, 4A, 4B, 5, 7, Cul 9),

and four adaptor proteins (Skp1, Elongin B/C and DDB1). Out of the many substrate receptors, there are 69 F-box proteins. The SCFs (Skp1-Cul1-Fbox) is the most well-studied multi-subunit RING-finger ligase, which contains Cullin 1 scaffolding protein, catalytic RING finger which recruits E2 enzyme and Skp1 which interacts with the F-box protein (**Figure 1.2**).

1.3 SCF^{Fbw7} E3 Ubiquitin Ligase

Fbw7 (F-box and WD repeat domain-containing 7) is the F-box protein that perform as the substrate receptor in SCF^{Fbw7} complex (**Figure 1.2**). Fbw7 is one of the most studied F-box proteins. Interestingly, it is one of the most highly mutated genes in human cancers (Akhoondi et al., 2007; R. J. Davis et al., 2014).

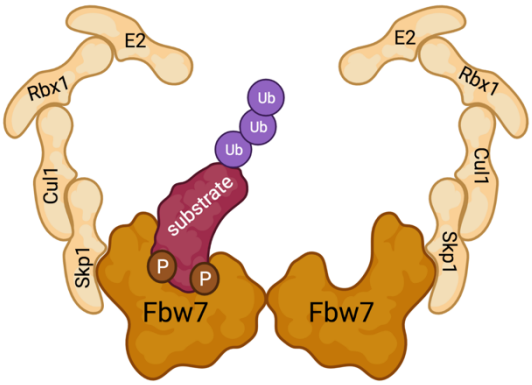

Figure 1.2 Schematic of SCF^{Fbw7} E3 ligase complex.

SCF^{Fbw7} complex consists of Cullin 1 which acts as a scaffold, SKP1 (S-phase kinase-associated protein 1), RBX1 (Ring Box 1) and Fbw7 (F-box and WD repeat domain-containing 7). RBX1 interacts with the E2 enzyme that brings in the ubiquitin molecule. Ubiquitin molecules are transferred by the E2 enzyme while substrate is bound to Fbw7.

Fbw7 is an evolutionarily conserved F box protein. Cdc4 in *S. cerevisiae*, sel-10 in *C.elegans* and Archipelago in *Drosophila* are Fbw7's orthologs that have been well-studied. The Fbw7 protein has three functional domains. The D domain mediates Fbw7 dimerization and F box links Fbw7 to Skp1. There is a stretch of eight WD40 repeats that form an eight-bladed barrel-shaped β-propeller structure that directly interacts with the substrates (**Figure 1.3**) (R. J. Davis et al., 2014; Welcker et al., 2013). The *FBXW7* gene produces three mRNAs, each independently regulated to generate three protein isoforms. These isoforms differ only by their N-terminal exons which specify subcellular localization (**Figure 1.3**). Fbw7α is nucleoplasmic, while Fbw7β and Fbw7γ are cytoplasmic and nucleolar, respectively. Fbw7α is the predominant isoform that is found in most cell types performing most Fbw7 functions. Fbw7β and Fbw7γ are mostly detected in the brain and muscle, respectively (Welcker & Clurman, 2008).

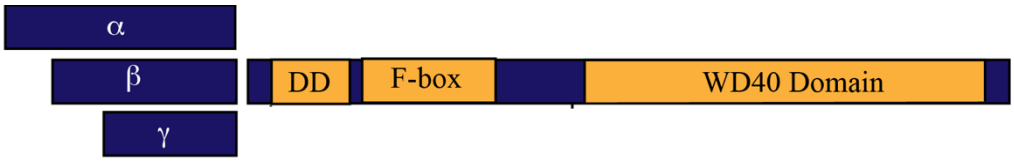

Figure 1.3 Schematic of Fbw7 protein domains.

Fbw7 protein isoforms (α, β, γ) differ by their first exon. All isoforms share three functional domains. DD: D domain that mediates Fbw7 dimerization. F-box: binds to Skp1 and interacts with rest of the SCF complex. WD40 Domain: WD40 repeat region forms the β propeller and interacts with phosphorylated substrates.

1.4 **Fbw7-Substrate Interactions**

Three highly conserved arginine residues that lie within repeats three and four of the β propeller structure form essential interactions with the substrates (Hao et al., 2007).

Specificity of substrates targeted by Fbw7 is determined by phosphorylation at the conserved Fbw7 recognition motif known as the Cdc4 phospho-degron (CPD). CPDs contain phosphorylated threonine or serine residues in the "0" and "+4" positions of the degron amino acid sequence and they interact with Fbw7 phosphate-binding pockets (Hao et al., 2007; Koepp et al., 2001). CPD affinity varies between substrates. High affinity substrates contain two phosphorylated sites within each degron while low affinity substrates contain a negatively charged amino acid in lieu of one phosphorylated site. Fbw7 dimerization also plays a role in substrate interactions (Tang et al., 2007; Welcker et al., 2013; Welcker & Clurman, 2007). Fbw7 monomer is sufficient to properly interact with optimal CPDs (high affinity) and target for ubiquitylation. However, weak degrons need to cooperate with neighboring degrons and interact with Fbw7 dimers.

Signaling pathways that regulate CPD phosphorylation are determinants of Fbw7 substrate degradation. Most proteins have multiple degradation pathways and SCF^{Fbw7} specificity is determined by the phosphorylated CPD. Glycogen synthase kinase 3 (GSK3) phosphorylates many CPDs (Crusio et al., 2010).

1.5 **Fbw7 Substrates**

Fbw7 targets more than two dozen proteins for degradation and many are transcription factors (TFs) (**Figure 1.4**). As an upstream regulator of multiple TFs, Fbw7 plays a critical role in controlling vital cellular processes such as proliferation, differentiation, apoptosis and metabolism (Crusio et al., 2010). While cyclin E is the firstly and most predominantly characterized Fbw7 substrate, c-Myc, c-Jun and Notch are oncogenic transcription factors that are also well studied Fbw7 substrates.

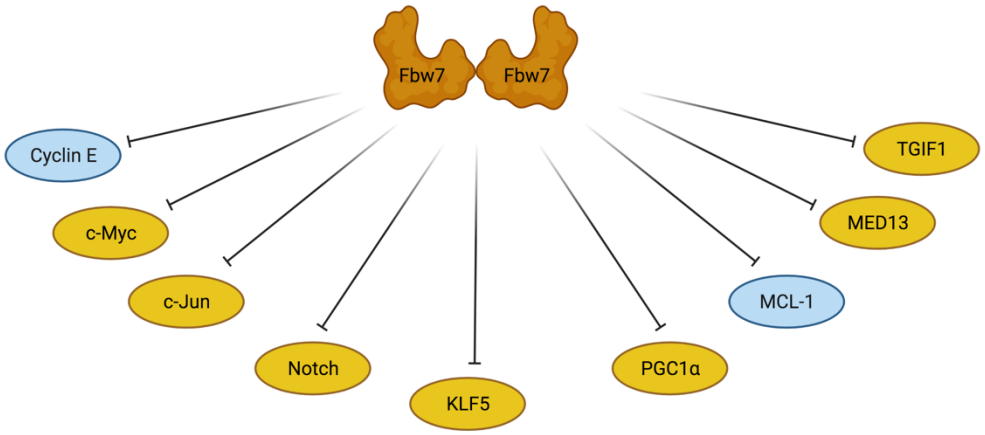

Figure 1.4 Fbw7 regulates a broad network of substrates

Most of the Fbw7 substrates are transcriptional regulators (shown in yellow) with a few exceptions (shown in blue).

1. c-Jun (hereafter also called Jun)

AP-1 (activator protein 1) transcription factor is a dimeric complex that mainly consists of JUN (Jun, JunB, JunD), FOS (cFos, FosB, Fra1, Fra2) and ATF(ATFa, ATF2, ATF3) proteins (Hess et al., 2004). AP1 proteins dimerize with each other in a context-specific manner to regulate a network of cellular processes including cell proliferation, death and differentiation. Fbw7 binds to a highly conserved CPD on Jun – "TPPLSP", which is phosphorylated by GSK3, and targets Jun

for ubiquitylation (Gao et al., 2004; Nateri et al., 2004; Wei et al., 2005; Wertz et al., 2004). Loss of Fbw7 causes accumulation of Jun, consequently deregulating downstream transcription leading to oncogenesis. Mutations in Jun itself has been found to cause human cancer (Shaulian & Karin, 2002).

2. c-Myc (hereafter also called Myc)

Myc has important roles in cell growth and mitogenic responses. Phosphorylated T58 CPD in Myc is bound by Fbw7 and targeted for ubiquitylation (Welcker et al., 2004; Yada et al., 2004). Phosphorylation of T58 by GSK3 is primed by the phosphorylation of S62 by Ras-ERK pathway. The T58 region often mutates in lymphomas which impairs degradation by Fbw7 (Bahram et al., 2000). Fbw7α targets Myc in the nucleoplasm while Fbw7γ targets Myc in the nucleolus (Grim et al., 2008; Welcker et al., 2011). In addition to Fbw7, Myc is regulated by other ubiquitin ligases such as Skp2 (S. Y. Kim et al., 2003). Myc has a very short half-life (~30 min) and Myc transcription is negatively auto-regulated by the occupancy of Myc protein at its own promoter (Penn et al., 1990).

3. Cyclin E

Cyclin E is one of the earliest identified Fbw7 substrates as well as an oncogenic driver (Clurman et al., 1996; Grim et al., 2008; Strohmaier H et al., 2001). Cyclin E binds to and activates CDK2. Cyclin E-CDK2 regulate cell cycle entry and progression, mainly the G1 to S transition. There are two CPDs on Cyclin E (T380 and T62) both of which are phosphorylated by GSK3 and CDK2 (Welcker et al., 2003). The “0” and “+4” positions of Cyclin E CPD are phosphorylated strengthening the degron and alleviating the requirement of an Fbw7 dimer. However, when the

"+4" position (S384) is not phosphorylated, the degron is weak and dimerized Fbw7 is essential to stably interact. Constitutive cyclin E/CDK2 activity due to impaired degradation causes genome instability which is a key mechanism of tumorigenesis (Loeb et al., 2005; Minella et al., 2007; Rajagopalan et al., 2004).

4. Notch

Notch is a transmembrane receptor that controls the differentiation of multiple cell types. Upon ligand activation, the receptor is cleaved by γ-secretase. The cleaved Notch intracellular domain (NICD) translocates into the nucleus and forms a transcriptional activator complex with RBPJ and MAML (H. Wang et al., 2015). Fbw7 targets NICD for ubiquitylation and degradation (Öberg et al., 2001). All four Notch paralogs contain CPDs, however Notch1 is the most well-studied. It has been shown that complete loss of Fbw7 in mice result in embryonic lethality (day ~ 10.5) because of defects in hematopoietic and vascular development which is likely due to the deregulation of Notch (Tetzlaff et al., 2004). *NOTCH1* gene itself harbors mutations in more than 50% of T-cell Acute Lymphoblastic Leukaemia (T-ALL) and these mutations often occur in the PEST domain. Fbw7 mutations in T-ALL are mutually exclusive with Notch PEST mutations (Malyukova et al., 2007; O'Neil et al., 2007; Thompson et al., 2007).

1.6 **Fbw7 and Cancer**

Fbw7 is known as a tumor suppressor; it is inactivated by mutations, resulting in accumulation of oncogenic protein substrates. Chromosome 4q32, the region *FBXW7* resides, is commonly deleted in cancers (>30% of cancers). *FBXW7* is mutated approximately in 6% of all human tumors (Akhoondi et al., 2007).

The majority of *FBXW7* mutations are single nucleotide substitutions, while the rest are small nucleotide deletions or insertions (Akhoondi et al., 2007). Those mutations result in either missense mutations or premature termination of protein. The majority of missense mutations occur at the three key arginine residues that directly interact with the substrates (Arg^{465}, Arg^{479}, Arg^{505}); known as hotspot mutations ($Fbw7^{Arg}$). Because these arginine residues are absolutely required for high-affinity Fbw7-substrate interactions, $Fbw7^{Arg}$ mutations have a profound impact on Fbw7 regulation compared with other missense mutations (Hao et al., 2007; Tang et al., 2007). These mutational hotspots are often on CG dinucleotides that are methylated and undergo spontaneous deamination (C:G→T:A)(Kemp et al., 2005).

Heterozygous $Fbw7^{Arg}$ ($Fbw7^{Arg/+}$) mutations are the most common Fbw7 mutation type in human cancers. Although *FBXW7* is recognized as a tumor suppressor gene, unlike other tumor suppressors such as *TP53* and *APC*, *FBXW7* does not follow the classic two-hit model. Biallelic mutagenesis or combination of mutation with loss of heterozygosity (LOH) has been observed but rare (Miyaki et al., 2009). Even then, the second hit was rare to occur when the first single base mutation was at one of the three key arginine residues. This suggests that a second hit may not be necessary for $Fbw7^{Arg/+}$ to exert a tumorigenic effect (Kemp et al., 2005). Cancers favor partial loss of Fbw7 function over complete loss of Fbw7. Studies suggest that heterodimeric complexes

of WT and mutated Fbw7 may act in a dominant negative manner, potentially by sequestering wild-type Fbw7 in inactive dimers (Akhoondi et al., 2007).

Fbw7 dimerization adds another layer of regulation (Welcker & Clurman, 2007). Each Fbw7 protomer contains a substrate-binding domain, therefore Fbw7 dimers can simultaneously bind to two CPDs, which is important for substrates with weak (suboptimal) CPDs. Substrates with high affinity optimal CPDs can form a sufficiently stable interaction with one Fbw7 protomer. As dimers, Fbw7 can tolerate many missense mutations that disable monomers.

The highest frequency of *FBXW7* mutations were observed in cholangiocarcinomas (35%) and T-cell acute lymphoblastic leukemia (T-ALL) (30%). Additionally, Fbw7 is mutated 6-10% in colorectal adenocarcinoma, uterine carcinosarcoma, uterine endometrial carcinoma and bladder carcinoma (R. J. Davis et al., 2014; Welcker & Clurman, 2008). Stomach adenocarcinoma, lung squamous cell carcinoma, cervical squamous cell carcinoma and head and neck squamous cell carcinoma also have a low level of Fbw7 mutations. In contrast, Fbw7 mutations are not found in certain cancers such as acute myeloid leukemia and multiple myeloma. TCGA studies provide a comprehensive overview of Fbw7 mutational spectrum in cancers (**Table 1.1**) (Kandoth, McLellan, et al., 2013; Kandoth, Schultz, et al., 2013; Muzny et al., 2012). Currently TCGA does not hold mutational data from T-ALL cancers, however, several independent studies discuss Fbw7 mutations in T-ALL (**Table 1.2**) (Malyukova et al., 2007; Maser et al., 2007; O'Neil et al., 2007; Thompson et al., 2007).

While T-ALLs almost exclusively harbor $Fbw7^{Arg/+}$ mutations, colorectal cancers contain deletions and nonsense mutations in addition to the missense mutations. This suggests that Fbw7 mutations arise in a tissue specific manner and presumably produce unique biological outcomes via specific substrates.

Table 1.1 Fbw7 mutations and homozygous deletion frequency in selected cancers (adapted from (R. J. Davis et al., 2014)**)**

Tumor Type	Number of samples	Arginine Hot Spot Mutations %	Nonsense Mutations %	Other Missense Mutations %	All Point Mutations %	Arginine Hot Spot Mutations/ Total Point Mutations %	Homozygous Deletions %
Uterine carcinosarcoma	56	23	4	14	39	59	0
Colon and rectal adenocarcinoma	212	8	3	6	17	49	0
Uterine corpus endometrial carcinoma	240	6	3	8	16	37	0
Stomach adenocarcinoma	219	5	2	2	9	59	<1
Urothelial bladder carcinoma	127	3	5	4	9	33	2

Table 1.2 Fbw7 mutation frequency in T-ALL cell lines and patient samples (adapted from (R. J. Davis et al., 2014)**)**

Study	Number of Samples	Source of Sample	Fbw7 Point Mutations %	Arginine Hot Spot Mutations/ Total Point Mutations
1 (O'Neil et al., 2007)	20	cell lines	35	86
	81	primary samples	9	100
2 (Maser et al., 2007)	23	cell lines	43	90
	38	primary samples	29	73
3 (Thompson et al., 2007)	89	primary samples	17	100
4 (Malyukova et al., 2007)	15	cell lines	33	100
	26	primary samples	31	88

Colorectal cancer (CRC)

Human colorectal cancers can be either hereditary (Hereditary Nonpolyposis Colorectal Cancer - HNPCC and Familial Adenomatous Polyposis - FAP) or sporadic. Both types of cancers have been detected with *FBXW7* mutations (Miyaki et al., 2009). Approximately 10% of colorectal tumors exhibit *FBXW7* mutations and it is the fourth most commonly mutated gene in CRCs after the tumor suppressors *TP53*, *RAS* and *APC* (adenomatous polyposis coli). Although Fbw7 mutations are present in early stage human colon adenomas, loss of Fbw7 alone is insufficient to cause colorectal tumors in mice (Grim et al., 2012; Rajagopalan et al., 2004). However co-occurrence with other tumor suppressor mutations such as in *APC* and *TP53* aggravates tumorigenesis (Babaei-Jadidi et al., 2011; H. Davis et al., 2014). Approximately 70% of *FBXW7* mutations in colorectal tumors are monoallelic while loss of heterozygosity (LOH) is uncommon. Compared to $Fbw7^{+/-}$ mice, $Fbw7^{Arg/+}$ mice exhibit increased tumorigenesis indicating mutation type-specific function of Fbw7 and unique role of $Fbw7^{Arg/+}$ mutation (H. Davis et al., 2014). TGIF1 and KLF5 were stabilized in $Fbw7^{Arg/+}$ tumors, but not in $Fbw7^{+/-}$ tumors indicating substrate-specific consequences of Fbw7 mutations (H. Davis et al., 2014). Tumors with loss of Fbw7 combined with APC mutations did not progress beyond the adenoma stage and metastasize. However, codeletion of Fbw7 and p53 from the mouse gut caused advanced adenocarcinomas (Grim et al., 2012). These tumors were highly invasive and metastatic. It is known that p53 suppresses cyclin E induced genomic instability caused by Fbw7 loss, and accordingly these adenocarcinomas with Fbw7 and p53 co-deleted exhibited chromosomal instability (CIN).

Hematologic cancer

Fbw7 deletion in either T cells or HSCs is sufficient to cause T-ALL and this is the only case where Fbw7 mutations are sufficient to cause cancer (Matsuoka et al., 2008). $Fbw7^{Arg/+}$ mice did not develop spontaneous T-ALL, however it cooperated with Notch deregulation to drive T-ALL (King et al., 2013). Moreover, studies show that Myc abundance in $Fbw7^{Arg/+}$ cells is tightly regulated that it is not too detrimental to affect HSC maintenance yet sufficient to cause a tumorigenic effect in leukemia initiating cells (King et al., 2013).

1.7 **Fbw7 in Stem Cells**

The role of Fbw7 in stem cells has been investigated using several stem cell types such as hematopoietic stem cells (HSCs), neural stem cells (NSCs) and intestinal stem cells (Takeishi & Nakayama, 2014). Fbw7 is known to play a role in tissue homeostasis by regulating quiescence and self-renewal in HSCs (Matsuoka et al., 2008; Thompson et al., 2008). Loss of Fbw7 causes HSCs to continuously proliferate eventually leading to exhaustion of HSCs, which is thought to be regulated by Myc overexpression (Reavie et al., 2010). Aberrant regulation of cyclin E also causes impaired self-renewal in HSCs (Siu et al., 2014). Interestingly, $Fbw7^{Arg/+}$ HSCs express Myc at an intermediate level to WT and Fbw7-/- HSCs suggesting a unique role for $Fbw7^{Arg/+}$ causing a "just-enough" level of Myc deregulation (King et al., 2013).

Conditional *FBXW7* deletion specifically in mice intestinal tissue demonstrates the role of Fbw7 in controlling differentiation and proliferation of intestinal progenitor cells and of tumor cells (Grim et al., 2012; Sancho et al., 2010). Loss of Fbw7 enhances the stability of Notch and Jun, while Myc and Cyclin E were less affected. Accumulation of actively proliferating progenitor cells were detected in $Fbw7^{-/-}$ intestines; however intestinal tumors were not instigated. Agreeing

with human data, co-occurrence of *FBXW7* loss-of-function with *APC* mutations resulted in tumor formation in mice. Neural stem cell differentiation and progenitor cell apoptosis is regulated by Fbw7 via Notch and c-Jun respectively (Hoeck et al., 2010). Differentiation of liver and epidermal stem cells are also deregulated by loss of Fbw7 in mice leading to impaired cell lineage decisions (Ishikawa et al., 2013; Onoyama et al., 2011).

1.8 Cleavage Under Targets and Release Using Nuclease (CUT&RUN)

CUT&RUN is a chromatin profiling strategy that has several advantages over the commonly known protein mapping technique, ChIP-Seq (chromatin immunoprecipitation and sequencing) (Skene & Henikoff, 2017) (**Figure 1.5**).

In ChIP-Seq, cells are crosslinked with formaldehyde, chromatin is fragmented and solubilized using sonication, and chromatin bound protein of interest is immunoprecipitated using antibodies (Solomon & Varshavsky, 1985). Then, DNA is extracted from the immunoprecipitated chromatin for sequencing. Although crosslinking helps to preserve the *in vivo* protein interactions, it can promote epitope masking and generate false positive binding sites. In ChIP-Seq, the disruption of the entire genome creates high background noise, therefore to generate good quality informative data genomic material need to be sequenced at a higher depth which is costly.

CUT&RUN uses native, non-crosslinked cells. Instead of randomly shearing the entire genome, CUT&RUN exploits a targeted cleavage approach. Antibodies that target the protein of interest (TF or histone modifications) are allowed into the cell and bind the protein. Antibodies are then bound by micrococcal nuclease (MNase) which cleaves DNA on both sides of the bound protein after it is activated by calcium. The cleaved protein-DNA complex is released out of the cell into the supernatant out of which DNA is extracted and sequenced. These steps can be

performed on nuclei isolated from native cells or directly on cells with the cell membrane permeabilized (Skene et al., 2018; Skene & Henikoff, 2017). Nuclei or cells can be immobilized on lectin-coated magnetic beads which makes the sample handling much easier.

In CUT&RUN, *in situ* protein interactions are preserved because the cells are not crosslinked. MNase cleaves DNA at the targeted sites and only the cleaved DNA is extracted out for sequencing leaving behind most of the genomic material. Therefore, DNA can be sequenced at a much less sequencing depth compared to ChIP-Seq (2-5 fold less). Extremely low backgrounds are produced with high signal to noise ratio making the method highly cost-effective. In comparison to ChIP-Seq, CUT&RUN is a robust, efficient and easy to optimize protocol that takes you from cells to data in 2-3 days. High quality data can be achieved with a much lower number of cells compared to ChIP-Seq. For these reasons and because our study included a large number of protein mapping experiments, inarguably CUT&RUN was the best choice of protein mapping technique. We used CUT&RUN to map several transcription factors and histone modification marks in different cell types. Different adaptations of the CUT&RUN protocol were used as the method continued to be optimized by the Henikoff lab. Initially we used isolated nuclei (Skene & Henikoff, 2017). Next the protocol was optimized to include cells permeabilized with Digitonin (Skene et al., 2018). It was further improved to be performed on an automated platform (Janssens et al., 2018). These modifications facilitated the use of lower cell numbers per sample and increased efficiency to process a large number of samples.

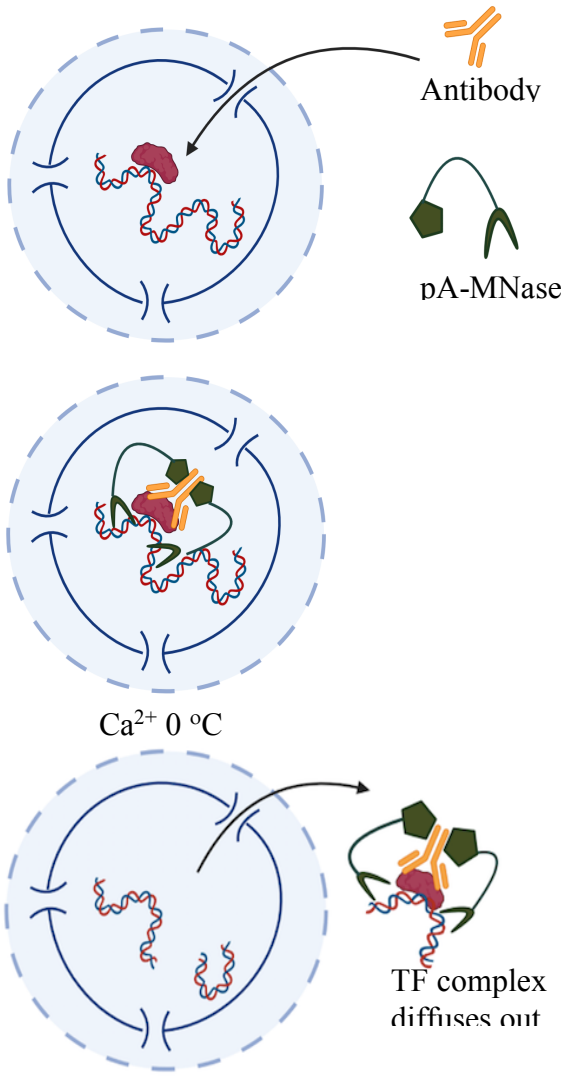

Figure 1.5 A schematic overview of the CUT&RUN protocol.

Cells are harvested and bound to concanavalin A-coated magnetic beads (optional). Cell membranes are permeabilized with digitonin. Antibody that targets the protein of interest is added followed by the protein A-Micrococcal nuclease conjugated protein (pA-MNase). After incubating cells with the antibody and pA-MNase, cells are chilled to 0 ^{o}C and digestion begins with the addition of Ca^{2+}. Digestion reaction is stopped by the addition of chelating agents (EDTA/EGTA). Digested DNA is released into the solution. DNA is extracted from the supernatant and sequenced.

1.9 **Thesis Overview**

Fbw7 targets many transcription factors (TFs) for degradation. Loss of Fbw7 function causes a widespread effect on TFs and their downstream target-genes, possibly leading to a network of impaired biological processes. Due to tissue-type and mutation-type specific deregulatory mechanisms, Fbw7's role in tumorigenesis is quite complex to unravel. Cellular level analysis of one or two substrates in one tissue type may not suffice the current need in the field to fully understand Fbw7's global transcriptional regulation and its role in tumorigenesis. To begin to address this gap in knowledge, in this thesis work, I took a holistic approach by investigating how Fbw7 regulates multiple TFs, genome-wide, in a mutation-type and cell-type specific manner. An important yet an unanswered question in the field is why $Fbw7^{Arg/+}$ is favored in tumors over complete loss of Fbw7. Chapter 3 presents unique and shared consequences of $Fbw7^{-/-}$ and $Fbw7^{Arg/+}$ mutations on two Fbw7 substrates – Myc and Jun, in Hct116 colon cancer cells. This study led to the discovery of class II HLA regulation by Fbw7. Moreover, the observations made in Hct116 cells were compared to neural stem cells. Chapter 4 elaborates on Fbw7's cell-type specific regulation of TFs using DLD1 colon cancer cells. The identification of exact genomic regions that Fbw7 associates with would provide greater insights to understand its transcriptional regulation. Therefore I attempted to map the genomic occupancy of Fbw7 and Chapter 5 entails the techniques and reagents that I used as well as future directions that I propose to optimize the method. Finally, in Chapter 6, I briefly present a secondary project carried out to determine Fbw7's role in stem cell maintenance, where we identified that Fbw7 promotes a G0 quiescent cell cycle phase. Overall, these findings have advanced our understanding of context-specific transcriptional regulation by Fbw7 and its relevance to human cancer.

Chapter 2. Material and Methods

2.1 RNA-Seq : RNA extraction and library preparation

Total RNA was isolated from three million cells per sample using the Qiagen RNeasy Mini Kit (Cat # 74104) following the manufacturer's instructions. Three replicates per cell type were included and for each replicate cells were harvested from separate cultured plates.

RNA quality was tested using the NanoDrop; A260/280 1.8 – 2.1, A260/230 > 1.7. Total RNA integrity was checked using an Agilent 4200 TapeStation (Agilent Technologies, Inc., Santa Clara, CA) and quantified using a Trinean DropSense96 spectrophotometer (Caliper Life Sciences, Hopkinton, MA). For all samples RIN $\geq$ 9.

Libraries were prepared by the Fred Hutch Genomics Center using the TruSeq RNA Samples Prep Kit v2 (Illumina Inc., San Diego CA, USA). Library size distribution was validated using an Agilent 4200 TapeStation (Agilent Technologies, Santa Clara, CA, USA). Additional library QC, blending of pooled indexed libraries, and cluster optimization was performed using Life Technologies' Invitrogen Qubit® 2.0 Fluorometer (Life Technologies-Invitrogen, Carlsbad, CA, USA). RNA-Seq libraries were pooled and clustered onto flow cell lanes; 6 samples per one lane. Sequencing was performed using an Illumina HiSeq 2500 in rapid mode employing a paired-end, 50 base read length (PE50) sequencing strategy. RNA-Seq for U5-NSCs was an exception – libraries were prepared using TruSeq Stranded mRNA and sequencing was performed using an Illumina NovaSeq 6000 employing a paired-end 50 base read length (PE50) sequencing strategy.

2.2 RNA-Seq data analysis

Fastq files were filtered to exclude reads that didn't pass Illumina's base call quality threshold. STAR v2.7.1 (https://pubmed.ncbi.nlm.nih.gov/23104886/) with 2-pass mapping was used to

align paired-end reads to human genome build hg19 and GENCODE gene annotation v31lift37 (https://www.gencodegenes.org/human/).

FastQC 0.11.8 (https://www.bioinformatics.babraham.ac.uk/projects/fastqc/) and RSeQC 3.0.0 (https://pubmed.ncbi.nlm.nih.gov/22743226/) were used for QC including insert fragment size, read quality, read duplication rates, gene body coverage and read distribution in different genomic regions. FeatureCounts (https://pubmed.ncbi.nlm.nih.gov/24227677/) in Subread 1.6.5 was used to quantify gene-level expression.

For stranded libraries, only coding strand derived reads were counted. Bioconductor package edgeR 3.26.8 (https://academic.oup.com/bioinformatics/article/26/1/139/182458) was used to detect differential gene expression between conditions. Genes with low expression were excluded by requiring at least one count per million in at least N samples (N is equal to one less than the number of samples in the smallest group). The filtered expression matrix was normalized by TMM method (https://genomebiology.biomedcentral.com/articles/10.1186/gb-2010-11-3-r25) and subject to significance testing using GLM LRT method. Genes were deemed differentially expressed if absolute fold changes were above 1.5 and FDRs were less than 0.05 in Hct116 and U5-NSCs and if absolute fold changes were above 2.0 and FDRs were less than 0.01 in DLD1 cells.

2.3 **CUT&RUN (Cleavage Under Target and Release Using Nuclease)**

Manual or automated CUT&RUN were performed as previously described (Janssens et al., 2018; Skene et al., 2018; Skene & Henikoff, 2017). Briefly, cells were harvested using Accutase, counted and washed twice with Wash Buffer (20mM HEPES pH 7.5, 150 mM NaCl, 0.5mM Spermidine and one Roche Complete EDTA free protein inhibitor tablet per 50 mL). Cells were bound to

Concanavalin A-coated magnetic beads (20uL per one million cells). Then cells were permeabilized with Dig Wash buffer (Wash Buffer with 0.05% Digitonin) while being incubated with primary antibody overnight at 4 ^{o}C. Cell-bead mixture was washed twice with Dig-Wash buffer and incubated with Protein A-MNase (pA-MN) for 1 hour at 4 ^{o}C. After washing the mix with Dig Wash buffer twice, cells were placed on an ice-cold block and incubated with 2 mM $CaCl_2$ in Dig Wash buffer to activate pA-MN digestion. After the specific digestion period the reaction was inhibited with 2X Stop Buffer (340 mM NaCl, 20mM EDTA, 4mM EGTA, 0.05% Digitonin, 0.05% mg/ml glycogen, 5 ug/mL RNase, 2pg/mL heterologous spike-in DNA). The samples were incubated at 37 ^{o}C for 30 min to release the digested DNA fragments in to the supernatant. The supernatant was collected and libraries were prepared as previously explained (Janssens et al., 2018). Paired-end 25 base read length (PE25) sequencing was performed using an Illumina HiSeq 2500 platform at Fred Hutch Genomics Shared Resources.

<u>Deviations from the above described protocol:</u>

1. Automated CUT&RUN. Cells were harvested, counted, washed, permeabilized with Digitonin and added antibody (manual preparation). Cells with the antibodies were incubated at 4 ^{o}C overnight. Next day samples were submitted for automated CUT&RUN which was performed by the Genomics and Bioinformatics Center at Fred Hutch on a BioMek platform.
2. Secondary antibody addition. When the primary antibody was of a mouse origin, a rabbit anti-mouse antibody was also included. After the cells incubated in primary antibody overnight, next day the secondary antibody was added after washing cells twice with the

Dig-Wash buffer. Cells were incubated at 4 °C overnight prior to submission for automated CUT&RUN.

3. Nuclei instead of cells. Nuclei was isolated from native cells. H3K4me1 and H3K4me2 were mapped using the CUT&RUN protocol as previously described using isolated nuclei (Skene & Henikoff, 2017).

A summary of all CUT&RUN data with experimental conditions and CUT&RUN protocol modifications is presented in **Appendix C**.

2.4 **CUT&RUN data analysis**

Basic analysis: Sequencing reads were aligned to hg19 using Bowtie2.

bowtie2 --end-to-end --very-sensitive --no-overlap --no-dovetail --no-unal --no-mixed --no-discordant -q -I 10 -X 700 -x path/to/Bowtie2/indices -1 read1.fastq.gz -2 read2.fastq.gz

CPM normalized bigwig files were generated using bedtools genomecov.

Peaks were called using MACS2. Peak calling was performed for each target with and without the IgG control.

Narrow peaks with IgG control: macs2 callpeak --name TARGET --treatment path/to/TARGET/hg19.bam --control path/to/IgG/hg19.bam --format BAMPE --gsize hs --keep-dup all -q 0.05

Narrow peaks without IgG control: macs2 callpeak --name TARGET --treatment path/to/TARGET/hg19.bam --format BAMPE --gsize hs --keep-dup all -q 0.05

IgG-controlled peaks that overlap with no-control peaks were retained for further analyses.

For each TF/histone mark mapped in each genotype, peaks from three replicates were considered to make a final peak-set to use for downstream analysis. For example, for Myc in DLD1 WT cells, pairwise intersection was performed using "bedtool intersect" tool (for 3 replicates : 1and2, 1and3, 2and3). Then the intersection of 2 previous intersected files (1and2 and 1and3) was considered as the final peak-set for Myc in DLD1 WT cells.

bedtools intersect -u -wa -a DLD1_Myc_rep1_peaks.bed -b DLD1_Myc_rep2_peaks.bed > Inters_DLD1_Myc_rep12_peaks.bed

Differential binding analysis in Hct116 and U5-NSCs: Merged peak set for each target was used for the analysis. FeatureCounts (https://pubmed.ncbi.nlm.nih.gov/24227677/) in Subread 1.6.5 was used to count reads mapped to merged peaks in each sample. Bioconductor package edgeR 3.26.8 (https://academic.oup.com/bioinformatics/article/26/1/139/182458) was used to detect differential peaks between conditions. Peaks with low read numbers were excluded using edgeR function filterByExpr with min.count = 10 and min.total.count = 15. The filtered count matrix was normalized by TMM method (https://genomebiology.biomedcentral.com/articles/10.1186/gb-2010-11-3-r25) and subjected to significance testing using generalized linear models and quasi-likelihood method. Peaks were deemed differentially bound if absolute fold changes were above 1.5 and FDRs were less than 0.01for H3K27ac and Jun data, and FDR 0.05 for Myc data.

Differential binding analysis in DLD1 cells: For all previous analysis the filtered count matrix was normalized by TMM method with the assumption that total protein levels and majority of peaks do not change (https://genomebiology.biomedcentral.com/articles/10.1186/gb-2010-11-3-r25). However, since Myc total protein levels were increased in DLD1 Fbw7$^{-/-}$ cells (based on

western blot), the assumption made for TMM normalization doesn't hold true. Therefore, read counts were normalized to yeast spike-in DNA. For consistency Jun counts were also normalized to yeast spike-in DNA. However, Jun analysis output was independent of the normalization method (its total protein level did not change) (**Appendix B: Table 1**), whereas output of Myc analysis was dependent on the normalization method. Normalized read counts were subjected to significance testing using generalized linear models and quasi-likelihood method. Peaks were deemed differentially bound if absolute fold changes (FC) were above 1.5 and FDRs were less than 0.01.

2.5 Other computational data analysis

Correlation matrix.

Correlations between various CUT&RUN samples were determined using deepTools (Ramírez et al., 2016). We generated a final peak-set for each correlation analysis by intersecting and merging peaks from three replicates per cell condition for each TF / histone mark. Using multiBamSummary, we computed the read coverages for 2 kb regions of each peak. Then plotCorrelation was used quantify Pearson correlation coefficients and visualize results as a heatmap.

Correlation between RNA-Seq and the distribution of histone marks around TSS.

A reference list of hg19 genes was downloaded from the UCSC Table Browser. Genes were oriented according to the directionality of gene transcription and specified a 2 kb window around TSSs. Genes that have overlapping TSS within the 2 kb window and mitochondrial genes were removed, creating a list of 22,222 TSSs. The gene list (TSSs) were sorted in descending order of

their RNA-Seq FPKM values. CUT&RUN H3K27ac and H3K27me3 signal (merged from three replicates) were mapped on to the ordered genomic sites. The coverage of histone marks was quantified using bedtools coverage and converted to FPKM values. Correlation between RNA-Seq and histone mark FPKM values was calculated using R cor function.

Gene set enrichment analysis

Enrichr web-based tool was used to determine Gene Ontology (GO) Terms enriched in gene lists.

Motif analysis

For all motif analysis we used the The MEME Suite (Bailey et al., 2009). We used bedtools getfasta to generate FASTA files for genomic sites of interest (Quinlan & Hall, 2010). For motif discovery analysis we submitted the center 100 bp sequence of peaks to MEME-ChIP. MEME-ChIP was used with default parameters in Classic mode. HOCOMOCO Human (v11 FULL) motif database was used (Ref). We used the position-weight matrix (PWM) of the motif discovered by MEME-ChIP as the input for FIMO, to quantify the abundance of the motif. We used FIMO with a threshold value of p.value =< 0.01 to capture all motif configurations and then filtered the output to select only the motifs with the highest FIMO motif scores (higher the score, similar to the input motif). For differential motif analysis, we used MEME-ChIP in Differential Enrichment mode with default parameters.

Annotations

To assign gene regions where peaks are located, we used ChIPseeker, an R/Bioconductor package (Yu et al., 2015).

We used the nearest gene method to assign a peak to a gene using the bedtools closest tool (Quinlan & Hall, 2010) Gencode Human Release 31 (GRCh37) Comprehensive gene annotation list was used to generate a list of genes with full gene coordinates which was used to annotate peaks to the nearest gene (https://www.gencodegenes.org/human/release_31lift37.html).

Venn diagrams

Intervene was used to determine intersections between multiple genomic ranges lists and plot Venn diagrams (Khan & Mathelier, 2017).

Sequencing file processing and data visualization

Tools for BAM and bigwig processing (bamCoverage, multiBamSummary, computeMatrix) and heatmap generation (plotHeatmap, plotProfile) were used to analyze sequence data (Ramírez et al., 2016). Plots were generated using Microsoft Excel, R (https://www.r-project.org) and ggplot2 (https://ggplot2.tidyverse.org/).

Primary cancer and cell line data analysis.

CIITA expression data from Fbw7 WT and mutated Colon and rectal cancers were collected from the TCGA COADREAD database via UCSC Xena (https://xenabrowser.net/). CIITA expression in Fbw7 WT and mutated colorectal cancer cell lines were collected from the DepMap Portal (https://depmap.org/portal/). Student t-test was performed on data to determine statistical significance of differential expression. GraphPad Prism was used for statistics and graph visualization.

2.6 **Antibodies**

We used Rabbit anti-H3K27ac (1:100, Abcam Cat #ab45173), anti-H3K27me3 (1:100, Cell Signaling Tech Cat#9733S), Rabbit anti-Jun (1:25, Santa Cruz Cat #sc-1694), Rabbit anti-Myc (1:25, Cell Signaling Tech D3N8F Cat #13987), Rabbit anti-H3K4me1 (1:10, Abcam Cat#ab8895), Rabbit normal IgG (1:50, Santa Cruz sc-2027) . Concentrations mentioned are for CUT&RUN.

We used Rabbit anti-Fbw7 (Bethyl A301-720), Rabbit Sigma anti-Flag (Anti-Flag Sigma Rb F7425), Mouse anti-Flag (Sigma Flag M2 F1804), Mouse anti-Flag (Sigma Flag M2 F3165), Rabbit anti-mouse (Abcam ab46540), Rabbit anti-Jun (BD Biosciences).

2.7 **Cell culture**

Hct116, DLD1 and 293A cells were grown in DMEM with 10% FBS and 1% 100X PenStrep solution. Raji cells were grown in RPMI media with 10% FBS and 1% 100X PenStrep solution. For CUT&RUN and RNA-Seq experiments 2 x 10^6 cells were plated per 10 cm dish two days prior to harvesting.

U5-NSCs were used for experiments in collaboration with Dr. Paddison's lab. Cells and culture media were provided by them. Human fetal tissue derived U5 NCSs were cultured in NeuroCult NS-A basal medium (Stem Cell Technologies) supplemented with N2 (made in-house 2x stock in Advacned DMEM/F-12 (Thermo Fisher Scientific)), B27 (Thermo Fisher Scientific), antibiotic-antimycotic (Thermo Fisher Scientific), glutamaz (Thermo Fisher Scientific), EGF and bFGF (Peprotech). Cells were cultured in Laminin coated plates. Accutase was used to harvest cells for experiments.

2.8 Molecular Biology and Biochemistry Techniques

Western blot and immunoprecipitations

Whole cell extracts (WCE) were made by lysing cells in 0.5% NP-40 lysis buffer (50mM Tris pH 8.0, 150 mM NaCl, 0.5% NP-40, 1mM DTT) with protease and phosphatase inhibitor cocktail (made in-house). Then WCE were sonicated and spun to remove debris. Samples were normalized to total protein using Bradford reagent. Protein was denatured by boiling for 10 minutes in Laemmli sample buffer. Eluted protein was run on 10% polyacrylamide gels and transferred to PVDF. Membranes were blocked in 5% milk/TNT and probed with primary antibodies overnight at 4^0C. After membranes were washed, they were probed with HRP conjugated anti-Rabbit secondary antibody (1:10,000). Membranes were treated with ECL (made in-house) and visualized on a BioRad ChemiDoc imaging system.

To immunoprecipitate Fbw7 from whole or fractionated cell lysates anti-Fbw7 Bethyl A301-720A antibody and Protein A beads were added and incubated for at least 2hrs at 4^0C. Beads were then washed with thrice with 1 ml NP40 lysis buffer. Eluted protein was run on 8% polyacrylamide gels and transferred to PVDF which was blotted against Fbw7 using anti-Fbw7 Bethyl A301-720A (1:1000).

Chromatin fractionation

Untreated and Bortezomib treated (0.5 uM for 10 hrs) cells were harvested and counted. Cells were resuspended in CSK buffer (10 mM HEPES pH 6.8, 100mM NaCl, 1mM EGTA, 1mM EDTA, 2mM $MgCl_2$, 300mM Sucrose, 0.1% Triton X-100 and Protease inhibitor - 50 ul per million cells)

(J. M. Kim et al., 2008). Cells were allowed to lyse for 5 min on ice and centrifuged for 5 min at 4^0C at 1500 g. The supernatant which is the soluble fraction (S) was removed to a new tube. The pellet was resuspended in 1 ml of CSK buffer, centrifuged for 5 min at 4^0C at 1500 g. The supernatant was thoroughly removed. Next, NP40 buffer with protease inhibitor and 250 U/ml benzonase was added to the cell pellet (same volume as CSK buffer was used to lyse cells). Cells were incubated for 30 min on ice. This was chromatin fraction (C). Both soluble and chromatin fractions were sonicated, spun to remove debris (5 min at 4^0C at maximum speed). Total protein in all chromatin fractions were quantified using Bradford and samples were normalized to total protein content. Equal volumes of chromatin and soluble fractions from each sample were used to immunoprecipitate Fbw7.

PCR amplification of CIITA

RNA was isolated from Hct116 and Raji cells using the Qiagen RNeasy Mini Kit (Cat # 74104). cDNA was prepared using the iScript Reverse Transcription Supermix (Cat # 1708841). CIITA PIII and PIV were amplified using specific primers (PIII : F – 5'GCTGGGATTCCTACACAATGC3', R – 5'GGGTTCTGAGTAGAGCTCAATC3' and PIV : F – 5'GGGAGCCCGGGGAACA3', R – 5'GATGGTGTCTGTGTCGGGTT3') at 60^0C annealing temperature for 38 cycles(Chen et al., 2015). GAPDH was amplified as the control (25 cycles) using primers F – 5'GGTCGGAGTCAACGGATTTG3' and R – 5'ATGAGCCCCAGCCTTCTCCAT3'. Platinum Taq DNA polymerase was used following the manufacturer's instructions.

siRNA

siRNA used to knockdown Myc was ordered from Qiagen: sense strand 5'-CGAUGUUGUUUCUGUGGAATT-3'. AllStars siRNA from Qiagen was used as the negative control. All siRNA transfections were performed using Lipofectamine RNAiMax (Life Technologies) by following the manufacturer's protocol.

2.9 **Homozygous Fbw7 null U5-NSC generation**

Previously described protocol to generate homozygous null mutations using CRISPR-Cas9 and nucleofection was followed (Hoellerbauer et al., 2020). Briefly the protocol is as follows:

CRISPR sgRNA design: Broad Institute's GPP Web Portal was used to design the sgRNAs. The output list of sgRNAs was manually curated to choose three sgRNAs targeting FBXW7. Exon 3, 4 and 9 in FBXW7 were targeted by 5'AAGAGCGGACCTCAGAACCA3', 5'CTGAGGTCCCCAAAAGTTGT3', 5'ACATTAGTGGGACATACAGG3' guides respectively. A control sgRNA was also included 5'GTAGCGAACGTGTCCGGCGT3'. sgRNAs were purchased from Synthego.

Cas9:sgRNA RNP nucleofection: Reconstituted sgRNAs by adding 10uL of 1X TE Buffer 1.5nmol of dried sgRNA. A working stock of 30uM sgRNA was used henceforth. A working stock of Cas9 (10.17 pmol/ul) was made. To prepare RNP complexes, sgRNA, sNLS-SpCas9-sNLS (Aldevron) and SG Cell Line Nucleofector Solution (Lonza) were mixed in 1.87 uL, 1.84 uL and 18.29 uL respectively to make a 20 uL final volume. The mixture was incubated at room temperature for 15 minutes to allow RNP complexes to form. To nucleofect, 0.13 x 10^6 cells were harvested. The cells were washed with PBS and resuspended with RNPs. (We were able to

successfully nucleofect up to 0.85 x 10^6 cells with the same volume of RNPs.) Cells were electroporated using the Amaxa 4D Nucleofector X unit and program EN-138. Nucleofected cells were plated in pre-warmed media.

CRISPR editing efficiency analysis: Extraction of genomic DNA, PCR amplification of target site and efficiency analysis was done as previously described (Hoellerbauer et al., 2020). The primer pairs used to amplify CRISPR target sites in Exon 3: 5'TCATCACACACTGTTCTTCTGGA3' and 5'TGTCTACCCTAGAACAGCTGT3', Exon 4: 5'TGTGTACCTGTGATCTCTGGG3' and 5'CACCTTGCTGTGCAACCATC3', Exon 9: 5'ACTGCTTTCATGTCGTGTTTCC3' and 5'AGGAAGCTGACAACACTAGCA3'. We found that the pool of three sgRNA was the most successful at deleting FBXW7. It was confirmed by blotting for immunoprecipitated Fbw7 in each nucleofected sample (Appendix A: Supplemental Figure 4A).

2.10 **Single Cell RNA-Seq (scRNA-Seq)**

U5-NSCs were harvested using Accutase. Approximately 5000 cells from WT and Fbw7$^{-/-}$ U5-NSCs were sequenced. Samples were prepared according to the 10X Genomics Single Cell Protocol (10X Genomic, 2019). Libraries were prepared using the Chromium Single Cell 3' v2 Libraries by Bielas lab. scRNA-Seq data analysis was performed by Dr. Sonali Aurora. Seurat package was used for the cell cycle analysis. Cell cycle scoring system developed by the Paddison lab was also subsequently used (ccAF) (O'Connor et al., 2021).

2.11 **Schematic figures and Genome Browser Views**

Schematic figures were created with BioRender.com. Bigwig files (three replicates merged) were viewed on Integrative Genome Viewer and screenshots taken to show examples of CUT&RUN binding data as peaks.

Chapter 3. Context-Specific Regulation of Transcription by Fbw7

This chapter was adapted from a manuscript in preparation.

Context-Specific Regulation of Transcription by Fbw7
[1,2]H. Nayanga Thirimanne, [3]Feinan Wu, [4]Derek Janssens, [5]Robert Amezquita, [2]Patrick Paddison, [4,7]Steven Henikoff, [2,3,6]Bruce Clurman
[1]Molecular Medicine and Mechanisms of Disease Program - Department of Pathology, [6]Department of Medicine, [7]Genomic Sciences, University of Washington, Seattle, WA, 98195, USA
[2]Division of Human Biology, [3]Division of Clinical Research and [4]Division of Basic Sciences, [5]Vaccine and Infectious Disease Division, [3]Bioinformatics and Genomics Center, Fred Hutchinson Cancer Research Center, Seattle, WA, 98109, USA

3.1 Introduction

Fbw7 is the substrate receptor of an SCF (Skp1-Cul1-F-box protein) E3 ubiquitin ligase that targets a network of substrates for ubiquitylation and degradation (Crusio et al., 2010; R. J. Davis et al., 2014). Fbw7 binds to substrates after they become phosphorylated within consensus recognition motifs called Cdc4-phosphodegrons that form high-affinity Fbw7 binding sites (Koepp et al., 2001). Substrate phosphorylation drives SCF^{Fbw7} mediated ubiquitylation and the signaling pathways that regulate degron phosphorylations determine when substrates are targeted for degradation.

Fbw7 exhibits an unusual mutational spectrum in tumors: the most frequent are heterozygous missense mutations that target arginine residues that comprise the Fbw7 substrate binding pockets, hereafter termed $Fbw7^{Arg/+}$ ($Fbw7^{R/+}$) (Hao et al., 2007; Spruck et al., 2002). These mutations weaken substrate binding and are thought to act as dominant negatives that heterodimerize with WT-Fbw7 and impair some Fbw7 functions. However, the oncogenic functions that drive $Fbw7^{Arg/+}$ selection in cancers are not known. Canonical loss of function Fbw7 mutations (e.g. nonsense, truncations, frame shifts, deletions) also occur, in addition to $Fbw7^{Arg/+}$. Different cancers have different mutational spectra: T-cell ALLs have almost exclusively

Fbw7$^{Arg/+}$ whereas colorectal cancers have both Fbw7$^{Arg/+}$ and canonical loss of function mutations (Malyukova et al., 2007).

Most Fbw7 substrates are master transcription factors (TFs) that control key cellular processes such as proliferation and differentiation, and these include c-Myc, Notch, c-Jun, PGC-1α, SREBP1/2, KLFs, and many others (R. J. Davis et al., 2014). Some of these TFs are oncoproteins that drive tumorigenesis when their activities are deregulated, and oncogenic Fbw7 substrates such as Myc and Notch are among the most important cancer drivers (King et al., 2013; Malyukova et al., 2007; Welcker et al., 2004). Fbw7 loss in tumors deregulates these oncoproteins. The biological consequences of Fbw7 function reflect the combined regulation of its large substrate network, many of which control complex transcriptional programs. In addition to its direct targets, Fbw7 may impact an even larger system of downstream effectors. However, the extent to which Fbw7 regulates these TFs and the transcriptional consequences of Fbw7$^{Arg/+}$ or Fbw7 null mutations are not fully understood.

In light of this complexity, we sought a holistic approach to understand how Fbw7 regulates TFs and gene expression. We used high resolution genome-wide protein mapping and RNA-Seq to study the consequences of Fbw7 mutations. Unlike T-ALL, colorectal cancers are known to have both Fbw7 missense and null mutations, therefore for this study we used an isogenic panel of Hct116 colorectal cancer cells that differ by their Fbw7 mutational status: WT-Fbw7, Fbw7 null (Fbw7$^{-/-}$) and heterozygous Fbw7$^{Arg/+}$ (Fbw7$^{R/+}$). Both mutations caused widespread transcriptional changes associated with active chromatin marks. We next mapped the chromatin occupancy of two TFs, c-Jun and c-Myc (hereafter Jun and Myc, respectively), which revealed that only a small fraction of their binding sites was deregulated by Fbw7 mutations, some in a mutation-type specific manner. Strikingly, Fbw7 loss preferentially deregulated TF occupancy at

distal regulatory regions, and we also identified sites in which Jun and Myc were co-regulated by Fbw7. We also studied neural stem cells (NSCs) in which Fbw7 was acutely deleted, which revealed transcriptional consequences of Fbw7 loss that were very analogous to those seen in Hct116 cells, although the differentially regulated genes were unique to each cell type.

One co-regulated site falls within an upstream regulatory region of *CIITA* (Class II Major Histocompatibility Complex Transactivator). CIITA is a transcriptional coactivator and the master regulator of MHC class II gene expression (Nagarajan et al., 2002; Steimle V, Otten LA, Zufferey M, 1993). CIITA is either constitutively expressed or induced, in a tissue-specific manner. Under normal conditions CIITA and its downstream MHC Class II molecules are constitutively expressed only in antigen presenting cells (APCs), however, CIITA expression can be induced in many other cell types by inflammatory cytokines such as IFNγ. Strikingly, Jun and Myc occupancy were both increased at upstream CIITA regulatory sites in Hct116 Fbw7$^{-/-}$ cells, leading to constitutive expression of CIITA and class II HLA expression. Fbw7 loss in NSCs also increased CIITA and class II HLA gene expression. These data suggest that Fbw7 loss is one mechanism leading to abnormal class II HLA expression in cancer.

Overall, these data revealed mutation-type specific and genomic region-specific co-regulation of TFs by Fbw7. Even with only two TF substrates we demonstrated the complex nature of direct Fbw7 targets and their downstream effectors, and potential multi-protein complexes that might interact with Fbw7. Lastly, we identified altered class II HLA expression as one important consequence of Fbw7 loss that may enable new prognostic and therapeutic strategies for Fbw7-associated cancers.

3.2 **Results**

3.2.1 Fbw7 null and missense mutations lead to distinct gene expression profiles.

We used an isogenic colon cancer cell line panel that differed only in Fbw7 mutational status to study how oncogenic Fbw7 mutations impact transcription and chromatin. Hct116 cells were engineered to mutate the endogenous wild-type (WT) *FBXW7* locus to either a heterozygous $Fbw7^{R505C/+}$ ($Fbw7^{R/+}$) or a homozygous null mutation ($Fbw7^{-/-}$) (**Figure 3.1A**) (R. J. Davis et al., 2018; Grim et al., 2008). We performed RNA sequencing on the WT, $Fbw7^{R/+}$ and $Fbw7^{-/-}$ Hct116 cells to identify the global transcriptome changes arising in response to these Fbw7 mutations. Principal component analysis (PCA) revealed that the $Fbw7^{R/+}$ and $Fbw7^{-/-}$ cells clustered apart from one another, indicating that the two *FBXW7* mutations have distinct effects on the transcriptome relative to WT cells **(Appendix A: Supplemental Figure 1A**). Compared with WT-cells, 11.3% and 5.4% of protein coding genes were differentially expressed in $Fbw7^{-/-}$ and $Fbw7^{R/+}$ respectively. Hierarchical clustering identified differentially expressed genes that are uniquely altered in the $Fbw7^{-/-}$ cells (clusters 1 and 2), as well as genes uniquely altered in $Fbw7^{R/+}$ cells (clusters 5 and 6**)** and genes that show similar expression changes in response to both types of *FBXW7* mutation (clusters 3 and 4) (**Figure 3.1B**). Gene set enrichment analysis (GSEA) revealed numerous pathways enriched in the differentially expressed genes common to both types of Fbw7 mutations or uniquely to $Fbw7^{-/-}$ cells (**Figure 3.1C**). For example, the Gene Ontology (GO) term "cholesterol biosynthetic processes" was identified in $Fbw7^{-/-}$ cells, which may reflect that SREBP, a master transcriptional regulator of cholesterol biosynthesis, is an Fbw7 substrate stabilized in $Fbw7^{-/-}$ Hct116 cells (Sundqvist et al., 2005; Welcker et al., 2013). MHC Class II components is the most enriched GO term in $Fbw7^{-/-}$ cells, which may underlie our previous finding that a signature of immune response related genes was highly predictive of Fbw7 mutations in primary

colorectal cancers (R. J. Davis et al., 2018). The two different *FBXW7* mutations thus led to both overlapping as well as distinct changes in the global transcription of Hct116 cells.

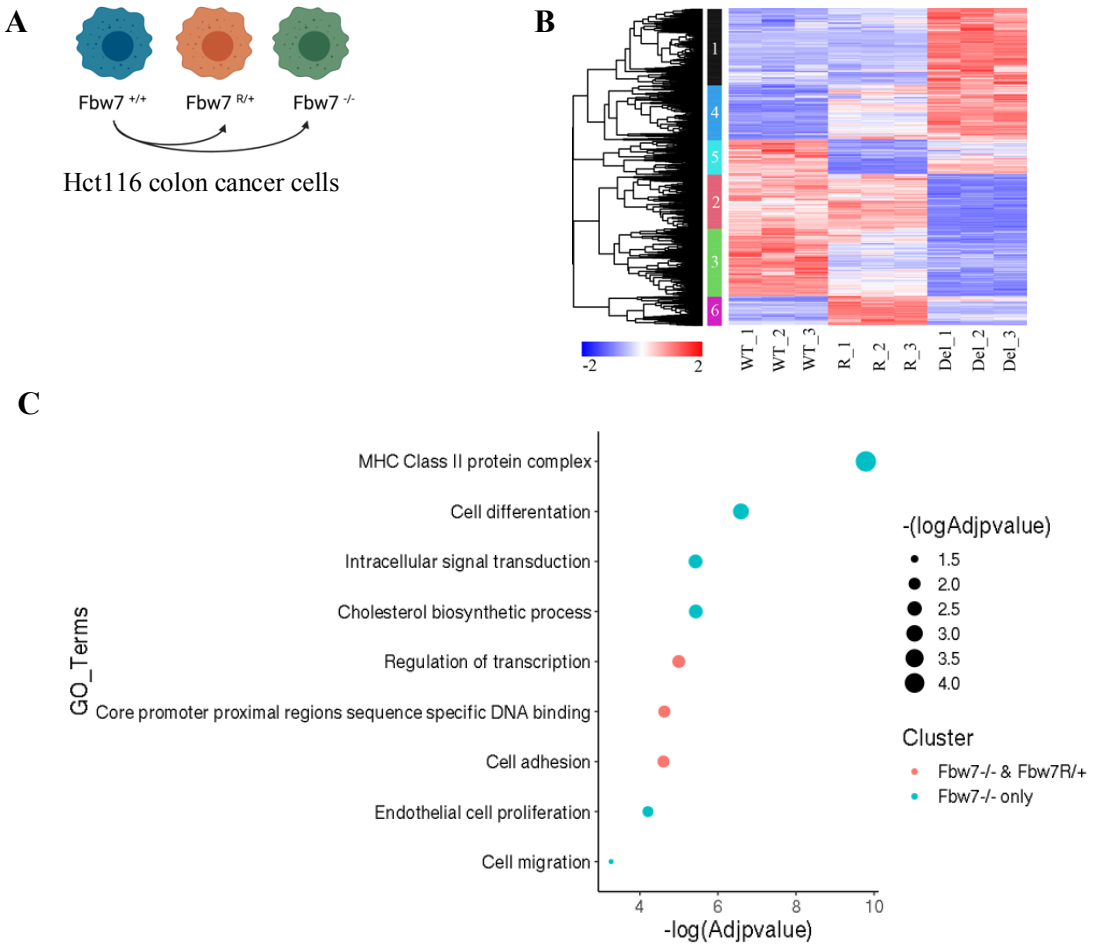

Figure 3.1 RNA-Seq analysis highlights differential global transcription in Hct116 Fbw7$^{-/-}$ and Fbw7$^{R/+}$ cells

(A) Schema depicting genetically engineered isogenic cell lines used in the study: Hct116 wild-type (WT), Fbw7$^{-/-}$ and Fbw7$^{R/+}$. (B) Hierarchical clustering analysis separates differentially expressed protein coding genes into six groups. The heatmap shows the intensity of expression of each gene (y axis) for three replicates per cell type (x axis). (C) Gene ontology terms that are enriched in gene clusters that are deregulated by both Fbw7$^{-/-}$ and Fbw7$^{R/+}$, and only by Fbw7$^{-/-}$. (R = Fbw7$^{R/+}$, Del = Fbw7$^{-/-}$).

3.2.2 Altered chromatin regulation in Fbw7 mutant cells

Altered gene expression in *FBXW7* mutant cell lines could be the cumulative result of altered degradation of multiple Fbw7 substrates that function as TFs and chromatin regulatory proteins. The histone H3 lysine-27 acetylation (H3K27ac) and histone H3 lysine-27 trimethylation (H3K27me3) provide a simple readout of transcriptionally active versus repressive chromatin, respectively (Karlic et al 2010 PNAS). We used CUT&RUN to map H3K27ac and H3K27me3 in each of the Hct116 cell lines (Skene et al., 2018; Skene & Henikoff, 2017). As expected, the H3K27ac signal within the 2 kb flanking the transcriptional start sites (TSSs) of genes was positively correlated with their expression (r = 0.44), whereas the amount of H3K27me3 was negatively correlated (r = -0.22) (**Figure 3.2A**).

Genome-wide analysis identified sites where H3K27ac is increased in *FBXW7*-mutant cells ($Fbw7^{-/-}$: 9.4%, $Fbw7^{R/+}$: 7.6%) compared with control cells, and sites where H3K27ac is decreased ($Fbw7^{-/-}$: 6.9% , $Fbw7^{R/+}$: 4.3%) (**Figure 3.2B**). While most H3K27ac sites in WT-cells are promoter proximal, the regions that show differential H3K27ac in both the $Fbw7^{R/+}$ and $Fbw7^{-/-}$ mutant background fall within introns or intergenic regions (p value 0.0003, Fisher's exact test) (**Figure 3.2C, Appendix A: Supplemental Figure 1C**). Thus, the changes in H3K27ac levels that occur in response to *FBXW7* mutation tend to occur at distal regulatory elements. To determine whether these changes potentially reflect altered binding of known Fbw7 substrates, we performed motif discovery analysis on the central 100 bp sequence of each peak. Strikingly, the AP-1 motif was enriched in H3K27ac sites that are upregulated in $Fbw7^{-/-}$ cells (**Figure 3.2D, Appendix A: Supplemental Figure 1D)**. The AP-1 motif is bound by the Jun family, and FIMO (Find Individual Motif Occurrences in MEME Suite) analysis revealed that the AP-1 motif was enriched in approximately 30-35% of H3K27ac sites that were upregulated in $Fbw7^{-/-}$ (p value $\leq$ 1.8e-5), downregulated in $Fbw7^{-/-}$ (p value $\leq$ 1.8e-5), upregulated in $Fbw7^{R/+}$ (30.2% p value $\leq$ 1.8e-5), or

downregulated in Fbw7$^{R/+}$ (35% p value $\leq$ 1.5e-5). In contrast, the AP-1 site was not enriched in H3K27ac sites that remained unchanged by the *FBXW7* mutations (**Appendix A: Supplemental Figure 1E)**. These data reveal widespread Fbw7-associated changes in chromatin marks in distal regulatory regions, and while RNA-Seq only determines changes in the transcriptional output, genome-wide analysis of chromatin marks also reveals exact genomic sites that are targeted by Fbw7 substrates. Moreover, the AP-1 site enrichment in differential sites suggests that Fbw7-dependent Jun regulation may account, at least in part, for some of these changes.

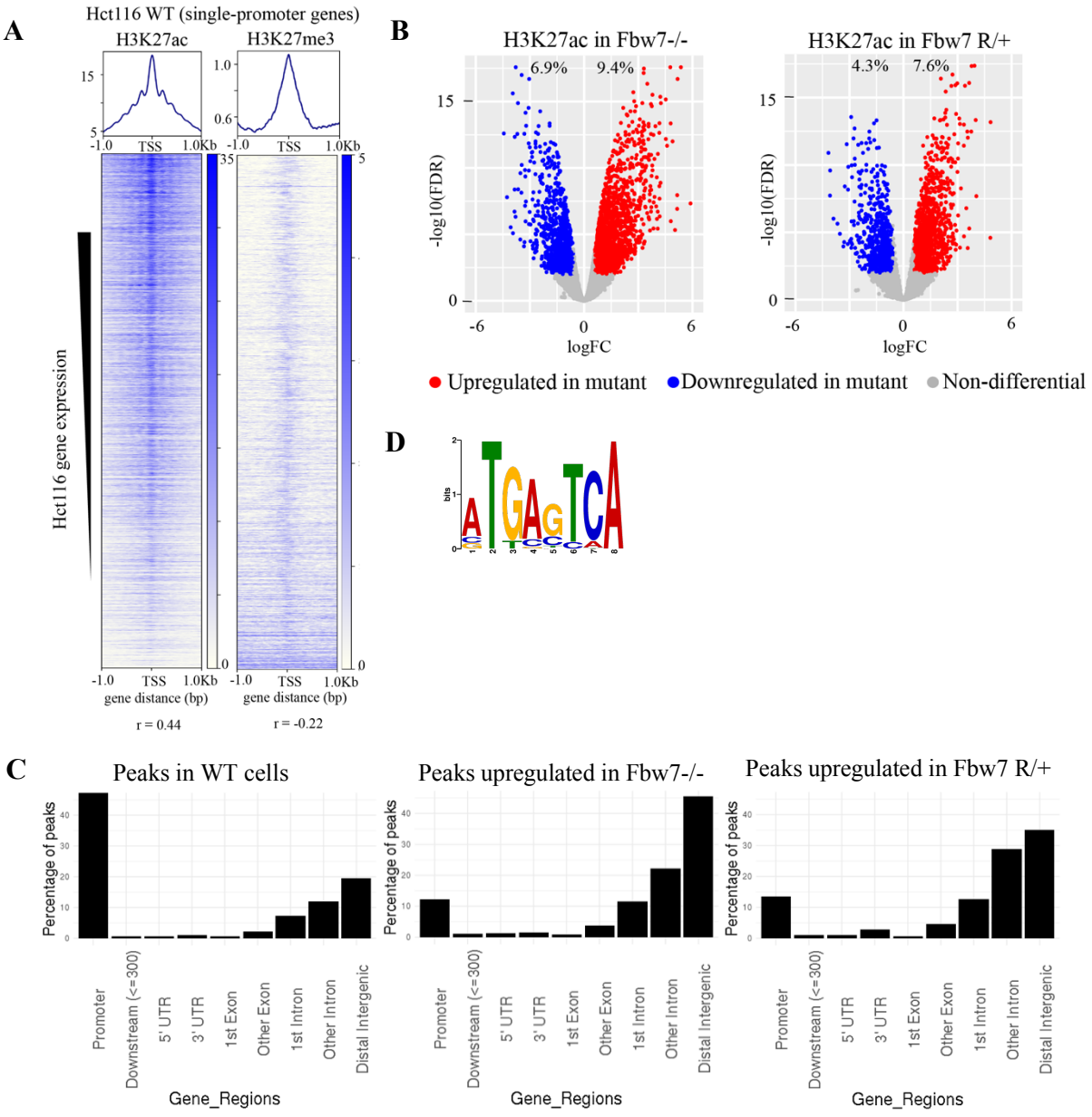

Figure 3.2 Differential H3K27ac signal in Hct116 Fbw7 mutant cells reveals specific genomic sites targeted by Fbw7.

(A) Heatmaps showing the correlation between CUT&RUN profiles of H3K27ac and H3K27me3, and RNA-Seq in Hct116 WT cells. (B) Volcano plots showing upregulated (red) and downregulated (blue) H3K27ac sites in Hct116 Fbw7$^{-/-}$ and Fbw7$^{R/+}$ cells compared to WT cells. Up- and downregulated differential sites indicated as a percent of total H3K27ac peaks in Hct116 WT cells. (C) Percentage of H3K27ac peaks located within different gene regions. (D) Sequence logo for AP1 motif enriched in H3K27ac peaks upregulated in Fbw7$^{-/-}$ cells (E value = 1.6e-3).

3.2.3 Fbw7 preferentially regulates Jun and Myc occupancy at distal regulatory regions.

Previous reports have shown that Fbw7 catalyzes the ubiquitylation of some TF substrates while they are bound to DNA, suggesting that binding to substrates may recruit Fbw7 to chromatin (Punga et al., 2006). We thus examined how mutations of the Fbw7 substrate binding domain impact its chromatin association in Hct116 cells with either heterozygous ($Fbw7^{R/+}$) or homozygous ($Fbw7^{R/R}$) mutations. Fbw7 is found in both the chromatin and soluble fractions of WT-Hct116 cellular lysates, but $Fbw7^{R/R}$ is exclusively found in the soluble fraction (**Figure 3.3A**). The only known consequence of $Fbw7^{R}$ mutations is to prevent substrate binding, hence the loss of chromatin-associated Fbw7 in $Fbw7^{R/R}$ cells suggests that Fbw7 is normally tethered to chromatin by binding to substrates such as TFs. Proteasome inhibition (+ bortezomib) prevents substrate degradation and stabilizes Fbw7-substrate complexes, and further shifted Fbw7 to chromatin, supporting the hypothesis that Fbw7 is recruited to chromatin by its substrates.

To directly test whether the altered transcription in *FBXW7* mutant Hct116 cells is the result of altered chromatin occupancy of Fbw7 substrates, we profiled genome-wide Jun and Myc occupancy. As expected, Jun-binding and Myc-binding site motifs were highly enriched in the respective datasets (**Appendix A: Supplemental Figure 2A**). Genome-wide differential binding analyses of the Jun and Myc peaks demonstrated that only 5.3% and 3.8% of the Jun sites and 2.2% and 3.3% of the Myc sites exhibited differential occupancy each in the $Fbw7^{-/-}$ and $Fbw7^{R/+}$ cells, respectively (**Figure 3.3B and 3.3C)**. Thus, rather than a global increase, Fbw7 mutations led to changes in Myc and Jun occupancy at specific loci.

Similar to H3K27ac, most of the Myc binding sites in control cells were promoter proximal, while almost all of the differential sites with increased Myc occupancy in Fbw7 mutant cells fell within introns and intergenic regions (**Figure 3.3D, Appendix A: Supplementary Figure 2C)**. Compared with Myc, a smaller proportion of the Jun sites in WT-Hct116 cells were

promoter-proximal, but again the differential sites were heavily biased to introns and intragenic regions (**Figure 3.3D**). These differential sites in introns and intergenic loci were enriched for histone modifications such as H3K27ac and H3K4me1, consistent with roles as distal regulatory elements such as enhancers (**Figure 3.3E**).

To study the functional significance of altered Jun and Myc binding, we examined the expression of transcripts that could be linked to differential Jun or Myc sites in Fbw7$^{-/-}$ cells (within the gene body or 10 kb upstream of Transcription Start Site (TSS)) (**Figure 3.3F).** Approximately 40% of genes with increased promoter proximal Jun and 46% of genes with decreased promoter proximal Jun in Fbw7$^{-/-}$ cells correlated with differentially expressed genes (differentially expressed genes logFC$\pm$0.6 and FDR$\leq$0.05, some differential genes were not statistically significant and some were not captured by RNA-Seq) (**Figure 3.3G**). Most genes with increased or decreased Jun occupancy in Fbw7$^{-/-}$ cells exhibited increased or decreased expression, respectively (**Figure 3.3G).** Similar findings were seen with Myc differential sites, although overall there were fewer genes that could be linked with differential Myc binding sites (**Appendix A: Supplemental Figure 2D**). Overall, the differential sites that could be linked with associated genes showed concordance between the amount of Jun and Myc binding and target gene transcription.

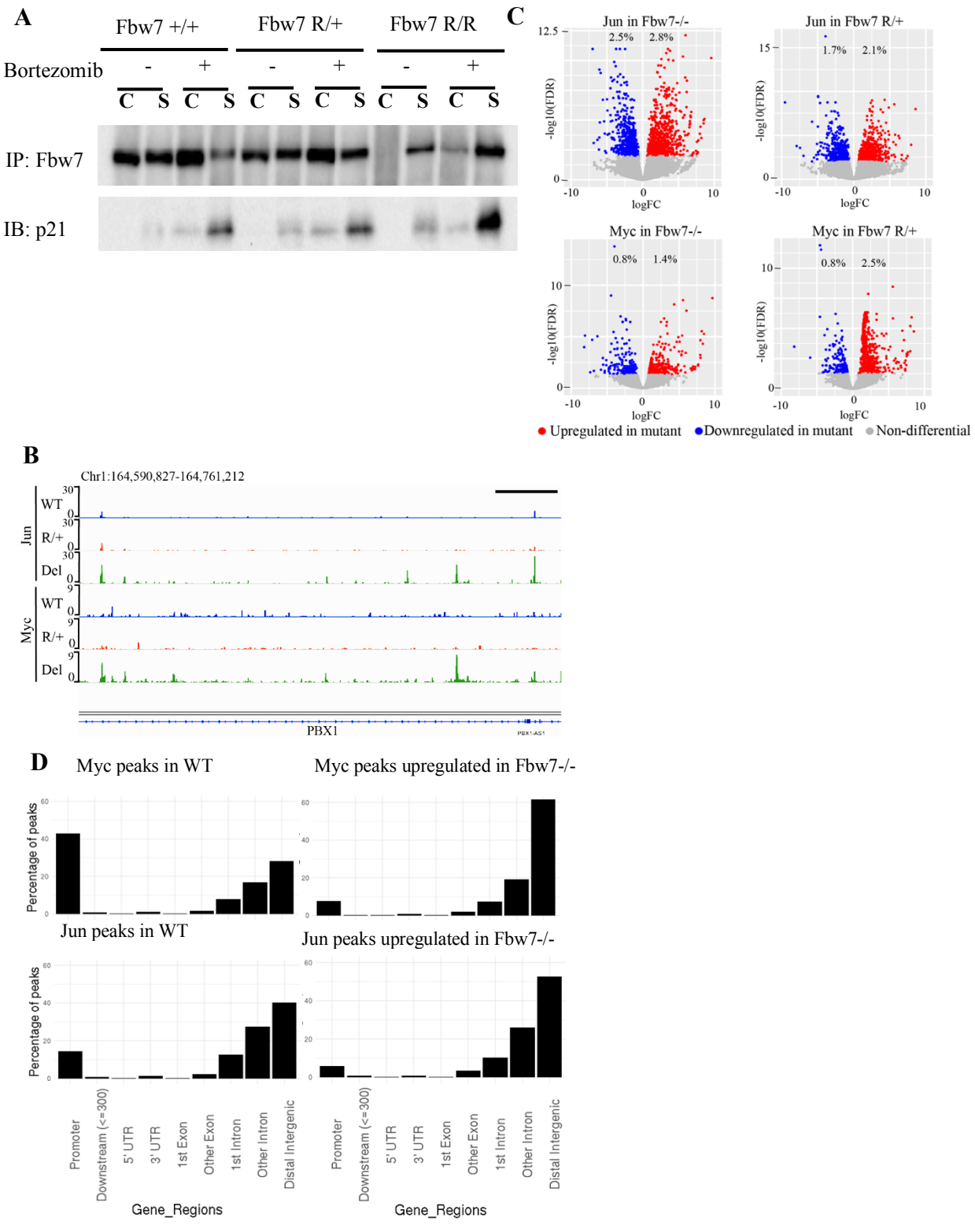
A
Fbw7 +/+
Fbw7 R/+
Fbw7 R/R
Bortezomib
- + - + - +
C S C S C S C S C S C S
IP: Fbw7
IB: p21
C
Jun in Fbw7-/-
2.5% 2.8%
Jun in Fbw7 R/+
1.7% 2.1%
Myc in Fbw7-/-
0.8% 1.4%
Myc in Fbw7 R/+
0.8% 2.5%
-log10(FDR)
logFC
Upregulated in mutant
Downregulated in mutant
Non-differential
B
Chr1:164,590,827-164,761,212
Jun
Myc
WT
R/+
Del
PBX1
D
Myc peaks in WT
Myc peaks upregulated in Fbw7-/-
Jun peaks in WT
Jun peaks upregulated in Fbw7-/-
Percentage of peaks
Promoter
Downstream (<=300)
5' UTR
3' UTR
1st Exon
Other Exon
1st Intron
Other Intron
Distal Intergenic
Gene_Regions

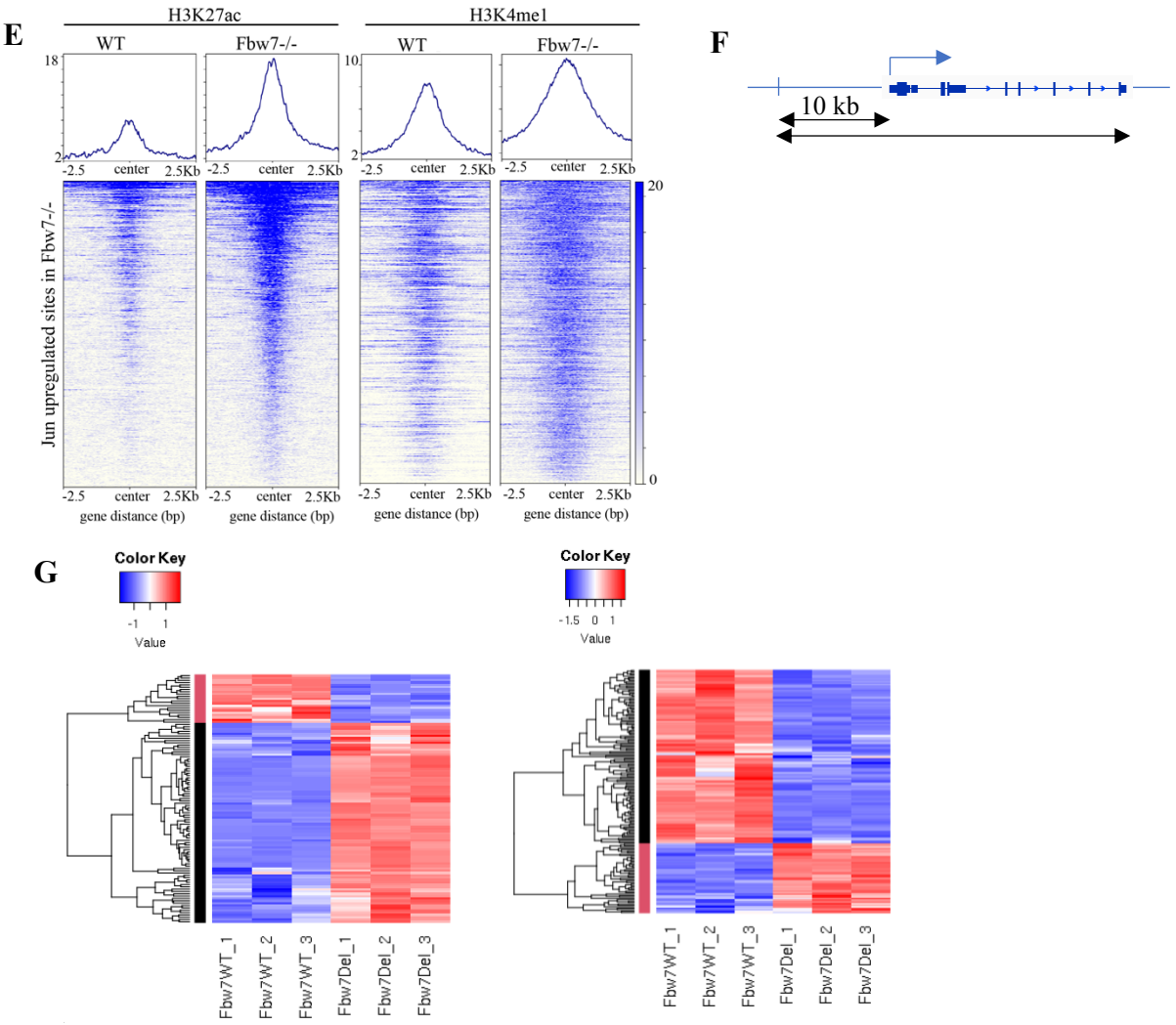

Figure 3.3 Fbw7 regulates Jun and Myc bound to DNA, preferentially at distal regulatory regions.

(A) Western blot showing Fbw7 in chromatin (C) and soluble (S) fractions in untreated and Velcade treated (0.5 uM 10hr) Hct116 WT, Fbw7$^{R/+}$ and Fbw7$^{R/R}$ cells. (B) Genome viewer tracks showing Jun and Myc occupancy in Hct116 WT, Fbw7$^{-/-}$ (Del) and Fbw7$^{R/+}$ (R/+) at a representative locus (PBX1). Black scale bar = 20kb. (C) Volcano plots showing upregulated (red) and downregulated (blue) Jun and Myc sites in Hct116 Fbw7$^{-/-}$ and Fbw7$^{R/+}$ cells compared to WT. (D) Percentage of Jun and Myc peaks located at different gene features. (E) H3K27ac and H3K4me1 CUT&RUN signal from Hct116 WT and Fbw7$^{-/-}$ cells mapped on genomic sites that have Jun upregulated in Fbw7$^{-/-}$ cells. (F) Schema depicting the filtering criteria applied to the annotated differential sites to select gene proximal sites. (G) Heatmaps showing the transcription of genes that have more and less Jun bound at a gene proximal site. (Each row is a gene and three replicates each from Hct116 WT and Fbw7$^{-/-}$ cells are shown.)

3.2.4 Shared and unique consequences of Fbw7$^{-/-}$ and Fbw7$^{R/+}$ mutations on TF occupancy.

Although heterozygous missense mutations are the most common Fbw7 mutations in cancers, their biological consequences and the selection pressure driving this striking mutational spectrum are not known. We thus examined how Jun occupancy is differentially affected by Fbw7$^{R/+}$ and Fbw7$^{-/-}$ mutations. A simple comparison shows that many differential Jun sites found in Fbw7$^{R/+}$ cells are also found in Fbw7$^{-/-}$ cells (48%, 252/530; p value <0.0001, Fisher's exact test) (**Figure 3.4A).** Conversely, many differential Jun sites in Fbw7$^{-/-}$ cells were also found in Fbw7$^{R/+}$ cells (35%, 252/715) (**Figure 3.4A).** Representative peaks of Jun upregulated in Fbw7$^{-/-}$ and/or Fbw7$^{R/+}$ are shown to elaborate on the observations we made (**Figure 3.4B**). At *KCNQ5* intronic sites, Jun signal was upregulated only in Fbw7$^{-/-}$ cells. In *ITGA2,* Jun was upregulated in both Fbw7$^{-/-}$ and Fbw7$^{R/+}$, but to a lesser extent in Fbw7$^{R/+}$. In *MAML2*, Jun was upregulated in Fbw7$^{R/+}$ more highly than in Fbw7$^{-/-}$. H3K27ac was also upregulated in mutant cells and followed the same trend exhibited by Jun at each of these sites (**Figure 3.4B**). In support thereof, differentially expressed genes (including the above mentioned genes) exhibited the same pattern of effect by mutations (**Figure 3.1B**). Genes in cluster 3 and 4 were deregulated in both Fbw7$^{-/-}$ and Fbw7$^{R/+}$, but to an intermediate level in Fbw7$^{R/+}$, while genes in cluster 5 and 6 were deregulated most strongly in Fbw7$^{R/+}$.

The Venn diagram was expanded to include upregulated Myc sites in Fbw7$^{-/-}$ and Fbw7$^{R/+}$ where we saw a similar overlap in the two cell types (234 Myc sites upregulated in Fbw7$^{-/-}$ and Fbw7$^{R/+}$ cells) (**Figure 3.4C**, marked with white stars). In summary, these data identified specific genomic sites that are uniquely affected by each Fbw7 mutation type and others that were shared between the two mutant cell lines. Because the Fbw7$^{-/-}$ and Fbw7$^{R/+}$ cells were derived independently, the shared sites found in Fbw7$^{-/-}$ and Fbw7$^{R/+}$ cells and the gradients in Jun

occupancy, H3K27ac, and RNA expression support the conclusion that these differences are directly attributable to Fbw7 status.

3.2.5 Fbw7 coordinately regulated Jun and Myc at co-occupied loci

Myc and Jun are oncogenic TFs with activities in shared pathways, and we examined how they might be coregulated at shared sites. Approximately 20% of the Myc and Jun binding sites overlap in Hct116 WT-cells (**Appendix A: Supplemental Figure 3A**). We identified 78 sites in which both Jun and Myc occupancy are upregulated in $Fbw7^{-/-}$ cells (**Figure 3.4C**, marked with yellow stars). We made similar observations regarding co-regulated sites with reduced Jun and Myc occupancy in $Fbw7^{-/-}$ cells: 53 sites where both Myc and Jun are downregulated (**Figure 3.4E,** marked with yellow stars). In contrast, no sites with discordant changes in Myc and Jun occupancy were found; i.e. no overlap between Jun upregulated sites with Myc downregulated sites nor vice versa (**Figure 3.4D, 3.4F**). Jun and Myc regulation in $Fbw7^{R/+}$ cells were also coordinately up- or downregulated. This data suggests coordinate regulation of multiple substrates by Fbw7. Presumably Fbw7 extends its impact towards other TFs that heterodimerize and form transcription factor complexes with its direct substrates.

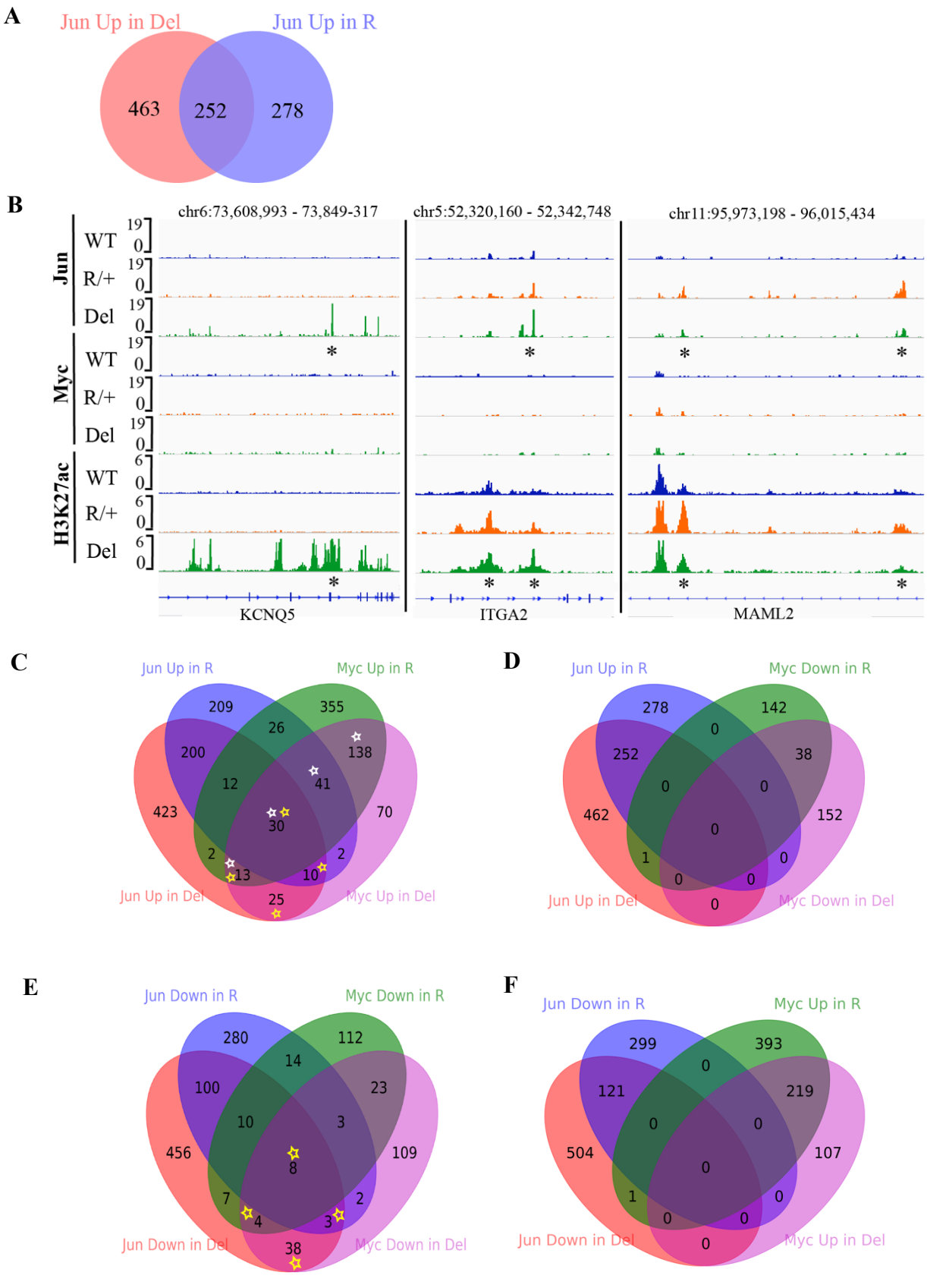
A
Jun Up in Del
Jun Up in R
463
252
278
B
chr6:73,608,993 - 73,849-317
chr5:52,320,160 - 52,342,748
chr11:95,973,198 - 96,015,434
Jun
Myc
H3K27ac
WT
R/+
Del
KCNQ5
ITGA2
MAML2
C
Jun Up in R
Myc Up in R
Jun Up in Del
Myc Up in Del
209
355
26
200
138
12
41
423
70
30
2
13
10
2
25
D
Jun Up in R
Myc Down in R
Jun Up in Del
Myc Down in Del
278
142
0
252
38
0
0
462
152
0
1
0
0
0
E
Jun Down in R
Myc Down in R
Jun Down in Del
Myc Down in Del
280
112
14
100
23
10
3
456
109
8
7
4
3
2
38
F
Jun Down in R
Myc Up in R
Jun Down in Del
Myc Up in Del
299
393
0
121
219
0
0
504
107
0
1
0
0
0

Figure 3.4 Fbw7 exhibits mutation-type specific regulation and coordinate regulation of multiple TFs.

(A) Venn diagram showing the overlap between upregulated Jun peaks in Fbw7$^{-/-}$ and Fbw7$^{R/+}$ cells. (B) Genome viewer tracks showing Jun and H3K27ac occupancy in Hct116 WT, Fbw7$^{-/-}$ and Fbw7$^{R/+}$ cells at representative loci. Myc was not bound at these sites. Asterisks refer to peaks that are upregulated uniquely in Fbw7$^{-/-}$ (*KCNQ5*), peaks upregulated in both Fbw7$^{-/-}$ and Fbw7$^{R/+}$ (intermediate level in Fbw7$^{R/+}$) (*ITGA2*) and peaks upregulated in Fbw7$^{R/+}$ higher than in Fbw7$^{-/-}$ (*MAML2*). (C) Venn diagram showing the overlap between upregulated Jun and Myc peaks in Fbw7$^{-/-}$ and Fbw7$^{R/+}$ cells. (D) Venn diagram showing the overlap between Jun upregulated in Fbw7$^{-/-}$ and Fbw7$^{R/+}$, and Myc downregulated in Fbw7$^{-/-}$ and Fbw7$^{R/+}$ (E)Venn diagram showing the overlap between Jun and Myc downregulated in Fbw7$^{-/-}$ and Fbw7$^{R/+}$ (F) Venn diagram showing the overlap between Jun downregulated in Fbw7$^{-/-}$ and Fbw7$^{R/+}$ and Myc upregulated in Fbw7$^{-/-}$ and Fbw7$^{R/+}$

3.2.6 MHC Class II regulation by Fbw7

Gene ontology analysis performed on differentially expressed genes showed MHC Class II gene enrichment (**Figure 3.1C**). Strikingly, we found that Myc and Jun occupancy was co-upregulated in Fbw7$^{-/-}$ cells at upstream regulatory regions of the *Class II Major Histocompatibility Transactivator (CIITA*) gene. The CIITA gene is regulated by a multi-promoter 14 kb region. Four independent promoters (hereafter referred to as PI – PIV) lead to four transcripts with four distinct first exons (Muhlethaler-Mottet et al., 1997). CIITA isoform I is expressed exclusively in dendritic cells (DCs), while isoform III is expressed in DCs, B lymphocytes, monocytes and activated T cells (van der Stoep et al., 2007). Isoform II is expressed at negligible levels and poorly studied. CIITA isoform PIV is the predominant IFNγ induced isoform. IFNγ can also induce isoform III in non-hematopoietic cells such as fibroblasts and epithelial cells.

PIII Upstream Regulatory Region (PURR), a 4kb region that is located 6kb upstream of PIII, consists of regulatory sites for both constitutive and IFNγ-induced CIITA expression (**Figure 3.5A**) (Deffrennes et al., 2001; van der Stoep et al., 2007). While PURR is not responsible for constitutive expression of isoform III in hematopoietic cells, it regulates IFNγ induced and constitutive expression of isoform III in melanomas (van der Stoep et al., 2007). The two modes of expression are regulated by distinct regions in PURR. PII exon I region of 437 bp, which overlaps with PURR, is essential for the melanoma-specific constitutive activating effect of PURR, while the 530 bp region with GAS boxes is involved in IFNγ-dependent activation. PURR cannot enhance the IFNγ induction of the PIV isoform. In addition to PURR, there are four other enhancer regions that regulate CIITA activity (**Figure 3.5A**) (Ni et al., 2008). Studies show that these regulator regions not only mediate gene expression, they also contribute to form three dimensional structures.

We found that both Myc and Jun bind to regulatory elements 6kb and 14kb upstream of CIITA-PIII and that their occupancy is increased in Fbw7$^{-/-}$ cells (**Figure 3.5B**). The AP-1 motif at the PURR site has been noted in previous studies (Martins et al., 2007). Jun and Myc occupancy increased at these sites in Fbw7$^{R/+}$ cells, but to a lesser extent than in Fbw7$^{-/-}$ cells. In addition, H3K72ac and H3K4me1, histone modifications that mark actively transcribed regions, also increased at these sites in Fbw7$^{-/-}$ cells. According to RNA-Seq CIITA mRNA expression is increased in Fbw7$^{-/-}$ cells (**Figure 3.5C**). Consistent with the finding of increased Myc and Jun occupancy at the PURR site, isoform-specific primers demonstrated that the pIII isoform is elevated in Fbw7$^{-/-}$ cells, but that the pIV isoform is not (**Figure 3.5D**). Raji cells are shown as a control cell that expresses both isoforms. The elevation of *CIITA* expression in Fbw7$^{-/-}$ cells is likely functionally significant as several MHC Class II genes that are targets of CIITA (HLA-DPA1, HLA-DPB1 and HLA-DRA) were highly expressed in Fbw7$^{-/-}$ cells (**Figure 3.5C)**. Moreover, we detected elevated expression of class II HLA-DR proteins in Fbw7$^{-/-}$ Hct116 cells, however, only in a small fraction of cells (**Appendix A: Supplemental Figure 3B**). Further research is required to fully understand the reason for heterogenous expression of class II HLA protein in Fbw7 mutant cells. We examined *CIITA* expression in colorectal primary tumors using TCGA data, which revealed increased *CIITA* expression in Fbw7 mutant cancers (**Figure 3.5E)**. Because these tumors also contain immune infiltrates, the CIITA expression could reflect tumor cell-autonomous immune cell expression. However, colorectal cancer cell lines also exhibited elevated CIITA expression in Fbw7 mutant cell lines (**Figure 3.5F**). These data support the idea

that Fbw7 directly regulates CIITA expression in colorectal cancer, likely due to coregulation of Myc and Jun at the PIII upstream regulatory sites.

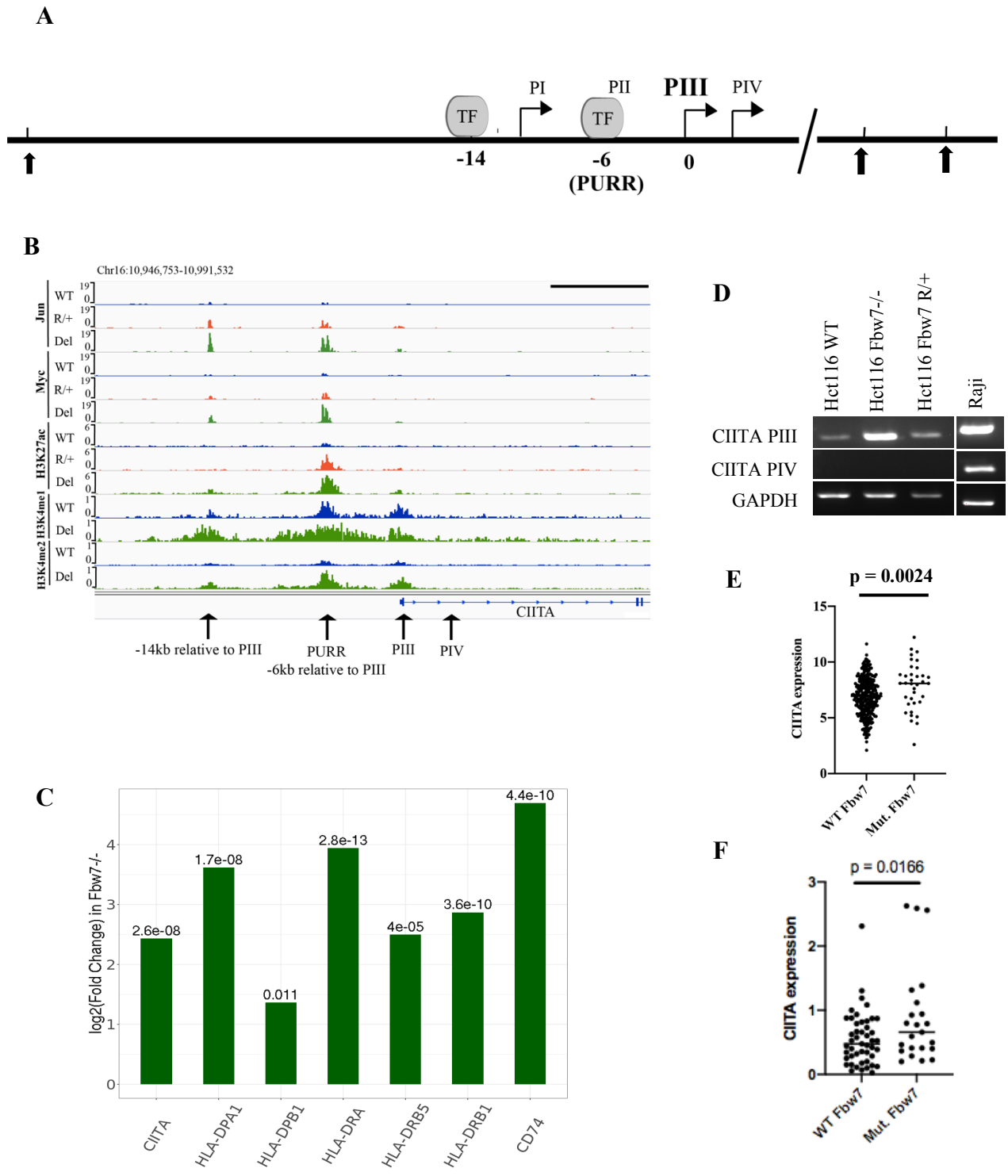

Figure 3.5 Fbw7 regulates the expression of MHC Class II genes.

(A) Schematic figure showing the gene features of CIITA. Distances are marked in kb with respect to PIII. Black arrows mark the additional distal regulatory sites. (B) Genome browser tracks showing TFs and histone modification marks enriched at the promoter and regulatory sites upstream of CIITA gene. Arrows point to (from right to left) PIV (promoter of isoform IV), PIII (promoter of isoform III), PURR (PIII Upstream Regulatory Regions, a known regulatory site 6 kb upstream of PIII), and a known regulatory site 14 kb upstream to PIII. Black scale bar = 10 kb (C) Expression fold change of CIITA and MHC Class II genes in Hct116 Fbw7$^{-/-}$ with respect to WT cells. FDR values are indicated at the top of each bar. (D) CIITA isoform III and IV amplified using isoform specific primers in Hct116 and Raji cells. (E) CIITA expression in primary cancer samples from TCGA COADREAD database that have WT Fbw7 (n=297) and mutated Fbw7 (n=43). (F) CIITA expression in colon and rectal cancer cell lines with WT Fbw7 (n=47) and mutated Fbw7 (n=23). Data collected from DepMap portal.

3.2.7 Acute inactivation of Fbw7 in neural stem cells recapitulates Jun regulation by Fbw7 in Hct116 cells.

Because this Hct116 panel bears Fbw7 mutations that were stably engineered into a transformed cell line, we examined how acute Fbw7 deletion in a non-transformed cell line impacts RNA expression and Jun occupancy. Fbw7 is known to play a role in neural stem cell (NSC) maintenance and Fbw7-mediated Jun regulation has been previously characterized in NSCs (Hoeck et al, 2010). An high efficiency CRISPR/nucleofection protocol to knockout genes without the need for selection was developed by the Paddison lab and optimized for U5 NSCs (Hoellerbauer et al., 2020)**.** Considering all these reason we chose to inactivate Fbw7 in U5 NSCs and further study its transcriptional regulation (**Figure 3.6A, Appendix A: Supplemental Figure 4A**). PCA analyses of gene expression data from both Hct116 and U5 NSCs revealed cell-type dependent (PC1) and mutation-type dependent (PC2) correlation (**Appendix A: Supplemental Figure 4B**). Analogous to the Hct116 cell panel, ~9% of protein coding genes were differentially expressed in Fbw7$^{-/-}$ cells compared with WT-U5 NSCs (**Figure 3.6B**). GSEA on the differentially expressed genes again revealed several enriched categories, some of which were shared with Hct116 cells whereas others were unique (**Figure 3.6C**). Notably, MHC class II genes were again one of the highly enriched processes in Fbw7 null U5 NSCs.

We mapped Jun genomic occupancy in WT and Fbw7$^{-/-}$ NSCs and also found results similar to those in the Hct116 cell panel: (1) only a minority of the Jun binding sites displayed differential occupancy after Fbw7 inactivation, including increased (8.3%) and decreased (4.1%) sites, and (2) most of the differentially regulated sites were found in introns and intergenic regions (**Figure 3.6D, 3.6E**). Thus, while the specific genes and loci differentially impacted by Fbw7 in

the Hct116 cells and NSCs differed, the scope of Fbw7's impact on Jun was quite similar in both contexts.

One striking similarity between the two systems is the upregulation of CIITA and MHC class II expression in Fbw7$^{-/-}$ cells (**Figure 3.6F**). Jun and Myc were bound at regulatory regions upstream of CIITA in NSCs while Myc was increased at the -14 kb site in Fbw7$^{-/-}$ NSCs (**Figure 3.6G**). Preliminary flow cytometry data from U5-NSCs indicated that WT U5-NSCs express a background level of class II HLA-DR protein and loss of Fbw7 upregulated the level by two-fold (**Appendix A: Supplemental Figure 3B**). Unlike in Hct116 WT cells, Jun and Myc are bound upstream of CIITA in WT U5-NSCs which might explain the background level of HLA protein expression. Overall, this data indicates that the function of Fbw7 to mediate activation of CIITA and the downstream MHC class II genes by preventing over-accumulation of Jun is shared in these distinct cell types, and is likely a critical function of Fbw7.

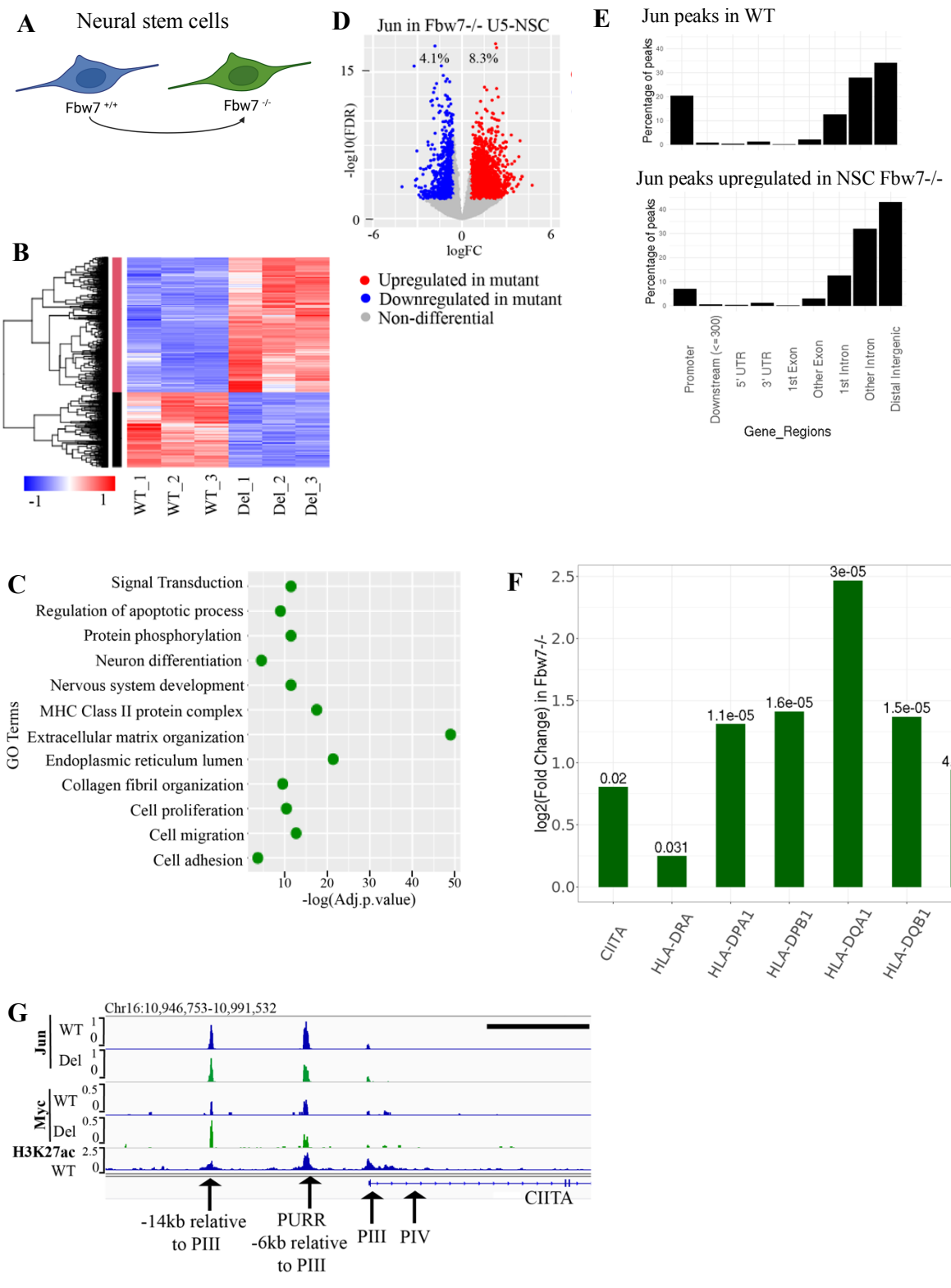
A
Neural stem cells
Fbw7 +/+
Fbw7 -/-
B
-1
1
WT_1
WT_2
WT_3
Del_1
Del_2
Del_3
D
Jun in Fbw7-/- U5-NSC
4.1%
8.3%
-log10(FDR)
logFC
Upregulated in mutant
Downregulated in mutant
Non-differential
E
Jun peaks in WT
Percentage of peaks
Jun peaks upregulated in NSC Fbw7-/-
Promoter
Downstream (<=300)
5' UTR
3' UTR
1st Exon
Other Exon
1st Intron
Other Intron
Distal Intergenic
Gene_Regions
C
Signal Transduction
Regulation of apoptotic process
Protein phosphorylation
Neuron differentiation
Nervous system development
MHC Class II protein complex
Extracellular matrix organization
Endoplasmic reticulum lumen
Collagen fibril organization
Cell proliferation
Cell migration
Cell adhesion
GO Terms
-log(Adj.p.value)
F
log2(Fold Change) in Fbw7-/-
0.02
0.031
1.1e-05
1.6e-05
3e-05
1.5e-05
4.6e-05
CIITA
HLA-DRA
HLA-DPA1
HLA-DPB1
HLA-DQA1
HLA-DQB1
CD74
G
Chr16:10,946,753-10,991,532
Jun
WT
Del
Myc
WT
Del
H3K27ac
WT
CIITA
-14kb relative to PIII
PURR -6kb relative to PIII
PIII
PIV

Figure 3.6 Loss of Fbw7 in neural stem cells recapitulates transcriptional changes in Hct116 cells.

(A) Schema depicting the genetically engineered non-transformed cells used in the study: U5 Neural Stem Cells (NSCs) (B) Clustering analysis separates differentially expressed protein coding genes in NSCs into 2 groups. Heatmap shows the intensity of expression of each gene (y axis) for three replicates per cell type (x axis). (C) Gene Ontology terms enriched in differentially expressed genes in $Fbw7^{-/-}$ NSCs. (D) Volcano plot showing upregulated (red) and downregulated (blue) Jun sites in $Fbw7^{-/-}$ NSCs compared to WT. (E) Percentage of Jun peaks located at different gene features. (F) Fold change of CIITA and MHC Class II genes in $Fbw7^{-/-}$ NSCs compared to WT. FDR values are indicated at each bar. (G) Genome browser tracks showing Myc, Jun and H3K27ac occupancy on CIITA regulatory regions in WT and $Fbw7^{-/-}$ (Del) NSCs. Black scale bar = 8 kb.

3.3 **Discussion**

The global transcriptional changes indicated by RNA-Seq are potentially the cumulative effect of multiple TFs deregulated by Fbw7. Thus, an analysis of the transcriptome might not be sufficient to characterize the transcriptional regulatory network of Fbw7. Genome-wide analysis of histone modifications such as H3K27ac provided a descriptive overview of exact genomic regions that are directly or indirectly targeted by Fbw7. TF motifs that overlap differential H3K27ac sites may indicate TFs bound to DNA that are targeted by Fbw7. Our analysis identified the AP-1 motif suggesting Jun deregulation.

Differential H3K27ac, Jun and Myc sites indicated that Fbw7 preferentially targets distal regulatory elements. The intronic and intergenic sites were enriched with histone modification marks H3K27ac and H3K4me1, suggesting they are enhancers. Additionally, we hypothesize that these sites might be involved in DNA looping to generate 3-dimensional genomic structures or that the intronic sites might be involved in RNA polymerase pause-release regulation. The majority of differential sites were not proximal to promoters; hence annotating them to genes was challenging and error-prone. Consequently, identifying gene signatures or biological pathways that were enriched among differentially regulated genomic sites was unsuccessful. Fbw7 directly and indirectly targets a large network of cellular pathways and that could also be why it was difficult to distinguish biological pathways that were deregulated in specific contexts. However, TF occupancy of many annotated differential sites correlated with the transcription of target genes, suggesting that the deregulated sites are functional and not mere noise. Changes in TF occupancy may not always correlate with transcription; however, it could also mean that CUT&RUN is more sensitive to capture changes in TF and histone marks than RNA-Seq is to capture changes in transcription. Therefore, we argue that genome-wide analysis of Fbw7 substrate occupancy

provides a deeper understanding of Fbw7's transcriptional regulation rather than assessing the final transcriptional output or total cellular level of substrates (R. J. Davis et al., 2018).

The data indicated unique and shared consequences of $Fbw7^{-/-}$ and $Fbw7^{R/+}$. We hypothesize that Fbw7's action as a dimer might play a role in context specific regulation. Although we determined the genomic occupancy of only two TFs, both Jun and Myc form heterodimers with many other proteins. Thus, Fbw7 might exert different regulatory effects on those heterodimers depending on how they interact with WT-Fbw7 and $Fbw7^{R/+}$. Some Fbw7 substrates have optimal degrons which can successfully interact with monomeric Fbw7 while others have suboptimal degrons that are Fbw7 dimer dependent. At some genomic sites substrates are affected the most by $Fbw7^{-/-}$ mutation and to an intermediate level by $Fbw7^{R/+}$ mutation. It is possible that these substrates have an optimal degron which can be regulated sufficiently with one Fbw7-WT monomer. These examples fit well with the "just enough" model of tumor suppressors where $Fbw7^{R/+}$ would be causing just the right amount of deregulatory effect to cause tumorigenesis, whereas complete loss of Fbw7 would be too detrimental to cells (H. Davis & Tomlinson, 2012). Some genomic sites are equally affected by both mutations and these sites are potentially bound by substrates with suboptimal degrons which cannot be degraded by impaired Fbw7 dimers (R/+). Strikingly, we identified a subset of genomic sites that is most affected by $Fbw7^{R/+}$ than $Fbw7^{-/-}$. Presumably, at these sites, $Fbw7^{R/+}$ exerts a dominant negative effect. When substrates are partially bound by $Fbw7^{R/+}$, yet not sufficiently targeted for ubiquitylation, they are masked from other compensatory protein turnover mechanisms, whereas in Fbw7 null cells, substrates are free to be targeted by compensatory mechanisms. The $Fbw7^{R/+}$ mutation is favored in cancers over complete loss of Fbw7 function, and the dominant negative effect has been the commonly hypothesized mechanism of action (R. J. Davis et al., 2014).

The canonical outcome of a ubiquitin ligase loss of function is the accumulation of otherwise degraded proteins. Hence we expected to see increased occupancy of TFs in Fbw7 mutant cells. Although most differential sites were of upregulated TFs, a smaller fraction of sites had downregulated TF occupancy in the mutant cells. Downregulated sites correlated with the transcription of target genes, indicating they have a functional outcome. We have not yet investigated the mechanism of action, however we hypothesize that at these sites TFs might be acting as pseudo-substrates that recruit Fbw7 to DNA to degrade a different protein or a different Fbw7 substrate that is even more elevated might be competing to bind the same site.

Constitutive expression of CIITA in normal conditions is confined to antigen presenting cells, therefore it was striking to find CIITA and MHC Class II genes expressed in Fbw7 mutated colon cancer cells. Previous studies have shown constitutive expression of CIITA and MHC Class II in a variety of tumors and melanoma cell lines (van der Stoep et al., 2007). Although MHC class II antigens are not expressed in normal colonic epithelial cells, they have been detected in colorectal carcinomas (38%), however information is very limited (Sconocchia et al., 2014). To the best of our knowledge, regulation of CIITA and its downstream targets by Fbw7 has not been discussed thus far. We hypothesize that, like in many other cancers, CIITA and class II HLA expression are correlated with favorable prognosis in Fbw7 mutant tumors (Sconocchia et al., 2014). In support thereof, data from previous studies show that in CRCs *FBXW7* mutations and distant metastasis almost never co-occur (Muzny et al., 2012). CIITA has been used as a marker associated with less aggressive CRCs. Furthermore, we believe that loss of Fbw7 could trigger a fail-safe mechanism in tumors. Because complete loss of Fbw7 can be detrimental to cells, class II HLA expression would make the tumor susceptible to immune responses. Opposed to $Fbw7^{-/-}$ cells, minor upregulation of MHC class II mRNA in $Fbw7^{R/+}$ cells might not trigger an immune

response and favor tumorigenesis. This model supports the mutational data that shows that human cancers favor $Fbw7^{R/+}$ over complete loss of Fbw7. A similar mechanism has been reported in HSCs with regard to Myc regulation by Fbw7 (King et al., 2013). However, further studies on MHC Class II protein expression and resulted immune responses are required to better understand the mutation type specific differences. In addition to directly regulating MHC Class II genes, CIITA has been found to mediate the expression of many other genes in B cells that impact diverse functions like antigen processing, signaling and proliferation. Although those genes cannot be directly linked to CIITA regulation in cancer cells, it is worth noting that constitutive CIITA expression in cancers may have a broader implication than our initial hypothesis of being limited to MHC Class II gene expression (Nagarajan et al., 2002). B lymphocytes express CIITA isoform III constitutively in normal conditions. It would be interesting to determine whether CIITA isoform III in B lymphocytes is not targeted by Fbw7 via Myc and Jun, in which case we can use this pathway to specifically target CIITA in cancerous cells. Further research is warranted to investigate the role of Fbw7 as a cancer-driver while implementing a potential fail-safe mechanism.

Overall, these data revealed global and context specific transcriptional control by mutation-type and genomic-region specific regulation of TFs by Fbw7. Our study demonstrated the complex nature of the effect of Fbw7 on the transcriptome; direct Fbw7 targets, their downstream effectors, and potential multi-protein complexes are all intertwined leading to complex deregulation of multiple cellular processes. Although UPS inhibition is a promising therapeutic strategy, targeting Fbw7, which regulates a large network of proteins including TFs, would result in broad cellular implications. Therefore, understanding context specific regulation by Fbw7 will enable to teasing apart the complex Fbw7 regulatory network and consequently strategizing more specific therapies.

Summary: Fbw7 regulates TFs at specific genomic sites; preferentially at regulatory elements within intronic and intergenic regions. Fbw7$^{-/-}$ and Fbw7$^{R/+}$ mutations exert unique and common deregulatory functions. Fbw7 coordinately co-regulates multiple TFs; for example, upstream regulatory regions of CIITA are co-occupied by Myc and Jun and they are co-regulated by Fbw7. Loss of Fbw7 upregulates CIITA and Class II HLA expression. Although cell type specific genes and loci are targeted by Fbw7, the general scope of transcriptional regulation seems to be similar across different cell types.

Chapter 4. Cell - Specific Transcriptional Regulation by Fbw7; DLD1 compared to Hct116

4.1 Introduction

The objective of this dissertation study was to understand Fbw7's role in global transcriptional regulation. An Hct116 colon cancer cell line panel which differed only in the Fbw7 mutational status was the first system we used to address our questions (see Chapter 3). Previous studies have shown tissue-specific Fbw7 regulation. We hypothesized that insights into Fbw7's regulation in another colon cancer cell line would support and strengthen our findings from Hct116 cells. Therefore we used the DLD1 colon cancer cell line panel: DLD1 wild-type (WT) and DLD1 Fbw7$^{-/-}$ cells. DLD1 Fbw7$^{-/-}$ isogenic cells were generated by the Clurman lab by genetically engineering the endogenous WT *FBXW7* locus to generate a homozygous null mutation (R. J. Davis et al., 2018).

We used RNA-Seq to study the global transcriptional changes in DLD1 cells and mapped genome-wide histone modification marks (H3K27ac) and TFs (Jun and Myc) in DLD1 WT and Fbw7$^{-/-}$ cells using CUT&RUN. Similar to the comparison between Hct116 and U5-NSCs (Chapter 3), the general scope of transcriptional regulation by Fbw7 was similar between Hct116 and DLD1 cells, however, the specific genes and loci targeted were cell-specific. The steady state level of Jun did not change in DLD1 Fbw7$^{-/-}$ cells, while a small fraction of specific Jun sites was differentially regulated. H3K27ac and Jun data showed that the majority of sites targeted by Fbw7 in DLD1 cells were also within intragenic and intergenic regions, and that some Jun and Myc co-occupied sites were coordinately co-regulated by Fbw7. The major discrepancy between the two cell types was that, in DLD1 Fbw7$^{-/-}$ cells, the steady state level of Myc was increased. Approximately 50% of Myc genomic sites in DLD1 cells were deregulated. Overall, the

similarities and discrepancies in transcriptional regulation by Fbw7 in the two colon cancer cell lines reiterates the context-specific and complex nature of Fbw7 regulation.

4.2 Results

4.2.1 Loss of Fbw7 leads to distinct gene expression profiles in DLD1 cells

To identify the global transcriptome changes that arise in response to loss of Fbw7, we performed RNA sequencing on WT and Fbw7$^{-/-}$ DLD1 cells. Principal component analysis (PCA) of these data revealed that Fbw7$^{-/-}$ cells cluster apart from WT cells, indicating the impact of loss of Fbw7 on global transcription (**Figure 4.1A**). Compared with WT cells, 15.1% of protein coding genes were downregulated and 13.8% of protein coding genes were upregulated in DLD1 Fbw7$^{-/-}$ cells (**Figure 4.1B**). Overall, RNA-Seq data revealed wide-spread changes in transcription resulted by loss of Fbw7.

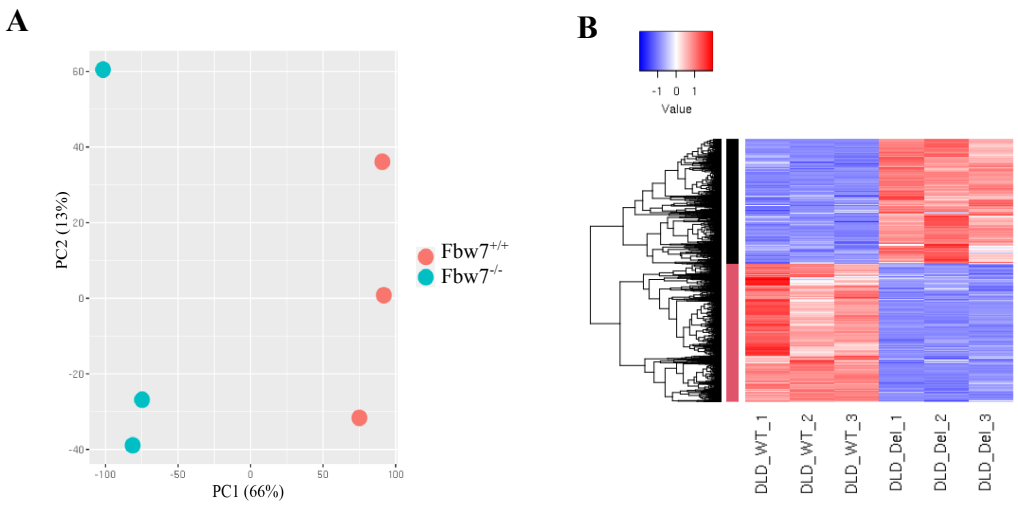

Figure 4.1 Loss of Fbw7 causes widespread changes in the DLD1 transcriptome.

(A) PCA plot of RNA-Seq data from DLD1 wild-type (WT) and DLD1 Fbw7$^{-/-}$ cells. (B) Hierarchical clustering on differentially expressed protein coding genes in DLD1 Fbw7$^{-/-}$ (Del) cells compared to WT cells. Only statistically significant differential genes are shown. (logFC >= 1.0 or =<(-1.0), FDR=<0.05)

4.2.2 Altered chromatin regulation in DLD1 Fbw7$^{-/-}$ cells

To identify the specific genomic sites directly or indirectly targeted by Fbw7 loss, we examined genome-wide chromatin modifications. Genome-wide analysis identified a larger collection of sites where H3K27ac was upregulated (38%) and less than 2% of sites where H3K27ac was downregulated in DLD1 Fbw7$^{-/-}$ cells (**Figure 4.2A**).

H3K27ac peaks in DLD1 WT cells were mostly promoter proximal (**Figure 4.2B**). However, similar to our observation in Hct116 mutant cells, the majority of differential H3K27ac sites in DLD1 Fbw7$^{-/-}$ cells were located within introns and intergenic regions (**Figure 4.2B**). Therefore, irrespective of the cell type our data indicates that Fbw7 controls transcription by preferentially impacting distal regulatory elements. To determine whether these changes potentially reflect altered binding of known Fbw7 substrates, we performed motif discovery analysis on the central 100 bp sequence of each peak. Similar to our findings in Hct116 cells, the AP1 motif was enriched in upregulated sites in DLD1 Fbw7$^{-/-}$ cells (E value 2.3e-2) (**Figure 4.2C**). FIMO (Find Individual Motif Occurrences) analysis showed a 30% enrichment of the AP-1 motif within the entire length of peaks (p value < 6.5e-5). This suggests the binding of the Fbw7 substrate, Jun. The SUH/RBPJ motif was also enriched in upregulated H3K27ac sites (E value 3.1e-2), however it was present only in 4% of peaks through their entire length (p value < 3.5e-9). The SUH/RBPJ motif suggests the regulation of the Fbw7 substrate, Notch1.

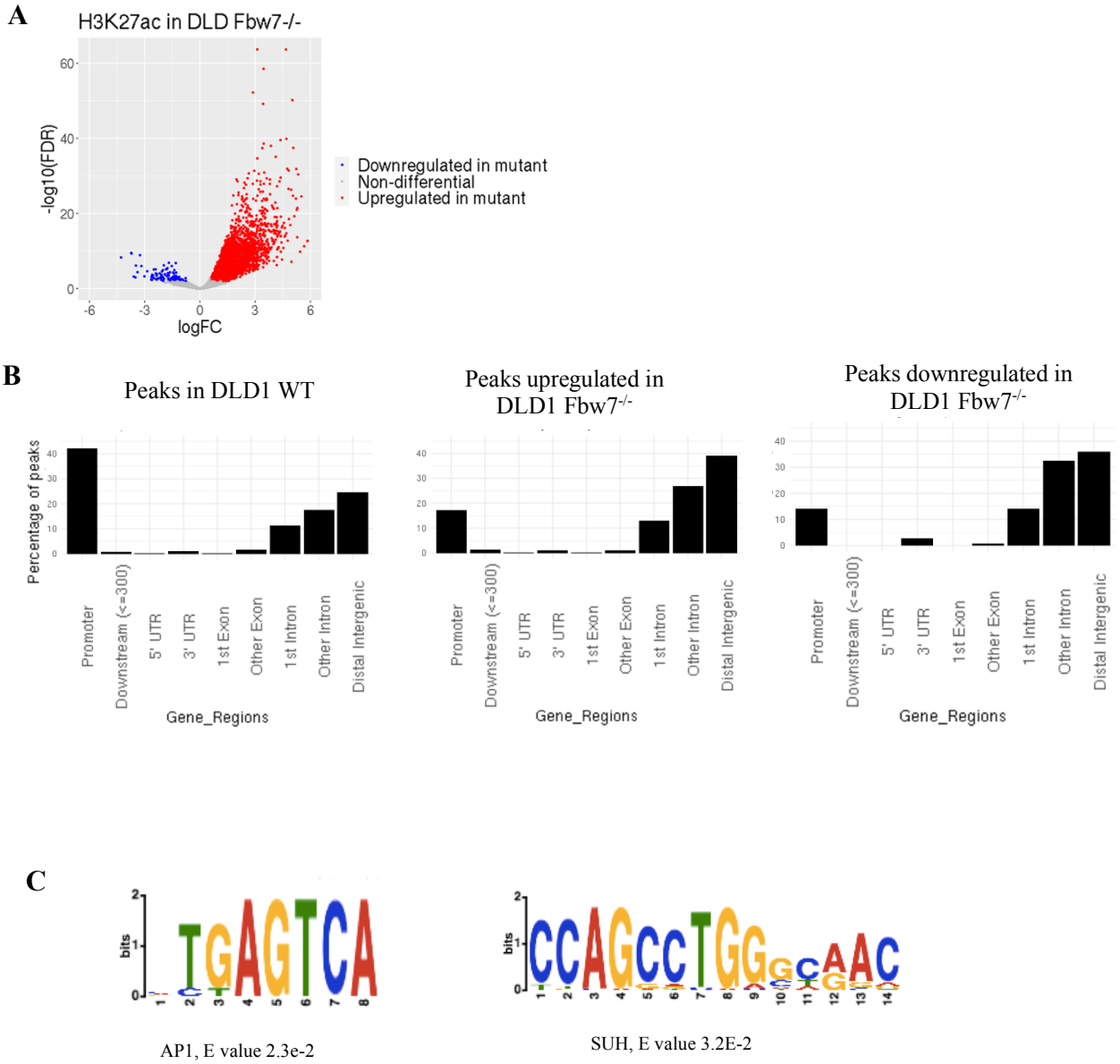

Figure 4.2 Differential H3K27ac signal in DLD1 Fbw7 mutant cells reveals specific genomic sites targeted by Fbw7

(A) Volcano plot showing upregulated (red) and downregulated (blue) H3K27ac sites in DLD Fbw7$^{-/-}$ cells compared to WT (B) Percentage of peaks located within each gene region **(C)** Sequence logo for AP1 and SUH/RBPJ motifs enriched in H3K27ac peaks upregulated in Fbw7$^{-/-}$ cells.

4.2.3 Fbw7 regulates TFs at specific genomic sites

Similar to Hct116 cells, the steady state level of Jun did not change in DLD1 Fbw7$^{-/-}$ cells; however, in contrast, the Myc steady state level was increased (**Figure 4.3A**). We leveraged this scenario to determine how informative a genomic level study on Fbw7 substrates would be as opposed to drawing conclusions based on total cellular protein levels. We mapped the genomic occupancy of Jun and Myc using AutoCUT&RUN (Automated CUT&RUN run BioMek) and validated the data by performing a motif discovery search. As expected, the AP-1 motif was enriched in Jun CUT&RUN data from DLD1 WT peaks (**Figure 4.3B**). In addition to the E-box motif, the AP-1 motif was also enriched in Myc CUT&RUN peaks, suggesting that Jun might be co-occupying with Myc (**Figure 4.3B**). Jun and Myc signals were enriched on genomics sites where H3K27ac was upregulated in Fbw7$^{-/-}$ DLD1 cells (**Figure 4.3C**). Jun and Myc levels correlated with the increasing trend of H3K27ac from WT to Fbw7$^{-/-}$ cells.

Similar to our findings in Hct116 cells, a small fraction of Jun sites was differentially regulated in DLD1 Fbw7$^{-/-}$ cells (**Figure 4.3D**). Approximately 14% of Jun sites were upregulated while 5% of sites were downregulated in Fbw7$^{-/-}$ cells. The deregulated fraction of Jun sites in DLD1 Fbw7$^{-/-}$ cells was higher than in Hct116 cells; however, the total number of Jun binding sites was also higher in DLD1 cells.

In contrast to Hct116 cells, approximately 50% of Myc peaks were upregulated in DLD1 Fbw7$^{-/-}$ cells (**Figure 4.3D**). This result recapitulates the bulk increase of Myc detected by western blot. To our surprise, a small fraction (1.3%) of Myc sites were downregulated in Fbw7$^{-/-}$ cells while almost half of Myc sites were non-differential. This suggests that, although a cellular level accumulation of the substrate was detected, a more fine-tuned regulation is carried out by Fbw7 at specific genomic sites.

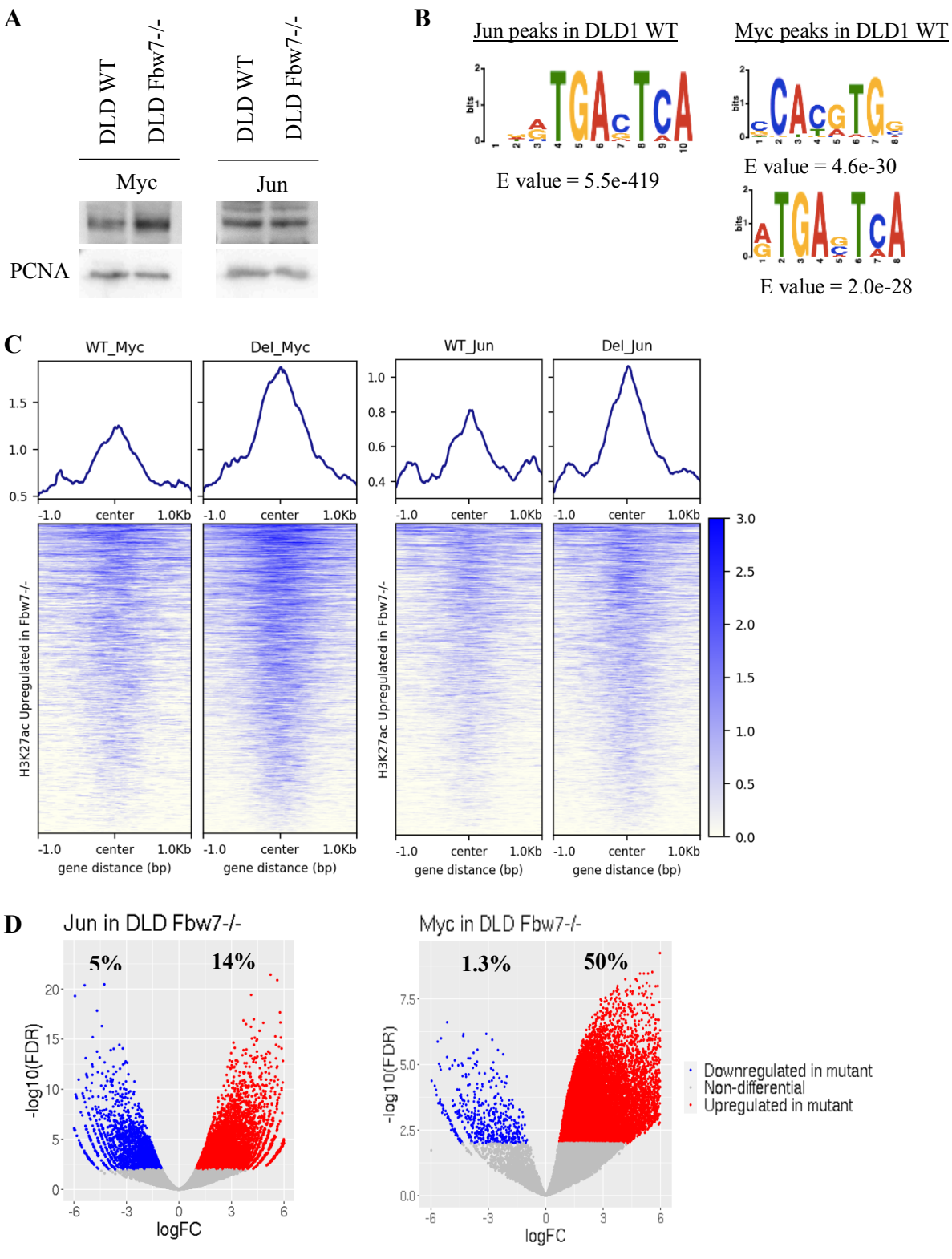
A
DLD WT
DLD Fbw7-/-
DLD WT
DLD Fbw7-/-
Myc
Jun
PCNA
B
Jun peaks in DLD1 WT
E value = 5.5e-419
Myc peaks in DLD1 WT
E value = 4.6e-30
E value = 2.0e-28
C
WT_Myc
Del_Myc
WT_Jun
Del_Jun
H3K27ac Upregulated in Fbw7-/-
-1.0
center
1.0Kb
gene distance (bp)
D
Jun in DLD Fbw7-/-
5%
14%
Myc in DLD Fbw7-/-
1.3%
50%
-log10(FDR)
logFC
Downregulated in mutant
Non-differential
Upregulated in mutant

Figure 4.3 Fbw7 regulates Jun and Myc at specific genomic sites in DLD1 cells

(A) Western blot showing total Myc and Jun protein levels in DLD1 WT and Fbw7$^{-/-}$ cells. (B) Sequence logo for AP1 and E-box motifs enriched in Jun and Myc peaks, respectively, in control cells. (C) Heatmaps showing Myc and Jun CUT&RUN signal mapped on a 2kb window of H3K27ac upregulated sites in DLD1 Fbw7$^{-/-}$ cells (D) Volcano plots showing upregulated (red and downregulated (blue) sites in DLD1 Fbw7$^{-/-}$ cells compared to WT cells.

4.2.4 Similar characteristics of transcriptional regulation by Fbw7 across multiple cell types

Similar to our findings in Hct116 and U5-NSCs, Jun differential sites were mostly within introns and intergenic regions; however, the shift may not seem very obvious since Jun is bound to distal regulatory elements in control cells to begin with (**Figure 4.4A**). The majority of Myc peaks in control cells were promoter proximal. Although the small fraction of Myc differential sites were mostly within intragenic and intergenic regions in Hct116 Fbw7$^{-/-}$ cells, Myc-upregulated sites in DLD1 Fbw7$^{-/-}$ cells were equally distributed between promoter proximal and distal regions. However, downregulated Myc sites in DLD1 Fbw7$^{-/-}$ cells were mostly within introns and intergenic regions. Differential sites were annotated to genes using proximity-based criteria (same as explained in Chapter 3 Figure 3.3F). Myc occupancy at ~22% of genes with increased promoter proximal Myc and at ~28% of genes with decreased promoter proximal Myc in Fbw7$^{-/-}$ DLD1 cells, correlated with the transcription of differentially expressed genes in Fbw7$^{-/-}$ DLD1 cells (differentially expressed genes logFC$\pm$1.0 and FDR < 0.05) (**Figure 4.4B**). Given the large number of promoter proximal Myc upregulated sites, it was surprising that the number of genes that correlated with transcription was modest. It could be because differential Myc occupancy may not always lead to changes in transcription, or because the magnitude of differential expression may be so small that it is filtered out by statistical parameters.

Approximately 25% of Myc and Jun peaks overlapped with each other in DLD1 WT cells (**Figure 4.4C**). Therefore, we examined how they might be coregulated by Fbw7 at shared sites. We identified 1663 sites in which both Jun and Myc occupancy was upregulated in Fbw7$^{-/-}$ cells and 157 sites where both TFs were downregulated (**Figure 4.4D**). Interestingly, similar to what we observed in Hct116 cells, Jun and Myc were coordinately regulated by Fbw7. Either both TFs were upregulated or both were downregulated, with the exception of a negligible overlap between

Myc upregulated and Jun downregulated sites (out of all Myc upregulated sites, 8% of sites overlapped with Jun upregulated sites while only 0.001% of Myc upregulated sites overlapped with Jun downregulated sites).

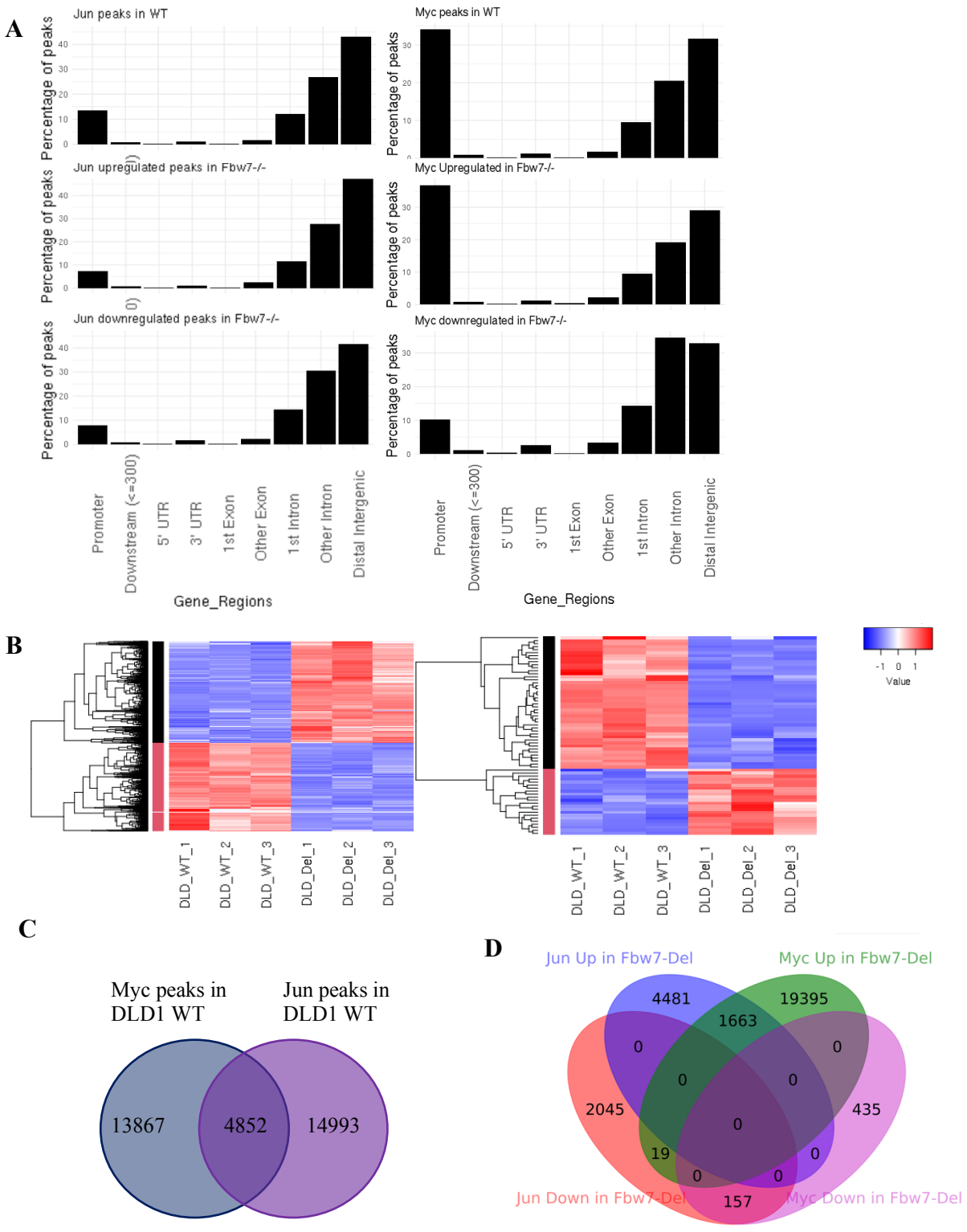
A
Jun peaks in WT
Myc peaks in WT
Jun upregulated peaks in Fbw7-/-
Myc Upregulated in Fbw7-/-
Jun downregulated peaks in Fbw7-/-
Myc downregulated in Fbw7-/-
Percentage of peaks
Promoter
Downstream (<=300)
5' UTR
3' UTR
1st Exon
Other Exon
1st Intron
Other Intron
Distal Intergenic
Gene_Regions
B
Value
DLD_WT_1
DLD_WT_2
DLD_WT_3
DLD_Del_1
DLD_Del_2
DLD_Del_3
C
Myc peaks in DLD1 WT
Jun peaks in DLD1 WT
13867
4852
14993
D
Jun Up in Fbw7-Del
Myc Up in Fbw7-Del
Jun Down in Fbw7-Del
Myc Down in Fbw7-Del
4481
19395
1663
0
2045
435
19
157

Figure 4.4 Fbw7 preferentially targets distal regulatory elements and coordinately regulates multiple substrates

(A) Percentage of peaks within each gene region. (B) Heatmap showing the change in transcription of genes with promoter proximal upregulated Myc (left) and downregulated Myc (right) (DL_WT = wildtype, DLD_Del = DLD1 Fbw7$^{-/-}$) (C) Overlap between Myc and Jun peaks in DLD1 WT cells. (D) Venn diagram showing the overlap between Jun upregulated and downregulated sites, and Myc upregulated and downregulated sites in DLD1 Fbw7$^{-/-}$ (Fbw7-Del) cells.

4.2.5 Fbw7 targets genes and genomic regions in a cell-specific manner

Hct116 and DLD1 are colorectal carcinoma cell lines. We hypothesized that Fbw7 mutations may impose similar deregulatory effects on transcription because they are from the same tissue and the same cancer type. We compared transcriptionally up- and downregulated genes in each cell line (**Figure 4.5A**). Approximately 13% of protein coding genes were deregulated in both Hct116 and DLD1 Fbw7$^{-/-}$ cells (significantly differential protein coding genes: 194/1490 in DLD1, 194/1470 in Hct116). Hierarchical clustering of differentially expressed protein coding genes in either cell type reveals that clusters 1 and 7 are downregulated and cluster 5 is upregulated in both Fbw7$^{-/-}$ cell types, whereas genes in other clusters are up- or down regulated in only one cell type (**Figure 4.5A**). Protein coding genes that are differentially expressed in both Hct116 and DLD1 cells were then hierarchically clustered separately (**Figure 4.5B**). Although the fold change of expression from WT to mutant cell differs between the two cell lines (note the heatmap color intensity), genes are concordantly regulated by Fbw7, i.e. either up- or downregulated in both cell types.

Next, we compared differential Jun and Myc occupancy in Hct116 and DLD1 Fbw7$^{-/-}$ cells. As the Venn diagrams depict, there was poor overlap between the two cell types for upregulated and downregulated TF sites (**Figure 4.5 C-F**). Taken together these observations demonstrate that there is cell-specific transcriptional regulation by Fbw7 even within the same tissue type.

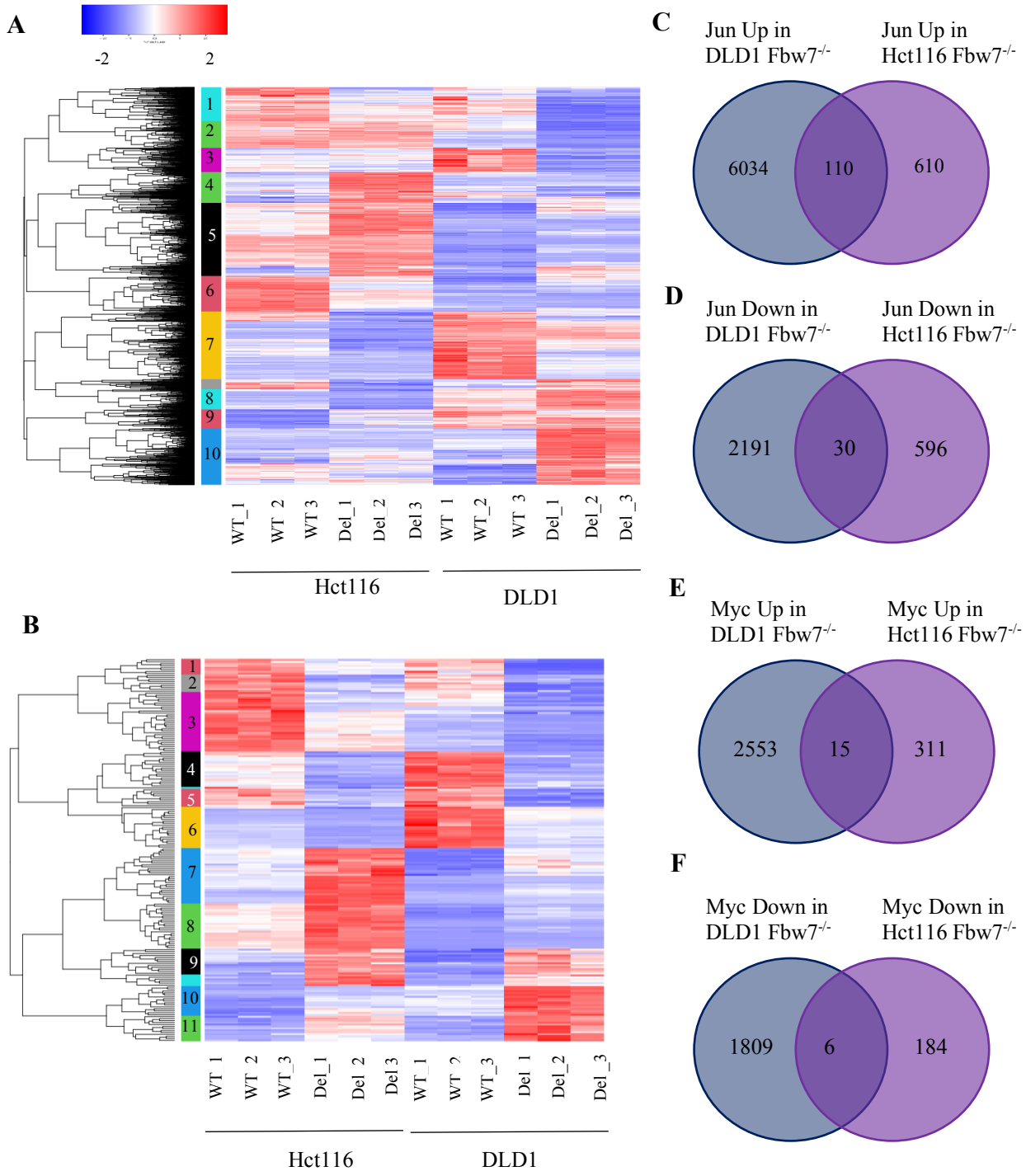
A
-2
2
1
2
3
4
5
6
7
8
9
10
WT_1
WT_2
WT_3
Del_1
Del_2
Del_3
WT_1
WT_2
WT_3
Del_1
Del_2
Del_3
Hct116
DLD1
B
1
2
3
4
5
6
7
8
9
10
11
WT_1
WT_2
WT_3
Del_1
Del_2
Del_3
WT_1
WT_2
WT_3
Del_1
Del_2
Del_3
Hct116
DLD1
C
Jun Up in DLD1 Fbw7-/-
Jun Up in Hct116 Fbw7-/-
6034
110
610
D
Jun Down in DLD1 Fbw7-/-
Jun Down in Hct116 Fbw7-/-
2191
30
596
E
Myc Up in DLD1 Fbw7-/-
Myc Up in Hct116 Fbw7-/-
2553
15
311
F
Myc Down in DLD1 Fbw7-/-
Myc Down in Hct116 Fbw7-/-
1809
6
184

Figure 4.5 Comparing Fbw7 transcriptional regulation in Hct116 and DLD1 cells

(A) Hierarchical clustering of protein coding genes differentially expressed in either Hct116 or DLD1 cells. (WT = wild-type, Del = Fbw7$^{-/-}$) (B) Hierarchical clustering of protein coding genes differentially expressed in both Hct116 and DLD1 cells. (C–F) Venn diagrams showing the overlap between Jun and Myc up- and downregulated peaks in Hct116 and DLD1 cells.

4.3 **Discussion**

Analysis across multiple cell types highlighted several aspects of transcriptional regulation by Fbw7 that were universal irrespective of the cell-type and mutation-type. First, Fbw7 regulates TFs at specific genomic sites. The signaling pathways that phosphorylate the degrons in substrates are likely a determinant of Fbw7 specificity. This body of work also revealed that Fbw7 preferentially targets genomic regions within introns and intergenic regions that are likely distal regulatory elements. Moreover, Fbw7 coordinately coregulates multiple TFs.

This study revealed that the genes and genomic regions targeted by Fbw7 were highly cell-specific. Different genes were targeted between different cell types of the same tissue and cancer type (Hct116 and DLD1 colon cancer cell lines). It is important to note the genetic background of the two cell types. Although they both are colon carcinoma cell lines, Myc is amplified in Hct116 cells and has a $KRAS^{+/-}$ mutation, while DLD1 cells are diploid for Myc. The background genetic composition influences the signaling pathways that phosphorylate substrate CPDs, which determine their recognition by Fbw7. While it is interesting to explore how Fbw7 regulation differs in various malignant cell types, to tease apart and understand the mechanism of tumorigenesis we suggest that further studies be performed on non-transformed cell lines with Fbw7 mutations incorporated.

We performed motif discovery analysis on H3K27ac differential genomic sites to identify Fbw7 substrates that are potentially bound and targeted by Fbw7 at these sites. AP-1 and SUH/RBPJ motifs were enriched. Interestingly, despite a large increase of Myc in $Fbw7^{-/-}$ cells, the E-box motif was not enriched in H3K27ac differential sites. When we mapped Myc using CUT&RUN in multiple cell lines, we observed that Myc signal was often enriched adjacent to an E-box motif instead of exactly overlapping the motif. Thus, we believe that the E-box motif was

not discovered in H3K27ac differential sites because the sequence scanned by MEME-ChIP was limited to the center 100 bp. FIMO analysis was performed to search for the canonical E-box motif (CACGTG) through the entire sequence of each peak, and 22% of peaks were enriched with the E-box motif (p value =< 0.0002). Moreover, it has been known that Myc binds to non-canonical E-boxes in addition to canonical E-boxes, as well as to sites where neither are present (Guo et al., 2014; Zeller et al., 2006).

Summary: Regardless of the cell type, Fbw7 regulates TFs in a genomic site-specific manner and preferentially targets distal regulatory elements. Fbw7 also coordinately co-regulates multiple substrates. However, Fbw7 targets specific genes and genomic sites in a cell-specific manner. Presumably the genetic background of each cell type is an indirect determinant of cell-specific substrate regulation because it controls the signaling pathways that phosphorylates Fbw7 substrates thus.

Chapter 5. Characterizing Chromatin Association of Fbw7

5.1 Introduction

Studies show that ectopic Fbw7 degrades its TF substrates such as SREBP and Notch while they are bound to their target genes (Fryer et al., 2004; Punga et al., 2006). Moreover, co-recruitment of ectopic Fbw7 and vitamin D receptor to Myc target genes has been shown using ChIP-qPCR (Salehi-Tabar et al., 2019). However, endogenous Fbw7 chromatin association has not been studied. The Clurman lab began to investigate the chromatin association of endogenous Fbw7 by immunoprecipitating Fbw7 from soluble and insoluble chromatin fractions of cellular lysates from different cell types (unpublished data by B. Clurman and J. Swanger). We found that WT-Fbw7 resides almost exclusively within the chromatin fraction, while $Fbw7^{Arg/Arg}$ was predominantly in the soluble fraction. Substrates interact with the arginine residues of the Fbw7 WD40 domain; therefore in $Fbw7^{Arg/Arg}$ mutant cells, substrates can no longer interact with Fbw7. In addition to recapitulating this data, I showed that more Fbw7 moves to the chromatin fraction when the proteasome complex is inhibited (**Figure 3.3A, Figure 5.1A**). Altogether, this data suggest that Fbw7 is associated with chromatin via its substrates.

The specific chromosomal contexts in which Fbw7 targets its TF substrates are not known and we believe that this information will provide useful insights into how Fbw7 regulates global transcription and drives tumorigenesis. We were interested in finding whether Fbw7 is preferentially occupied at specific genomic regions such as super-enhancers. Therefore, using highly sensitive protein mapping techniques we attempted to map the genomic occupancy of Fbw7. Despite many attempts using various reagents and techniques, we were unable to successfully map Fbw7 genomic occupancy. However, this chapter includes various adaptations that we tested and suggestions for future experiments.

5.2 **Results**

5.2.1 Fbw7 forms a stable interaction with a small portion of Myc

Stable interactions between Fbw7 and its substrates are hard to capture unless Fbw7 binding is uncoupled from substrate turnover. Therefore, we hypothesized that Fbw7 associates with chromatin by binding to pseudo-substrates. Ebp2 and SV40 Large T antigen are examples of pseudo-substrates that have been identified so far, that bind to Fbw7 but don't get degraded (Welcker et al., 2011; Welcker & Clurman, 2005).

Myc is a well-known canonical Fbw7 substrate (Welcker et al., 2004; Yada et al., 2004). Strikingly, Fbw7 co-immunoprecipitated with Myc in the absence of proteasome inhibition, which indicates that Myc forms a stable interaction with Fbw7 (**Figure 5.1B**). Therefore, we hypothesized that Fbw7 is recruited to chromatin via Myc. However, chromatin association of Fbw7 did not change upon the loss of Myc, indicating that Myc is not crucial in recruiting Fbw7 to chromatin (**Figure 5.1B-C)**. Fbw7 did not co-immunoprecipitate with Myc in Fbw7 dimer mutant (ΔD) cells, suggesting that the interaction between Fbw7 and Myc is dimer-dependent (**Figure 5.1D**). Even after immunoprecipitating almost all of Myc from cell lysates, the amount of stably bound Fbw7 did not increase. The majority of Fbw7 was still left in the lysate, suggesting that only a small fraction of Fbw7 stably interacts with Myc (**Figure 5.1E**).

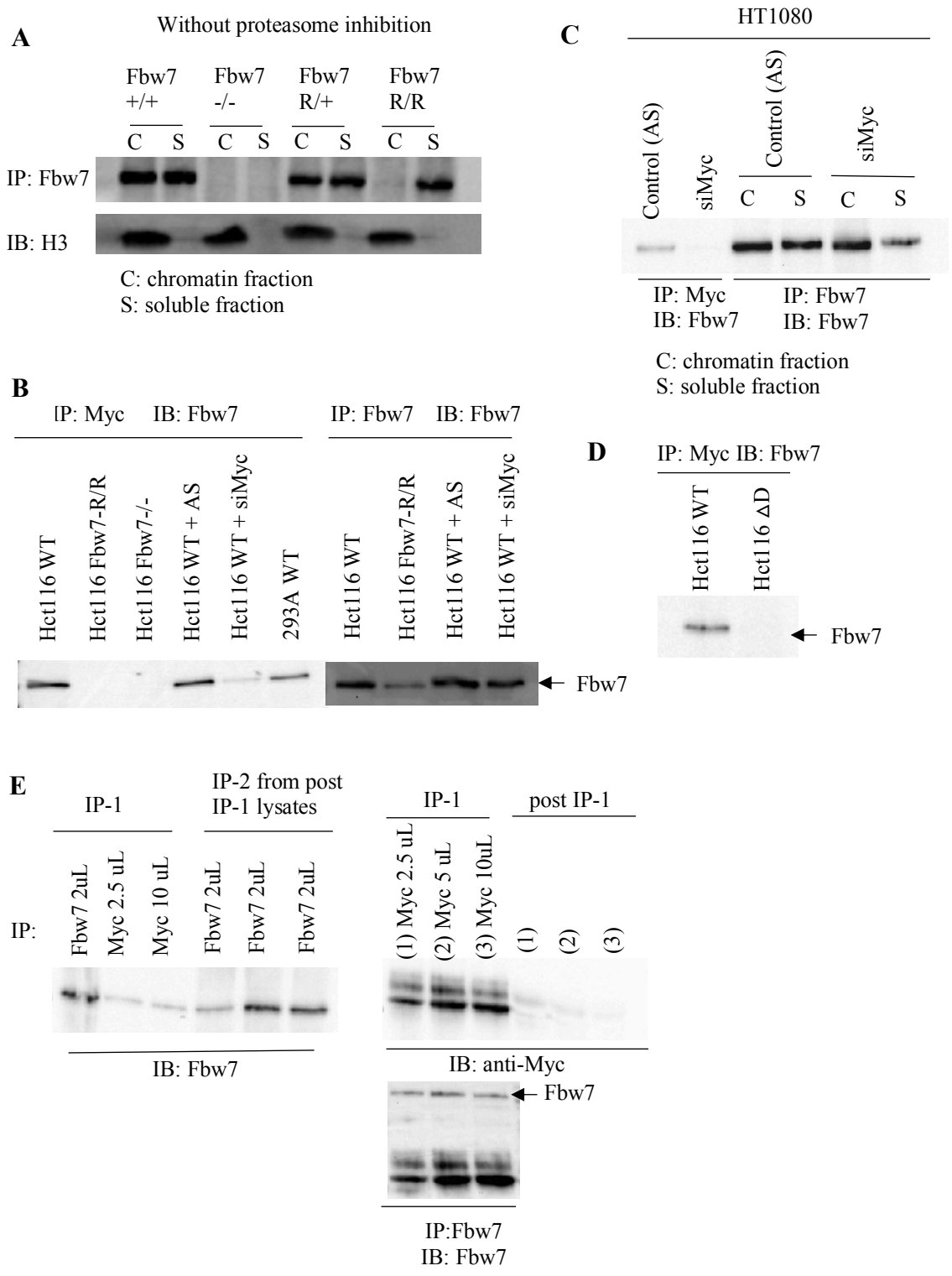
A
Without proteasome inhibition
Fbw7 +/+
Fbw7 -/-
Fbw7 R/+
Fbw7 R/R
C S C S C S C S
IP: Fbw7
IB: H3
C: chromatin fraction
S: soluble fraction
C
HT1080
Control (AS)
siMyc
Control (AS)
siMyc
C S C S
IP: Myc
IB: Fbw7
IP: Fbw7
IB: Fbw7
C: chromatin fraction
S: soluble fraction
B
IP: Myc IB: Fbw7
IP: Fbw7 IB: Fbw7
Hct116 WT
Hct116 Fbw7-R/R
Hct116 Fbw7-/-
Hct116 WT + AS
Hct116 WT + siMyc
293A WT
Hct116 WT
Hct116 Fbw7-R/R
Hct116 WT + AS
Hct116 WT + siMyc
Fbw7
D
IP: Myc IB: Fbw7
Hct116 WT
Hct116 ΔD
Fbw7
E
IP-1
IP-2 from post IP-1 lysates
IP:
Fbw7 2uL
Myc 2.5 uL
Myc 10 uL
Fbw7 2uL
Fbw7 2uL
Fbw7 2uL
IB: Fbw7
IP-1
post IP-1
(1) Myc 2.5 uL
(2) Myc 5 uL
(3) Myc 10uL
(1)
(2)
(3)
IB: anti-Myc
Fbw7
IP:Fbw7
IB: Fbw7

Figure 5.1 Stable interaction between Myc and Fbw7 in the absence of proteasome inhibition.

(A) Fbw7 in chromatin (C) and soluble (S) fractions of Hct116 WT, $Fbw7^{-/-}$, $Fbw7^{R/+}$ and $Fbw7^{R/R}$ cell lysates. Histone H3 was blotted as a control for fractionation. (B) Fbw7 co-immunoprecipitated with Myc in Hct116 and 293A WT cells, but not in Hct116 $Fbw7^{R/R}$ cells. Hct116 WT cells were treated with either siRNA against Myc or AllStars Negative Control siRNA (AS), and lysates thereof were immunoprecipitated for Myc and blotted for Fbw7 as shown in the first blot. Fbw7 levels in Hct116 WT, R/R, AS and siMyc cells are shown in the second blot. (C) Fbw7 was co-immunoprecipitated with Myc in HT1080 cells. Fbw7 in chromatin and soluble cellular fractions of HT1080 cells treated with AllStars Negative siRNA control or siRNA against Myc (D) Co-immunoprecipitation of Fbw7 and Myc in Hct116 WT and Fbw7 dimer mutant cells. (E) Qualitative comparison of the amount of Fbw7 immunoprecipitated with anti-Fbw7 and anti-Myc antibodies (IP-1) and the amount of Fbw7 left in the post-IP-1 lysate (IP-2). Comparison of the amount of Myc immunoprecipitated by different quantities of anti-Myc antibody from the same IP-1 lysates. This same blot was probed using anti-Fbw7 to compare the amount of Fbw7 co-immunoprecipitated with Myc. Post-IP-1 lysates were probed with anti-Myc to determine the amount of Myc left in post-IP-1 lysates.

5.2.2 Characterizing Fbw7 genomic occupancy

First, we used anti-Fbw7 antibodies to map Fbw7 in Hct116 WT cells. Hct116 Fbw7$^{-/-}$ cells were used as a negative control. We were unsuccessful at mapping Fbw7, however our choices were limited since ChIP-grade Fbw7 antibodies were not available. The low abundance of Fbw7 protein in cells was another challenge we had to deal with. Thus, we attempted to map ectopically expressed Flag-Fbw7 using anti-Flag antibodies, using non-transfected cells as the negative control. Flag-Fbw7 transfected cells exhibited genome-wide enrichment of sequencing reads, which seemed like background noise. Next, we used cells with endogenously Flag-tagged Fbw7. Despite the availability of good quality anti-Flag antibodies, we failed to map Fbw7, likely because these cells contained only one allele tagged with 1X Flag sequence which further diminished the mappable pool of Fbw7. Finally, we genetically engineered Hct116 WT cells and incorporated a 3X-Flag tag to both endogenous Fbw7 alleles (Hct116 $^{\text{Flag-Fbw7/Flag-Fbw7}}$). Our attempts to map Flag-Fbw7 using three different anti-Flag antibodies failed. The Cleavage Under Target and Release Using Nuclease (CUT&RUN) protein mapping technique was used to map Fbw7, and over the years various modifications to the protocol were tested, as explained in Table 5.1 and in Chapter 2 (Janssens et al., 2018; Skene et al., 2018; Skene & Henikoff, 2017).

Table 5.1 Techniques and reagents used to map the genomic occupancy of Fbw7: modifications to the CUT&RUN protocol, antibodies and cell types.

Trial	Cell type	Protocol	Modifications	Antibody
01	Hct116 WT Hct116 Fbw7$^{-/-}$	CUT and RUN (*nuclei)	- nuclei generated - extracted DNA from nuclei instead of supernatant	Bethyl A301-721A
02	Hct116 Flag-Fbw7$^{R/+}$ Hct116 Fbw7$^{-/-}$	CUT and RUN	- crosslinked cells	Anti-Flag Sigma Flag M2 F3165 and Anti-mouse Rb Secondary Ab Abcam ab46540 Anti-Fbw7; Bethyl A301-721A Anti-Flag; Cell Signaling 147935 Rb
03	Hct116 Flag-Fbw7$^{R/+}$ Hct116 Fbw7$^{-/-}$	CUT and RUN (*nuclei)		Sigma Flag M2 F3165 and Secondary Ab Abcam ab46540
04	293A cells with and without Flag-Fbw7 transfected	CUT and RUN	- crosslinked cells	Anti-Flag Sigma Flag M2 F3165 and Anti-mouse Rb Secondary Ab Abcam ab46540
05	Hct116 Flag-Fbw7$^{R/+}$ Hct116 Fbw7$^{-/-}$	CUT and RUN (*Digitonin)	- cells permeabilized with Digitonin	
06	Hct116 WT Hct116 Fbw7$^{-/-}$ Hct116 Fbw7$^{-/-}$ (generated by R. Davis)	CUT and RUN (*Direct Ligation)		Anti-Fbw7: Bethyl A301-720
07	Hct116 Flag-HA-Fbw7 Hct116 Fbw7-/-	CUT and RUN (*Direct Ligation)		Anti-Flag Sigma Flag M2 F1804 and Anti-mouse Rb Secondary Ab Abcam ab46540

				Anti-Fbw7: Bethyl A301-720
08	Hct116 Flag-Fbw7/+ Hct116 Fbw7-/-	CUT and RUN (*Automated)	- cells treated with and without Velcade	Anti-Flag Sigma Flag M2 F3165 and Anti-mouse Rb Secondary Ab Abcam ab46540 Anti-Flag Sigma Rb F7425
09	Hct116 Flag-Fbw7 (homozygous knockin) Hct116 WT	CUT and RUN (*Automated)	- cells treated with and without Velcade - different cell counts per sample were tested (1 million cells and 0.1 million cells per sample)	Anti-Flag Sigma Flag M2 F3165 and Anti-mouse Rb Secondary Ab Abcam ab46540 Anti-Flag Sigma Rb
10	Hct116 Flag-Fbw7 (homozygous knockin) Hct116 WT	CUT and RUN (*Automated)	- cells treated with and without Velcade - different cell counts per sample were tested (1 million cells and 0.1 million cells per sample)	Anti-Flag Sigma Flag M2 F1804 and Anti-mouse Rb Secondary Ab Abcam ab46540

** An IgG control and secondary antibody only control were also tested as negative controls

5.3 **Discussion**

This study revealed a stable interaction between Myc and Fbw7. Myc is a well-known Fbw7 substrate, and stably bound Myc-Fbw7 had not thus far been detected unless binding was uncoupled from turnover. I was able to detect Fbw7 co-immunoprecipitated with Myc in multiple cell types in the absence of proteasome inhibition. It was very difficult to detect Myc co-immunoprecipitating with Fbw7 (reciprocal immunoprecipitation), which is not surprising because Fbw7 binds to a large number of proteins and only a small fraction of Fbw7 might interact with Myc. Further investigations showed that only a small fraction of Myc is stably bound to Fbw7 and that it is not a critical part of Fbw7-chromatin association.

I attempted to map the exact genomic regions Fbw7 is associated with using a series of different techniques and reagents. Since specific and high quality Fbw7 antibodies were not available, we generated cells with endogenous Fbw7 tagged with Flag sequence. Different Flag antibodies were also tested to map Flag-Fbw7. The reason for failure could be twofold. First, a technical failure could be responsible. However, CUT&RUN has been widely used to map many proteins that directly and indirectly bind to DNA, as well as proteins in large complexes. Therefore it is hard to explain why Fbw7 occupancy was unmappable even if it was indirectly bound as part of a large protein complex. Secondly, it could be because Fbw7 is loosely associated with chromatin and it is accordingly difficult to capture a snapshot of its occupancy. Since CUT&RUN uses native cells and includes multiple washing steps to remove non-specific binding, it is possible that Fbw7 is easily removed from DNA. Kinetic studies have used measurements with millisecond time resolution to demonstrate substrate ubiquitylation after binding to SCF^{Fbw7}, which indicates that the interaction between Fbw7 and substrate is short-lived (Pierce et al., 2009). The alternative approach that we propose is to use crosslinked MNase ChIP-Seq that would presumably retain the

Fbw7-substrate interaction. The low abundance of cellular Fbw7 has been another challenge in our studies. Other Clurman lab members have tried to map the intracellular localization of Fbw7 using immunohistochemistry techniques, however have not been successful. The same anti-Flag and anti-Fbw7 antibodies mentioned above have been tested. Flow cytometry has also been exploited however unsuccessful at identified Fbw7. Mapping ectopic Flag-Fbw7 expressed at near physiologic levels might be also worth considering, using crosslinked ChIP-Seq. It is possible that Fbw7-substrate interactions are extremely short-lived and difficult to capture with currently available mapping techniques. However, if successful, we believe that knowledge of the exact genomic regions targeted by Fbw7 will be highly beneficial in understanding its biology and role in disease development.

CENP-A, an essential histone H3 variant specifically found at centromeres, is phosphorylated by Cyclin E / CDK2. A recent study showed that loss of Fbw7 causes hyperphosphorylation of CENP-A by increased Cyclin E/ CDK2 activity, and that hyperphosphorylated CENP-A loses its centromeric location and leads to chromosome instability (CIN) (Grim et al., 2012; Takada et al., 2017). It has also been shown that CENP-A is overexpressed in several colorectal cancer cell lines and accumulates at transcription factor binding sites that are noncentromeric locations (Athwal et al., 2015). If Fbw7 localizes to centromeric regions to regulate Cyclin E occupancy, it is possible that we could not map the DNA occupancy of Fbw7 because centromeric alpha-satellites get removed when repeat-masked libraries were used with regular CUT&RUN. Alternatively, the recent developments by the Henikoff lab to map CENP-A and CENP-B might be beneficial in testing this hypothesis.

Summary: We attempted to map the genomic occupancy of Fbw7 using anti-Fbw7 antibodies as well as anti-Flag antibodies that targeted endogenous Flag-Fbw7 using CUT&RUN, however we couldn't achieve our goal. Alternatively, we propose crosslinked MNase ChIP-Seq method to map Flag-Fbw7 using anti-Flag antibodies.

Chapter 6. Role of Fbw7 in Neural Stem Cell Maintenance - Insights from Single-Cell RNA-Seq

Fbw7 mutant U5 neural stem cells were generated in collaboration with Dr. Paddison's laboratory. Single cell RNA library preparation was done in collaboration with Dr. Bielas's laboratory and sequenced by Genomics Center at Fred Hutch. scRNA-Seq data were analyzed by Dr. Sonali Aurora.

6.1 Introduction

Neural stem cells (NSCs) give rise to differentiated cell types such as neurons, astrocytes and oligodendrocytes in the nervous system. Maintenance of NSCs is essential to produce the right type of cells in the right amounts for normal brain development. Dysregulation of stem cell maintenance leads to several disorders, including cancer.

Fbw7 is known to play a role in stem cell maintenance and differentiation. While the majority of studies on Fbw7 in stem cell biology are done in hematopoietic and embryonic stem cells (HSCs and ESCs), some studies show that Fbw7 plays an important role in NSCs (Matsumoto et al., 2011; Matsuoka et al., 2008; Takeishi & Nakayama, 2014; Z. Wang et al., 2012). In the mouse brain, loss of Fbw7 causes impaired stem cell differentiation and increased progenitor cell death (Hoeck et al., 2010). In mice, the Fbw7 substrates Jun and Notch regulate NSC viability and neural differentiation, respectively. Interestingly, loss of Fbw7 function has been observed in gliomas, a type of tumor that occurs in the brain and spinal cord (Mackay et al., 2017). The expression of Fbw7 in gliomas is correlated with survival and considered a favorable prognostic marker (Hagedorn et al., 2007).

A balance between quiescent and proliferative stem cells is important to maintain tissue homeostasis. Cyclin-dependent kinases (CDKs) are crucial mediators of the cell cycle and it is known that buildup of CDK2 activity in M phase from an intermediate level commits cells to enter the next cell cycle, whereas cells that lack CDK2 activity enter a transient G0 quiescent state

(Spencer et al., 2013). Interestingly, O'Connor *et al*. recently identified a "Neural G0" state in U5-NSCs (O'Connor et al., 2021). Loss of Fbw7 impairs Cyclin E degradation and consequently upregulates Cyclin E – CDK2 activity. Therefore we hypothesize that increased Cyclin E-CDK2 levels causes stem cells to skip the G0 quiescent state and continue to proliferate. Single-cell RNA-Seq (scRNA-Seq) analysis on WT and Fbw7$^{-/-}$ U5-NSCs revealed that indeed much fewer Fbw7$^{-/-}$ stem cells entered the G0 phase than did WT cells. This "G0 skip" phenotype has been previously observed in mouse Fbw7$^{-/-}$ HSCs, however it has been thought to be regulated by accumulated Myc (Reavie et al., 2010; Thompson et al., 2008). We will continue to investigate cell cycle regulation in NSCs to determine if Cyclin E – CDK2 plays a role in NSC maintenance.

6.2 **Results**

6.2.1 scRNA-Seq analysis identified different cell clusters in WT and Fbw7$^{-/-}$ U5-NSCs

Unsupervised clustering of all scRNA-Seq data identified outlying clusters based on the following quality control criteria: nFeature_RNA (the number of genes detected in each cells) (>2000), nCount_RNA (the total number of molecules detected within a cell) (5000-50,000), percent of ribosomal genes (<0.4), and percent of mitochondrial genes (<0.4) (**Figure 6.1A-B**). Cluster 6 had very low numbers for nCount and nFeature RNA with a high percentage of mitochondrial and ribosomal genes; thus it was identified as an outlying cluster and was removed. Quality controlled data was re-analyzed and a total of 7 clusters were identified (**Figure 6.1C-D**). Next the cells were separated by sample condition, WT vs. Fbw7$^{-/-}$ NSCs (**Figure 6.1E**). UMAP (Uniform Manifold Approximation and Projection) plot reveals that clusters 0 and 2 are unique to WT cells while cluster 1 is unique to Fbw7$^{-/-}$ cells.

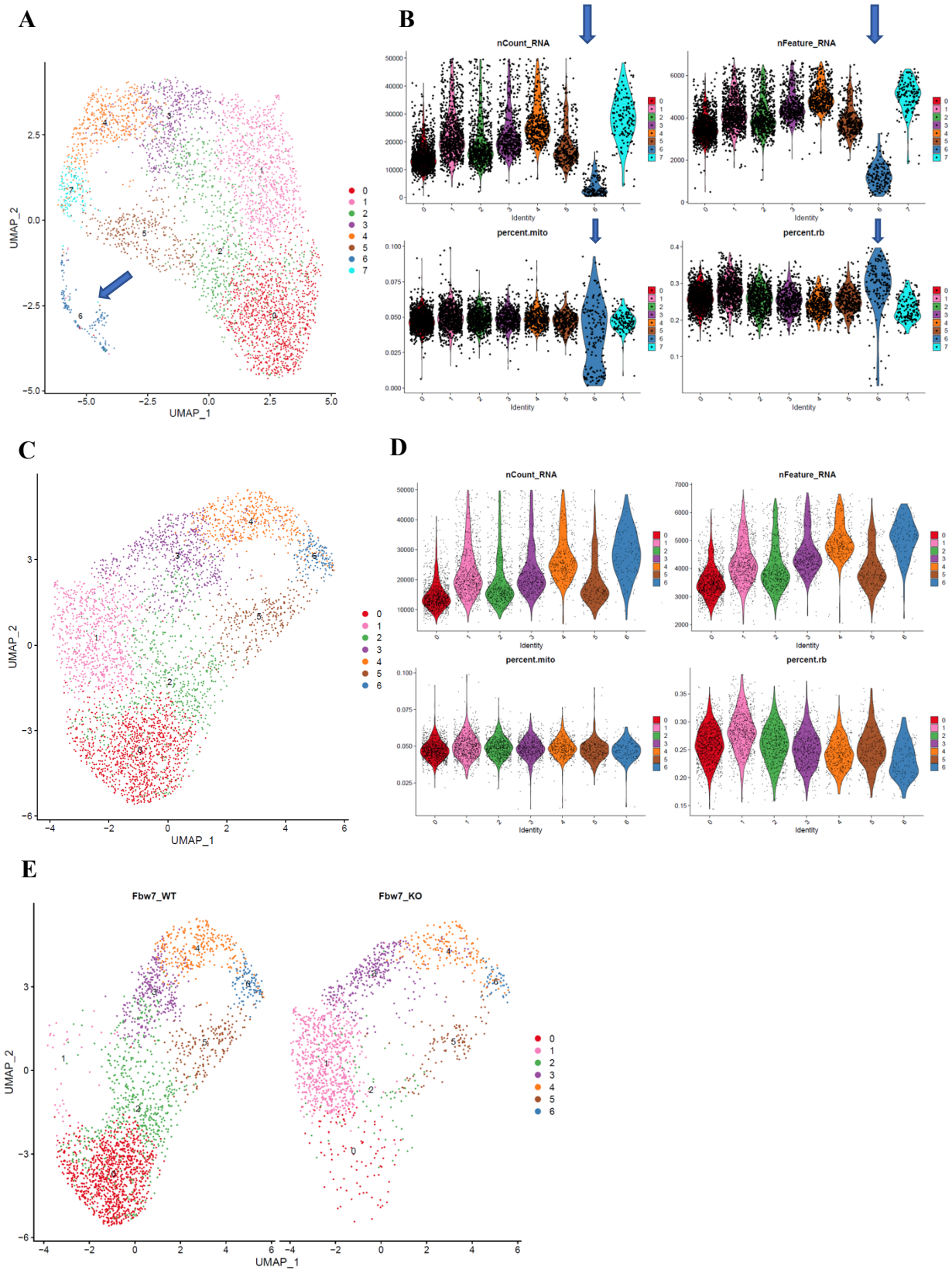
A
B
C
D
E
UMAP_1
UMAP_2
nCount_RNA
nFeature_RNA
percent.mito
percent.rb
Identity
Fbw7_WT
Fbw7_KO

Figure 6.1 Unsupervised clustering of U5-NSCs identified differential clusters between WT and Fbw7$^{-/-}$ samples.

(A) Single cells are displayed in a two-dimensional space using Uniform Manifold Approximation and Projection (UMAP). Unsupervised graph-based clustering identified seven transcriptional clusters of U5-NSCs. (B) Cluster 6 exhibited lower nCount and nFeature RNA than the expected threshold and higher than optimal percentage of mitochondrial and ribosomal genes (blue arrows) (C) UMAP plot showing the clustering output after removing the outlying cluster 6. (D) Total genes expressed per cell and the number of mitochondrial and ribosomal genes in each cell from all clusters were within the expected optimal range. (E) UMAP plot of cells separated by sample condition (WT vs. Fbw7$^{-/-}$) highlights the clusters unique to each condition (Fbw7$^{-/-}$ = Fbw7_KO) .

6.2.2 ccAF analysis identified the Neural G0 cell cycle phase

scRNA-Seq data was analyzed using the Seurat R package (Butler et al., 2018). Because we hypothesized that loss of Fbw7 might impact cell cycle regulation, cells were clustered based on the Seurat cell cycle classifier (ccSeurat). However, the output was not very informative except for showing that the Fbw7$^{-/-}$ sample had fewer cells in G1 phase (**Figure 6.2A**). The cell cycle classifier developed by the Paddison lab (ccAF) which identifies finer cell cycle changes was then applied to the U5-NSCs (**Figure 6.2B**) (O'Connor et al., 2021). While ccSeurat clustered cells into G1, S and G2/M phases, ccAF distinguished between Neural G0, M/early G1, G1, Late G1, S/G2 and G2/M phases. Neural G0 and Late G1 are novel cell cycle stages that were observed in U5-NSCs as a result of unsupervised clustering of cells and characterizing enriched genes (O'Connor et al., 2021). Genes specific to each cell cycle phase were enriched in respective U5-NSC clusters (**Figure 6.2C**).

6.2.3 U5-NSC Fbw7$^{-/-}$ cells skip the Neural G0 state

In comparison to U5-NSC WT cells, Fbw7$^{-/-}$ cells exhibit much fewer cells in the Neural G0 state, suggesting that loss of Fbw7 triggers cells to skip G0 state and enter the cell cycle (**Figure 6.2B**). Accordingly there are more Fbw7$^{-/-}$ NSCs in G1 phase.

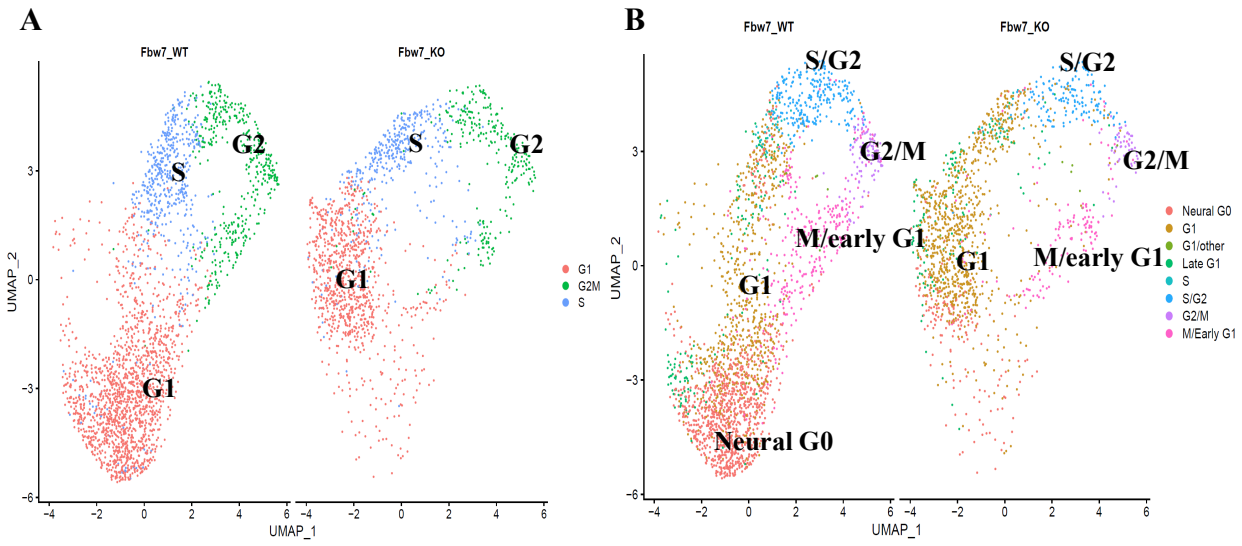

C

Fbw7$^{+/+}$ U5-NSCs

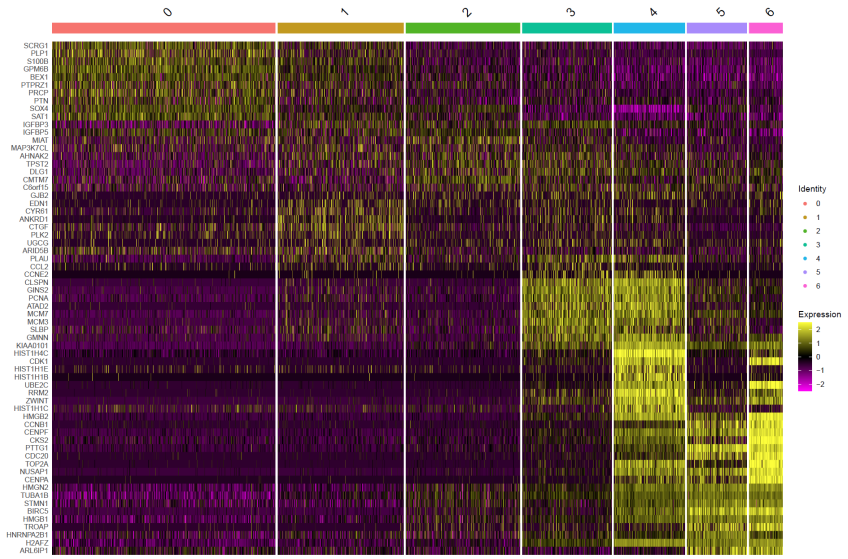

Fbw7$^{-/-}$ U5-NSCs

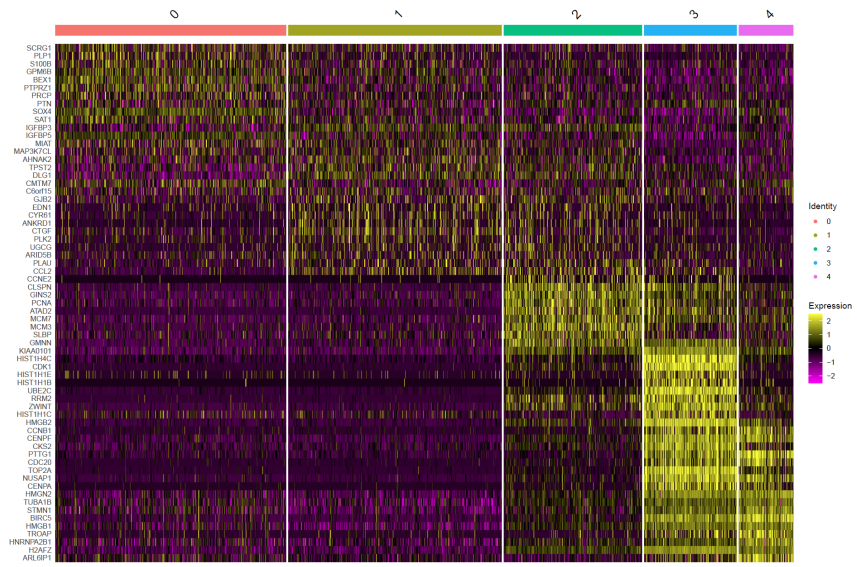

Figure 6.2 ccAF analysis identified that Fbw7$^{-/-}$ U5-NSCs skip the Neural G0 phase.

(A) UMAP plot of U5-NSCs clustered using ccSeurat cell cycle classifier. (Fbw7_KO = Fbw7$^{-/-}$) (B) UMAP plot of U5-NSCs clustered using ccAF cell cycle classifier (D) Heatmap showing the enrichment of cell cycle stage-specific gene expression in each cluster in WT and Fbw7$^{-/-}$ U5-NSCs.

6.3 **Discussion**

Single Cell RNA-Seq analysis revealed that Fbw7 plays a role in maintaining a Neural G0 cell cycle phase in U5-NSCs. Loss of Fbw7 caused NSCs to skip the G0 state and enter the cell cycle, however we are yet to determine the mechanism of regulation thereof. Previous studies suggest that accumulated Myc in Fbw7 null HSCs might be causing the G0 skip phenotype (Reavie et al., 2010; Thompson et al., 2008). Preliminary studies indicated that Myc is lowly expressed in U5-NSCs. Myc was difficult to detect on a western blot and Myc CUT&RUN signal was very poor. In contrast to Myc, Cyclin E was stabilized in Fbw7$^{-/-}$ U5 NSCs (data not shown) and high CDK2 activity has been detected in NSCs that skip the Neural G0 phase (O'Connor et al., 2021). While current observations support our hypothesis that Fbw7 mediates quiescence of NSCs via the regulation of Cyclin E, further research is necessary to determine the exact mechanism of regulation.

As we cultured the U5-NSCs, we observed that Fbw7$^{-/-}$ NSCs grow more slowly than WT cells. However, we did not quantify the magnitude of the growth difference. Theoretically cells that skip the G0 phase should proliferate faster. Previous studies suggest that Fbw7$^{-/-}$ stem cells cycle excessively, eventually leading to stem cell exhaustion. Thus, we assume that we might have registered loss of Fbw7$^{-/-}$ NSCs as slower growth. We will determine whether the NSCs are apoptosing in the absence of Fbw7 or whether they are differentiating to a mature cell type.

When we continued to culture the newly engineered Fbw7$^{-/-}$ NSCs for more than 3-4 weeks, we detected Fbw7 protein in cellular lysates. This suggested that the few WT NSCs that were left in the genetically engineered cell pool might be outcompeting the Fbw7$^{-/-}$ NSCs (note that we made sure to use cells cultured for less than two weeks for experiments). A similar observation

has been made in mouse HSCs where Fbw7 deficient HSCs lost their repopulating capability and were competed out by wild-type HSCs (Matsuoka et al., 2008).

Quiescent leukemia initiating cells (LICs) that escape anti-leukemia therapy cause relapse of the disease. Studies show that ablating Fbw7 in LICs causes them to continue to progress through the cell cycle so that they can be targeted by therapies directed to actively proliferating cells (Takeishi 2013). It would be interesting to determine if Fbw7 plays a similar role in glioma stem cells (GSCs), as this would likely be beneficial in developing therapeutic strategies.

Summary: Fbw7 plays a role in NSC maintenance by mediating the Neural G0 quiescent state, and loss of Fbw7 causes NSCs to skip the G0 state.

Chapter 7. Conclusions and Future Directions

A large number of Fbw7 substrates have been identified over the past several years, and many studies have shown cellular level deregulation of one or two substrates leading to a specific malignancy. However, such context-specific studies may not suffice to fully understand the complex regulatory network of Fbw7. Therefore, in this thesis work I sought a holistic approach to understand how Fbw7 mutations deregulate global transcription. A genome-scale analysis was performed to determine how different Fbw7 mutation types deregulate multiple TFs and their target genes in multiple cell types. I believe that genomic level analysis of TFs provides better insights to understand Fbw7's role in diseases than does a superficial overview of the transcriptome and cellular protein levels.

While RNA-Seq data provided an overview of changes in the transcriptome, analysis of histone modification marks identified the exact genomic regions that are potentially targeted by Fbw7 (directly or indirectly) as well as their transcriptional status. Motif enrichment analysis might be used in identifying TFs that are targeted at sites with differential histone marks. Genomic analysis of H3K27ac, Jun and Myc occupancy revealed cell-specific and ubiquitous characteristics of Fbw7's transcriptional regulation. Our study indicated that Fbw7 preferentially targets distal regulatory elements within introns and intergenic regions. Although total TF protein levels did not seem to change in mutant cells, we found that TFs at specific genomic sites were deregulated by Fbw7 (Jun in Hct116, DLD1 and U5-NSCs). Myc in DLD1 cells was an exception, where total cellular protein level was increased by $Fbw7^{-/-}$. Even then, instead of upregulating all DNA-bound Myc, Fbw7 targeted Myc at specific genomic sites. Furthermore, co-regulation of Jun and Myc displays Fbw7's ability to coordinately regulate multiple substrates at a specific genomic site. Jun and Myc both heterodimerize on DNA with other TFs and transcription mediators. Thus,

presumably, Fbw7's impact on Jun and Myc is amplified beyond the direct protein target. The nature of the phosphodegrons of substrates, whether they are high or low affinity, determines the interaction with WT and mutant Fbw7 dimers.

One of the most important questions I was eager to address was why $Fbw7^{R/+}$ mutations are favored in human cancers. We identified genes that were differentially expressed specifically in $Fbw7^{R/+}$ cells. Some Jun and Myc sites were more strongly affected by $Fbw7^{R/+}$ than by $Fbw7^{-/-}$. Our data also indicated a group of genes and genomic sites that were deregulated by $Fbw7^{R/+}$ at a level intermediate to WT and $Fbw7^{-/-}$ mutation. However, it was challenging to characterize the genes and genomic regions that were uniquely targeted by R/+ mutation. They did not enrich for any DNA motifs or biological pathways. Given the widespread effect that Fbw7 imposes on cellular homeostasis, it is believed that Fbw7 might be following a fail-safe mechanism during tumorigenesis. Presumably $Fbw7^{R/+}$ mutation causes a tumorigenic effect without being destructive to cells, which is possibly why it is favored over complete loss of Fbw7 in cancers. It is possible that the modest deregulatory impact by $Fbw7^{R/+}$ does not stand out sufficiently to be recognized and characterized. Furthermore, the majority of differential sites were within introns and intergenic regions; therefore it was challenging to accurately annotate them to genes, which limited our potential to identify enriched gene signatures and biological pathways.

To negate any concerns related to genetically engineered transformed cell lines such as Hct116 and DLD1, neural stem cells (NSCs) were also included in the study. Fbw7 in NSCs was deleted using a high efficiency CRISPR technique which did not require clonal selection (ribonucleoprotein complexes (RNP) composed of sgRNA and Cas9 nucleofected into cells). Similar to Hct116 and DLD1 cells, total Jun protein level did not increase in $Fbw7^{-/-}$ U5-NSCs, however a small fraction of Jun genomic sites was deregulated. The majority of deregulated sites

were within introns and intergenic regions. In addition to transcriptional regulation, we investigated cell cycle regulation in stem cells by Fbw7. U5-NSCs exhibited a G0 quiescent cell cycle phase (O'Connor et al., 2021). Loss of Fbw7 caused NSCs to skip the G0 state and continue through the cell cycle. We will continue to investigate this phenotype to determine whether it is regulated via Cyclin E – CDK2. We are also eager to find the consequences of continuous cycling of NSCs, whether it is apoptosis or differentiation.

The discovery of CIITA and MHC Class II upregulation by loss of Fbw7 was the culmination of our work. In normal conditions, constitutive expression of CIITA and MHC Class II genes is limited to antigen presenting cells (APCs). Although it has been observed in tumors before, we were the first group to link MHC Class II expression to Fbw7 mutant tumors. We envision the Fbw7 – MHC Class II pathway as a fail-safe mechanism that protects cells from Fbw7 loss. Increased expression of MHC Class II genes in $Fbw7^{-/-}$ cells, but intermediate upregulation in $Fbw7^{R/+}$ cells, might explain how tumors with R/+ mutations are successful at tumorigenesis. We propose further investigation of this phenotype particularly in Fbw7 mutant primary tumor samples. We found that loss of Fbw7 upregulates *CIITA* expression, presumably by increased occupancy of Jun and Myc at *CIITA* distal regulatory regions. Further research is required to fully understand the mechanistic details of how MHC Class II genes are regulated by Fbw7.

Although therapeutics that target E3 ligases have been developed, they are not considered highly successful, due to their lack of specificity, as inhibition of a broad spectrum of ligases eventually results in non-specific effects (Zhao & Sun, 2013). As many studies reveal, including ours, SCF^{Fbw7} E3 ligase degrades its substrates in a context-specific manner. Improving our knowledge of the spatial and temporal aspects of how different protein complexes are targeted by Fbw7 WT, and mutant hetero- and homodimers, will be useful for the development of more

specific targeted therapies. I believe that this study lays a solid foundation for future studies to broaden our understanding of context-specific transcriptional regulation by Fbw7.

Bibliography

10X Genomic. (2019). *Chromium Next GEM Single Cell V (D) J Reagent Kits User Guide*. *1000152*(D), 1–3.

Akhoondi, S., Sun, D., Von Der Lehr, N., Apostolidou, S., Klotz, K., Maljukova, A., Cepeda, D., Fiegl, H., Dofou, D., Marth, C., Mueller-Holzner, E., Corcoran, M., Dagnell, M., Nejad, S. Z., Nayer, B. N., Zali, M. R., Hansson, J., Egyhazi, S., Petersson, F., … Spruck, C. (2007). FBXW7/hCDC4 is a general tumor suppressor in human cancer. *Cancer Research*, *67*(19), 9006–9012. https://doi.org/10.1158/0008-5472.CAN-07-1320

Athwal, R. K., Walkiewicz, M. P., Baek, S., Fu, S., Bui, M., Camps, J., Ried, T., Sung, M. H., & Dalal, Y. (2015). CENP-A nucleosomes localize to transcription factor hotspots and subtelomeric sites in human cancer cells. *Epigenetics and Chromatin*, *8*(1), 1–23. https://doi.org/10.1186/1756-8935-8-2

Babaei-Jadidi, R., Li, N., Saadeddin, A., Spencer-Dene, B., Jandke, A., Muhammad, B., Ibrahim, E. E., Muraleedharan, R., Abuzinadah, M., Davis, H., Lewis, A., Watson, S., Behrens, A., Tomlinson, I., & Nateri, A. S. (2011). FBXW7 influences murine intestinal homeostasis and cancer, targeting Notch, Jun, and DEK for degradation. *J Exp Med*, *208*(2), 295–312. https://doi.org/10.1084/jem.20100830

Bahram, F., von der Lehr, N., Cetinkaya, C., & Larsson, L. G. (2000). c-Myc hot spot mutations in lymphomas result in inefficient ubiquitination and decreased proteasome-mediated turnover. *Blood*, *95*(6), 2104–2110.

Bailey, T. L., Boden, M., Buske, F. A., Frith, M., Grant, C. E., Clementi, L., Ren, J., Li, W. W., & Noble, W. S. (2009). MEME Suite: Tools for motif discovery and searching. *Nucleic Acids Research*, *37*(SUPPL. 2), 202–208. https://doi.org/10.1093/nar/gkp335

Butler, A., Hoffman, P., Smibert, P., Papalexi, E., & Satija, R. (2018). Integrating single-cell transcriptomic data across different conditions, technologies, and species. *Nature Biotechnology*, *36*(5), 411–420. https://doi.org/10.1038/nbt.4096

Chen, H., Li, Y., Lin, X., Cui, D., Cui, C., Li, H., & Xiao, L. (2015). Functional disruption of human leukocyte antigen II in human embryonic stem cell. *Biological Research*, *48*, 1–9. https://doi.org/10.1186/s40659-015-0051-6

Clurman, B. E., Sheaff, R. J., Thress, K., Groudine, M., & Roberts, J. M. (1996). Turnover of cyclin E by the ubiquitin-proteasome pathway is regulated by cdk2 binding and cyclin phosphorylation. *Genes and Development*, *10*(16), 1979–1990. https://doi.org/10.1101/gad.10.16.1979

Crusio, K. M., King, B., Reavie, L. B., & Aifantis, I. (2010). The ubiquitous nature of cancer: The role of the SCFFbw7 complex in development and transformation. *Oncogene*, *29*(35), 4865–4873. https://doi.org/10.1038/onc.2010.222

Davis, H., Lewis, A., Behrens, A., & Tomlinson, I. (2014). Investigation of the atypical FBXW7 mutation spectrum in human tumours by conditional expression of a heterozygous propellor tip missense allele in the mouse intestines. *Gut*, *63*(5), 792–799. https://doi.org/10.1136/gutjnl-2013-304719

Davis, H., & Tomlinson, I. (2012). CDC4/FBXW7 and the "just enough" model of tumourigenesis. *Journal of Pathology*, *227*(2), 131–135. https://doi.org/10.1002/path.4004

Davis, R. J., Gönen, M., Margineantu, D. H., Handeli, S., Swanger, J., Hoellerbauer, P., Paddison, P. J., Gu, H., Raftery, D., Grim, J. E., Hockenbery, D. M., Margolin, A. A., & Clurman, B. E. (2018). Pan-cancer transcriptional signatures predictive of oncogenic

mutations reveal that Fbw7 regulates cancer cell oxidative metabolism. *Proceedings of the National Academy of Sciences of the United States of America*, *115*(21), 5462–5467. https://doi.org/10.1073/pnas.1718338115

Davis, R. J., Welcker, M., & Clurman, B. E. (2014). Tumor suppression by the Fbw7 ubiquitin ligase: mechanisms and opportunities. *Cancer Cell*, *26*(4), 455–464. https://doi.org/10.1016/j.ccell.2014.09.013

Deffrennes, V., Vedrenne, J., Stolzenberg, M.-C., Piskurich, J., Barbieri, G., Ting, J. P., Charron, D., & Alcaïde-Loridan, C. (2001). Constitutive Expression of MHC Class II Genes in Melanoma Cell Lines Results from the Transcription of Class II Transactivator Abnormally Initiated from Its B Cell-Specific Promoter. *The Journal of Immunology*, *167*(1), 98–106. https://doi.org/10.4049/jimmunol.167.1.98

Fryer, C. J., White, J. B., & Jones, K. A. (2004). Mastermind recruits CycC:CDK8 to phosphorylate the Notch ICD and coordinate activation with turnover. *Molecular Cell*, *16*(4), 509–520. https://doi.org/10.1016/j.molcel.2004.10.014

Gao, M., Labuda, T., Xia, Y., Gallagher, E., Fang, D., Liu, Y. C., & Karin, M. (2004). Jun turnover is controlled through JNK-dependent phosphorylation of the E3 ligase itch. *Science*, *306*(5694), 271–275. https://doi.org/10.1126/science.1099414

Grim, J. E., Gustafson, M. P., Hirata, R. K., Hagar, A. C., Swanger, J., Welcker, M., Hwang, H. C., Ericsson, J., Russell, D. W., & Clurman, B. E. (2008). Isoform- and cell cycle-dependent substrate degradation by the Fbw7 ubiquitin ligase. *Journal of Cell Biology*, *181*(6), 913–920. https://doi.org/10.1083/jcb.200802076

Grim, J. E., Knoblaugh, S. E., Guthrie, K. A., Hagar, A., Swanger, J., Hespelt, J., Delrow, J. J., Small, T., Grady, W. M., Nakayama, K. I., & Clurman, B. E. (2012). Fbw7 and p53 Cooperatively Suppress Advanced and Chromosomally Unstable Intestinal Cancer. *Molecular and Cellular Biology*, *32*(11), 2160–2167. https://doi.org/10.1128/mcb.00305-12

Guo, J., Li, T., Schipper, J., Nilson, K. A., Fordjour, F. K., Cooper, J. J., Gordân, R., & Price, D. H. (2014). Sequence specificity incompletely defines the genome-wide occupancy of Myc. *Genome Biology*, *15*(10), 482. https://doi.org/10.1186/preaccept-2808268741329873

Hagedorn, M., Delugin, M., Abraldes, I., Allain, N., Belaud-Rotureau, M. A., Turmo, M., Prigent, C., Loiseau, H., Bikfalvi, A., & Javerzat, S. (2007). FBXW7/hCDC4 controls glioma cell proliferation in vitro and is a prognostic marker for survival in glioblastoma patients. *Cell Division*, *2*, 1–12. https://doi.org/10.1186/1747-1028-2-9

Hao, B., Oehlmann, S., Sowa, M. E., Harper, J. W., & Pavletich, N. P. (2007). Structure of a Fbw7-Skp1-Cyclin E Complex: Multisite-Phosphorylated Substrate Recognition by SCF Ubiquitin Ligases. *Molecular Cell*, *26*(1), 131–143. https://doi.org/10.1016/j.molcel.2007.02.022

Hershko, A., and Ciechanover, A. (1998). The Ubiquitin System. *Annu Rev Biochem*, *67*, 425–479.

Hess, J., Angel, P., & Schorpp-Kistner, M. (2004). AP-1 subunits: Quarrel and harmony among siblings. *Journal of Cell Science*, *117*(25), 5965–5973. https://doi.org/10.1242/jcs.01589

Hoeck, J. D., Jandke, A., Blake, S. M., Nye, E., Spencer-Dene, B., Brandner, S., & Behrens, A. (2010). Fbw7 controls neural stem cell differentiation and progenitor apoptosis via Notch and c-Jun. *Nature Neuroscience*, *13*(11), 1365–1372. https://doi.org/10.1038/nn.2644

Hoeller, D., & Dikic, I. (2009). Targeting the ubiquitin system in cancer therapy. *Nature*, *458*(7237), 438–444. https://doi.org/10.1038/nature07960

Hoellerbauer, P., Kufeld, M., Arora, S., Wu, H. J., Feldman, H. M., & Paddison, P. J. (2020). A

simple and highly efficient method for multi-allelic CRISPR-Cas9 editing in primary cell cultures. *Cancer Reports*, *3*(5), 1–14. https://doi.org/10.1002/cnr2.1269

Ishikawa, Y., Hosogane, M., Okuyama, R., Aoyama, S., Onoyama, I., Nakayama, K. I., & Nakayama, K. (2013). Opposing functions of Fbxw7 in keratinocyte growth, differentiation and skin tumorigenesis mediated through negative regulation of c-Myc and Notch. *Oncogene*, *32*(15), 1921–1932. https://doi.org/10.1038/onc.2012.213

Janssens, D. H., Wu, S. J., Sarthy, J. F., Meers, M. P., Myers, C. H., Olson, J. M., Ahmad, K., & Henikoff, S. (2018). Automated in situ chromatin profiling efficiently resolves cell types and gene regulatory programs. *Epigenetics and Chromatin*, *11*(1), 1–14. https://doi.org/10.1186/s13072-018-0243-8

Kandoth, C., McLellan, M. D., Vandin, F., Ye, K., Niu, B., Lu, C., Xie, M., Zhang, Q., McMichael, J. F., Wyczalkowski, M. A., Leiserson, M. D. M., Miller, C. A., Welch, J. S., Walter, M. J., Wendl, M. C., Ley, T. J., Wilson, R. K., Raphael, B. J., & Ding, L. (2013). Mutational landscape and significance across 12 major cancer types. *Nature*, *502*(7471), 333–339. https://doi.org/10.1038/nature12634

Kandoth, C., Schultz, N., Cherniack, A. D., Akbani, R., Liu, Y., Shen, H., Robertson, A. G., Pashtan, I., Shen, R., Benz, C. C., Yau, C., Laird, P. W., Ding, L., Zhang, W., Mills, G. B., Kucherlapati, R., Mardis, E. R., & Levine, D. A. (2013). Integrated genomic characterization of endometrial carcinoma. *Nature*, *497*(7447), 67–73. https://doi.org/10.1038/nature12113

Kemp, Z., Rowan, A., Chambers, W., Wortham, N., Halford, S., Sieber, O., Mortensen, N., Von Herbay, A., Gunther, T., Ilyas, M., & Tomlinson, I. (2005). CDC4 mutations occur in a subset of colorectal cancers but are not predicted to cause loss of function and are not associated with chromosomal instability. *Cancer Research*, *65*(24), 11361–11366. https://doi.org/10.1158/0008-5472.CAN-05-2565

Khan, A., & Mathelier, A. (2017). Intervene: A tool for intersection and visualization of multiple gene or genomic region sets. *BMC Bioinformatics*, *18*(1), 1–8. https://doi.org/10.1186/s12859-017-1708-7

Kim, J. M., Kee, Y., Gurtan, A., & D'Andrea, A. D. (2008). Cell cycle-dependent chromatin loading of the Fanconi anemia core complex by FANCM/FAAP24. *Blood*, *111*(10), 5215–5222. https://doi.org/10.1182/blood-2007-09-113092

Kim, S. Y., Herbst, A., Tworkowski, K. A., Salghetti, S. E., & Tansey, W. P. (2003). Skp2 regulates Myc protein stability and activity. *Molecular Cell*, *11*(5), 1177–1188. https://doi.org/10.1016/S1097-2765(03)00173-4

King, B., Trimarchi, T., Reavie, L., Xu, L., Mullenders, J., Ntziachristos, P., Aranda-Orgilles, B., Perez-Garcia, A., Shi, J., Vakoc, C., Sandy, P., Shen, S. S., Ferrando, A., & Aifantis, I. (2013). XThe ubiquitin ligase FBXW7 modulates leukemia-initiating cell activity by regulating MYC stability. *Cell*, *153*(7), 1552. https://doi.org/10.1016/j.cell.2013.05.041

Koepp, D. M., Schaefer, L. K., Ye, X., Keyomarsi, K., Chu, C., Harper, J. W., & Elledge, S. J. (2001). Phosphorylation-dependent ubiquitination of cyctin E by the SCFFbw7 ubiquitin ligase. *Science*, *294*(5540), 173–177. https://doi.org/10.1126/science.1065203

Lecker, S. H., Goldberg, A. L., & Mitch, W. E. (2006). Protein degradation by the ubiquitin-proteasome pathway in normal and disease states. *Journal of the American Society of Nephrology*, *17*(7), 1807–1819. https://doi.org/10.1681/ASN.2006010083

Loeb, K. R., Kostner, H., Firpo, E., Norwood, T., Tsuchiya, K. D., Clurman, B. E., & Roberts, J. M. (2005). A mouse model for cyclin E-dependent genetic instability and tumorigenesis.

Cancer Cell, *8*(1), 35–47. https://doi.org/10.1016/j.ccr.2005.06.010
Mackay, A., Burford, A., Carvalho, D., Izquierdo, E., Fazal-Salom, J., Taylor, K. R., Bjerke, L., Clarke, M., Vinci, M., Nandhabalan, M., Temelso, S., Popov, S., Molinari, V., Raman, P., Waanders, A. J., Han, H. J., Gupta, S., Marshall, L., Zacharoulis, S., … Jones, C. (2017). Integrated Molecular Meta-Analysis of 1,000 Pediatric High-Grade and Diffuse Intrinsic Pontine Glioma. *Cancer Cell*, *32*(4), 520-537.e5. https://doi.org/10.1016/j.ccell.2017.08.017
Malyukova, A., Dohda, T., von der Lehr, N., Akhoondi, S., Akhondi, S., Corcoran, M., Heyman, M., Spruck, C., Grandér, D., Lendahl, U., & Sangfelt, O. (2007). The tumor suppressor gene hCDC4 is frequently mutated in human T-cell acute lymphoblastic leukemia with functional consequences for Notch signaling. *Cancer Research*, *67*(12), 5611–5616. https://doi.org/10.1158/0008-5472.CAN-06-4381
Martins, I., Deshayes, F., Baton, F., Gorget, A., Ciechomska, I., Sylla, K., Aoudjit, F., Charron, D., Al-Daccak, R., & Alcaide-Loridan, C. (2007). Pathologic expression of MHC class II is driven by mitogen-activated protein kinases. *European Journal of Immunology*, *37*(3), 788–797. https://doi.org/10.1002/eji.200636620
Maser, R. S., Choudhury, B., Campbell, P. J., Feng, B., Wong, K. K., Protopopov, A., O'Neil, J., Gutierrez, A., Ivanova, E., Perna, I., Lin, E., Mani, V., Jiang, S., McNamara, K., Zaghlul, S., Edkins, S., Stevens, C., Brennan, C., Martin, E. S., … DePinho, R. A. (2007). Chromosomally unstable mouse tumours have genomic alterations similar to diverse human cancers. *Nature*, *447*(7147), 966–971. https://doi.org/10.1038/nature05886
Matsumoto, A., Onoyama, I., Sunabori, T., Kageyama, R., Okano, H., & Nakayama, K. I. (2011). Fbxw7-dependent degradation of notch is required for control of "Stemness" and neuronal-glial differentiation in neural stem cells. *Journal of Biological Chemistry*, *286*(15), 13754–13764. https://doi.org/10.1074/jbc.M110.194936
Matsuoka, S., Oike, Y., Onoyama, I., Iwama, A., Arai, F., Takubo, K., Mashimo, Y., Oguro, H., Nitta, E., Ito, K., Miyamoto, K., Yoshiwara, H., Hosokawa, K., Nakamura, Y., Gomei, Y., Iwasaki, H., Hayashi, Y., Matsuzaki, Y., Nakayama, K., … Suda, T. (2008). Fbxw7 acts as a critical fail-safe against premature loss of hematopoietic stem cells and development of T-ALL. *Genes and Development*, *22*(8), 986–991. https://doi.org/10.1101/gad.1621808
Minella, A. C., Grim, J. E., Welcker, M., & Clurman, B. E. (2007). p53 and SCFFbw7 cooperatively restrain cyclin E-associated genome instability. *Oncogene*, *26*(48), 6948–6953. https://doi.org/10.1038/sj.onc.1210518
Miyaki, M., Yamaguchi, T., Iijima, T., Takahashi, K., Matsumoto, H., & Mori, T. (2009). Somatic mutations of the CDC4 (FBXW7) gene in hereditary colorectal tumors. *Oncology*, *76*(6), 430–434. https://doi.org/10.1159/000217811
Muhlethaler-Mottet, A., Otten, L. A., Steimle, V., & Mach, B. (1997). Expression of MHC class II molecules in different cellular and functional compartments is controlled by differential usage of multiple promoters of the transactivator CIITA. *EMBO Journal*, *16*(10), 2851–2860. https://doi.org/10.1093/emboj/16.10.2851
Muzny, D. M., Bainbridge, M. N., Chang, K., Dinh, H. H., Drummond, J. A., Fowler, G., Kovar, C. L., Lewis, L. R., Morgan, M. B., Newsham, I. F., Reid, J. G., Santibanez, J., Shinbrot, E., Trevino, L. R., Wu, Y. Q., Wang, M., Gunaratne, P., Donehower, L. A., Creighton, C. J., … Thomson., E. (2012). Comprehensive molecular characterization of human colon and rectal cancer. *Nature*, *487*(7407), 330–337. https://doi.org/10.1038/nature11252
Nagarajan, U. M., Bushey, A., & Boss, J. M. (2002). Modulation of Gene Expression by the MHC Class II Transactivator. *The Journal of Immunology*, *169*(9), 5078–5088.

https://doi.org/10.4049/jimmunol.169.9.5078
Nateri, A. S., Riera-Sans, L., Da, C. C., & Behrens, A. (2004). The ubiquitin ligase SCFFbw7 antagonizes apoptotic JNK signaling. *Science*, *303*(5662), 1374–1378. https://doi.org/10.1126/science.1092880
Ni, Z., Hassan, M. A. El, Xu, Z., Yu, T., & Bremner, R. (2008). The chromatin-remodeling enzyme BRG1 coordinates CIITA induction through many interdependent distal enhancers. *Nature Immunology*, *9*(7), 785–793. https://doi.org/10.1038/ni.1619
O'Connor, S. A., Feldman, H. M., Arora, S., Hoellerbauer, P., Toledo, C. M., Corrin, P., Carter, L., Kufeld, M., Bolouri, H., Basom, R., Delrow, J., McFaline-Figueroa, J. L., Trapnell, C., Pollard, S. M., Patel, A., Paddison, P. J., & Plaisier, C. L. (2021). Neural G0: a quiescent-like state found in neuroepithelial-derived cells and glioma. *Molecular Systems Biology*, *17*(6). https://doi.org/10.15252/msb.20209522
O'Neil, J., Grim, J., Strack, P., Rao, S., Tibbitts, D., Winter, C., Hardwick, J., Welcker, M., Meijerink, J. P., Pieters, R., Draetta, G., Sears, R., Clurman, B. E., & Look, A. T. (2007). FBW7 mutations in leukemic cells mediate NOTCH pathway activation and resistance to -secretase inhibitors. *Journal of Experimental Medicine*, *204*(8), 1813–1824. https://doi.org/10.1084/jem.20070876
Öberg, C., Li, J., Pauley, A., Wolf, E., Gurney, M., & Lendahl, U. (2001). The Notch Intracellular Domain is Ubiquitinated and Negatively Regulated by the Mammalian Sel-10 Homolog. *Journal of Biological Chemistry*, *276*(38), 35847–35853. https://doi.org/10.1074/jbc.M103992200
Onoyama, I., Suzuki, A., Matsumoto, A., Tomita, K., Katagiri, H., Oike, Y., Nakayama, K., & Nakayama, K. I. (2011). Fbxw7 regulates lipid metabolism and cell fate decisions in the mouse liver. *Journal of Clinical Investigation*, *121*(1), 342–354. https://doi.org/10.1172/JCI40725
Penn, L. J. Z., Brooks, M. W., Laufer, E. M., & Land, H. (1990). Negative autoregulation of c-myc transcription. *EMBO Journal*, *9*(4), 1113–1121. https://doi.org/10.1002/j.1460-2075.1990.tb08217.x
Pierce, N. W., Kleiger, G., Shan, S. O., & Deshaies, R. J. (2009). Detection of sequential polyubiquitylation on a millisecond timescale. *Nature*, *462*(7273), 615–619. https://doi.org/10.1038/nature08595
Punga, T., Bengoechea-Alonso, M. T., & Ericsson, J. (2006). Phosphorylation and ubiquitination of the transcription factor sterol regulatory element-binding protein-1 in response to DNA binding. *Journal of Biological Chemistry*, *281*(35), 25278–25286. https://doi.org/10.1074/jbc.M604983200
Quinlan, A. R., & Hall, I. M. (2010). BEDTools: A flexible suite of utilities for comparing genomic features. *Bioinformatics*, *26*(6), 841–842. https://doi.org/10.1093/bioinformatics/btq033
Rajagopalan, H., Jallepalli, P. V., Rago, C., Velculescu, V. E., Kinzler, K. W., Vogelstein, B., & Lengauer, C. (2004). Inactivation of hCDC4 can cause chromosomal instability. *Nature*, *428*(6978), 77–81. https://doi.org/10.1038/nature02313
Ramírez, F., Ryan, D. P., Grüning, B., Bhardwaj, V., Kilpert, F., Richter, A. S., Heyne, S., Dündar, F., & Manke, T. (2016). deepTools2: a next generation web server for deep-sequencing data analysis. *Nucleic Acids Research*, *44*(W1), W160–W165. https://doi.org/10.1093/nar/gkw257
Reavie, L., Gatta, G. Della, Crusio, K., Aranda-Orgilles, B., Buckley, S. M., Thompson, B., Lee,

E., Gao, J., Bredemeyer, A. L., Helmink, B. A., Zavadil, J., Sleckman, B. P., Palomero, T., Ferrando, A., & Aifantis, I. (2010). Regulation of hematopoietic stem cell differentiation by a single ubiquitin ligase-substrate complex. *Nature Immunology*, *11*(3), 207–215. https://doi.org/10.1038/ni.1839

Salehi-Tabar, R., Memari, B., Wong, H., Dimitrov, V., Rochel, N., & White, J. H. (2019). The tumor suppressor Fbw7 and the Vitamin D receptor are mutual cofactors in protein turnover and transcriptional regulation. *Molecular Cancer Research*, *17*(3), 709–719. https://doi.org/10.1158/1541-7786.MCR-18-0991

Sancho, R., Jandke, A., Davis, H., Diefenbacher, M. E., Tomlinson, I., & Behrens, A. (2010). F-box and WD repeat domain-containing 7 regulates intestinal cell lineage commitment and is a haploinsufficient tumor suppressor. *Gastroenterology*, *139*(3), 929–941. https://doi.org/10.1053/j.gastro.2010.05.078

Sconocchia, G., Eppenberger-Castori, S., Zlobec, I., Karamitopoulou, E., Arriga, R., Coppola, A., Caratelli, S., Spagnoli, G. C., Lauro, D., Lugli, A., Han, J., Iezzi, G., Ferrone, C., Ferlosio, A., Tornillo, L., Droeser, R., Rossi, P., Attanasio, A., Ferrone, S., & Terracciano, L. (2014). HLA class II antigen expression in colorectal carcinoma tumors as a favorable prognostic marker. *Neoplasia (United States)*, *16*(1), 31–42. https://doi.org/10.1593/neo.131568

Shaulian, E., & Karin, M. (2002). AP-1 as a regulator of cell life and death. *Nature Cell Biology*, *4*(5), E131–E136. https://doi.org/10.1038/ncb0502-e131

Siu, K. T., Xu, Y., Swartz, K. L., Bhattacharyya, M., Gurbuxani, S., Hua, Y., & Minella, A. C. (2014). Chromosome Instability Underlies Hematopoietic Stem Cell Dysfunction and Lymphoid Neoplasia Associated with Impaired Fbw7-Mediated Cyclin E Regulation. *Molecular and Cellular Biology*, *34*(17), 3244–3258. https://doi.org/10.1128/mcb.01528-13

Skene, P. J., Henikoff, J. G., & Henikoff, S. (2018). Targeted in situ genome-wide profiling with high efficiency for low cell numbers. *Nature Protocols*, *13*(5), 1006–1019. https://doi.org/10.1038/nprot.2018.015

Skene, P. J., & Henikoff, S. (2017). An efficient targeted nuclease strategy for high-resolution mapping of DNA binding sites. *ELife*, *6*, 1–35. https://doi.org/10.7554/eLife.21856

Solomon, M. J., & Varshavsky, A. (1985). Formaldehyde-mediated DNA-protein crosslinking: A probe for in vivo chromatin structures. *Proceedings of the National Academy of Sciences of the United States of America*, *82*(19), 6470–6474. https://doi.org/10.1073/pnas.82.19.6470

Spencer, S. L., Cappell, S. D., Tsai, F. C., Overton, K. W., Wang, C. L., & Meyer, T. (2013). XThe proliferation-quiescence decision is controlled by a bifurcation in CDK2 activity at mitotic exit. *Cell*, *155*(2), 369. https://doi.org/10.1016/j.cell.2013.08.062

Spruck, C. H., Strohmaier, H., Sangfelt, O., Müller, H. M., Hubalek, M., Müller-Holzner, E., Marth, C., Widschwendter, M., & Reed, S. I. (2002). hCDC4 gene mutations in endometrial cancer. *Cancer Research*, *62*(16), 4535–4539.

Steimle V, Otten LA, Zufferey M, M. B. (1993). Complementation cloning of an MHC class II transactivator mutated in hereditary MHC class II deficiency (or bare lymphocyte syndrome). *Cell*, *Oct 8*.

Strohmaier H, Spruck C, Kaiser P, Won K, Sangfelt O, & Reed S. (2001). Human F-box protein hCdc4 targets cyclin E for proteolysis and is mutated in a breast cancer cell line. *Nature*, *413*(September), 316–322.

Sundqvist, A., Bengoechea-Alonso, M. T., Ye, X., Lukiyanchuk, V., Jin, J., Harper, J. W., &

Ericsson, J. (2005). Control of lipid metabolism by phosphorylation-dependent degradation of the SREBP family of transcription factors by SCFFbw7. *Cell Metabolism*, *1*(6), 379–391. https://doi.org/10.1016/j.cmet.2005.04.010

Takada, M., Zhang, W., Suzuki, A., Kuroda, T. S., Yu, Z., Inuzuka, H., Gao, D., Wan, L., Zhuang, M., Hu, L., Zhai, B., Fry, C. J., Bloom, K., Li, G., Karpen, G. H., Wei, W., & Zhang, Q. (2017). FBW7 loss promotes chromosomal instability and tumorigenesis via cyclin E1/CDK2–mediated phosphorylation of CENP-A. *Cancer Research*, *77*(18), 4881–4893. https://doi.org/10.1158/0008-5472.CAN-17-1240

Takeishi, S., & Nakayama, K. I. (2014). Role of Fbxw7 in the maintenance of normal stem cells and cancer-initiating cells. *British Journal of Cancer*, *111*(6), 1054–1059. https://doi.org/10.1038/bjc.2014.259

Tang, X., Orlicky, S., Lin, Z., Willems, A., Neculai, D., Ceccarelli, D., Mercurio, F., Shilton, B. H., Sicheri, F., & Tyers, M. (2007). Suprafacial Orientation of the SCFCdc4 Dimer Accommodates Multiple Geometries for Substrate Ubiquitination. *Cell*, *129*(6), 1165–1176. https://doi.org/10.1016/j.cell.2007.04.042

Tetzlaff, M. T., Yu, W., Li, M., Zhang, P., Finegold, M., Mahon, K., Harper, J. W., Schwartz, R. J., & Elledge, S. J. (2004). Defective cardiovascular development and elevated cyclin E and Notch proteins in mice lacking the Fbw7 F-box protein. *Proceedings of the National Academy of Sciences of the United States of America*, *101*(10), 3338–3345. https://doi.org/10.1073/pnas.0307875101

Thompson, B. J., Buonamici, S., Sulis, M. L., Palomero, T., Vilimas, T., Basso, G., Ferrando, A., & Aifantis, I. (2007). The SCFFBW7 ubiquitin ligase complex as a tumor suppressor in T cell leukemia. *The Journal of Experimental Medicine*, *204*(8), 1825–1835. https://doi.org/10.1084/jem.20070872

Thompson, B. J., Jankovic, V., Gao, J., Buonamici, S., Vest, A., Lee, J. M., Zavadil, J., Nimer, S. D., & Aifantis, I. (2008). Control of hematopoietic stem cell quiescence by the E3 ubiquitin ligase Fbw7. *Journal of Experimental Medicine*, *205*(6), 1395–1408. https://doi.org/10.1084/jem.20080277

van der Stoep, N., Quinten, E., Alblas, G., Plancke, A., van Eggermond, M. C. J. A., Holling, T. M., & van den Elsen, P. J. (2007). Constitutive and IFNγ-induced activation of MHC2TA promoter type III in human melanoma cell lines is governed by separate regulatory elements within the PIII upstream regulatory region. *Molecular Immunology*, *44*(8), 2036–2046. https://doi.org/10.1016/j.molimm.2006.09.013

Wang, H., Zang, C., Liu, X. S., & Aster, J. C. (2015). The role of notch receptors in transcriptional regulation. *Journal of Cellular Physiology*, *230*(5), 982–988. https://doi.org/10.1002/jcp.24872

Wang, Z., Inuzuka, H., Fukushima, H., Wan, L., Gao, D., Shaik, S., Sarkar, F. H., & Wei, W. (2012). Emerging roles of the FBW7 tumour suppressor in stem cell differentiation. *EMBO Reports*, *13*(1), 36–43. https://doi.org/10.1038/embor.2011.231

Wei, W., Jin, J., Schlisio, S., Harper, J. W., & Kaelin, W. G. (2005). The v-Jun point mutation allows c-Jun to escape GSK3-dependent recognition and destruction by the Fbw7 ubiquitin ligase. *Cancer Cell*, *8*(1), 25–33. https://doi.org/10.1016/j.ccr.2005.06.005

Weissman, A. M. (2001). Themes and Variations on Ubiquitylation. *Nature Reviews. Molecular Cell Biology*, *2*.

Welcker, M., & Clurman, B. E. (2005). The SV40 large T antigen contains a decoy phosphodegron that mediates its interactions with Fbw7/hCdc4. *Journal of Biological*

Chemistry, *280*(9), 7654–7658. https://doi.org/10.1074/jbc.M413377200
Welcker, M., & Clurman, B. E. (2007). Fbw7/hCDC4 dimerization regulates its substrate interactions. *Cell Division*, *2*, 7. https://doi.org/10.1186/1747-1028-2-7
Welcker, M., & Clurman, B. E. (2008). FBW7 ubiquitin ligase: A tumour suppressor at the crossroads of cell division, growth and differentiation. *Nature Reviews Cancer*, *8*(2), 83–93. https://doi.org/10.1038/nrc2290
Welcker, M., Larimore, E. A., Swanger, J., Bengoechea-Alonso, M. T., Grim, J. E., Ericsson, J., Zheng, N., & Clurman, B. E. (2013). Fbw7 dimerization determines the specificity and robustness of substrate degradation. *Genes and Development*, *27*(23), 2531–2536. https://doi.org/10.1101/gad.229195.113
Welcker, M., Larimore, E. a, Frappier, L., & Clurman, B. E. (2011). Nucleolar targeting of the fbw7 ubiquitin ligase by a pseudosubstrate and glycogen synthase kinase 3. *Molecular and Cellular Biology*, *31*(6), 1214–1224. https://doi.org/10.1128/MCB.01347-10
Welcker, M., Orian, A., Jin, J., Grim, J. E., Grim, J. A., Harper, J. W., Eisenman, R. N., & Clurman, B. E. (2004). The Fbw7 tumor suppressor regulates glycogen synthase kinase 3 phosphorylation-dependent c-Myc protein degradation. *Proceedings of the National Academy of Sciences of the United States of America*, *101*(24), 9085–9090. https://doi.org/10.1073/pnas.0402770101
Welcker, M., Singer, J., Loeb, K. R., Grim, J., Bloecher, A., Gurien-West, M., Clurman, B. E., & Roberts, J. M. (2003). Multisite phosphorylation by Cdk2 and GSK3 controls cyclin E degradation. *Molecular Cell*, *12*(2), 381–392. https://doi.org/10.1016/S1097-2765(03)00287-9
Wertz, I. E., O'Rourke, K. M., Zhang, Z., Dornan, D., Arnott, D., Deshaies, R. J., & Dixit, V. M. (2004). Human De-Etiolated-Regulates c-Jun by Assembling a CUL4A Ubiquitin Ligase. *Science*, *303*(5662), 1371–1374. https://doi.org/10.1126/science.1093549
Yada, M., Hatakeyama, S., Kamura, T., Nishiyama, M., Tsunematsu, R., Imaki, H., Ishida, N., Okumura, F., Nakayama, K., & Nakayama, K. I. (2004). Phosphorylation-dependent degradation of c-Myc is mediated by the F-box protein Fbw7. *EMBO Journal*, *23*(10), 2116–2125. https://doi.org/10.1038/sj.emboj.7600217
Yu, G., Wang, L. G., & He, Q. Y. (2015). ChIP seeker: An R/Bioconductor package for ChIP peak annotation, comparison and visualization. *Bioinformatics*, *31*(14), 2382–2383. https://doi.org/10.1093/bioinformatics/btv145
Zeller, K. I., Zhao, X. D., Lee, C. W. H., Kuo, P. C., Yao, F., Yustein, J. T., Hong, S. O., Orlov, Y. L., Shahab, A., How, C. Y., Fu, Y. T., Weng, Z., Kuznetsov, V. A., Sung, W. K., Ruan, Y., Dang, C. V., & Wei, C. L. (2006). Global mapping of c-Myc binding sites and target gene networks in human B cells. *Proceedings of the National Academy of Sciences of the United States of America*, *103*(47), 17834–17839. https://doi.org/10.1073/pnas.0604129103
Zhao, Y., & Sun, Y. (2013). Cullin-RING Ligases as Attractive Anti-cancer Targets. *Current Pharmaceutical Design*, *19*(18), 3215–3225. https://doi.org/10.2174/1381612811319999030

APPENDIX A

This Appendix provides the supplemental data for **Chapter 3**.

Supplemental Figure 1

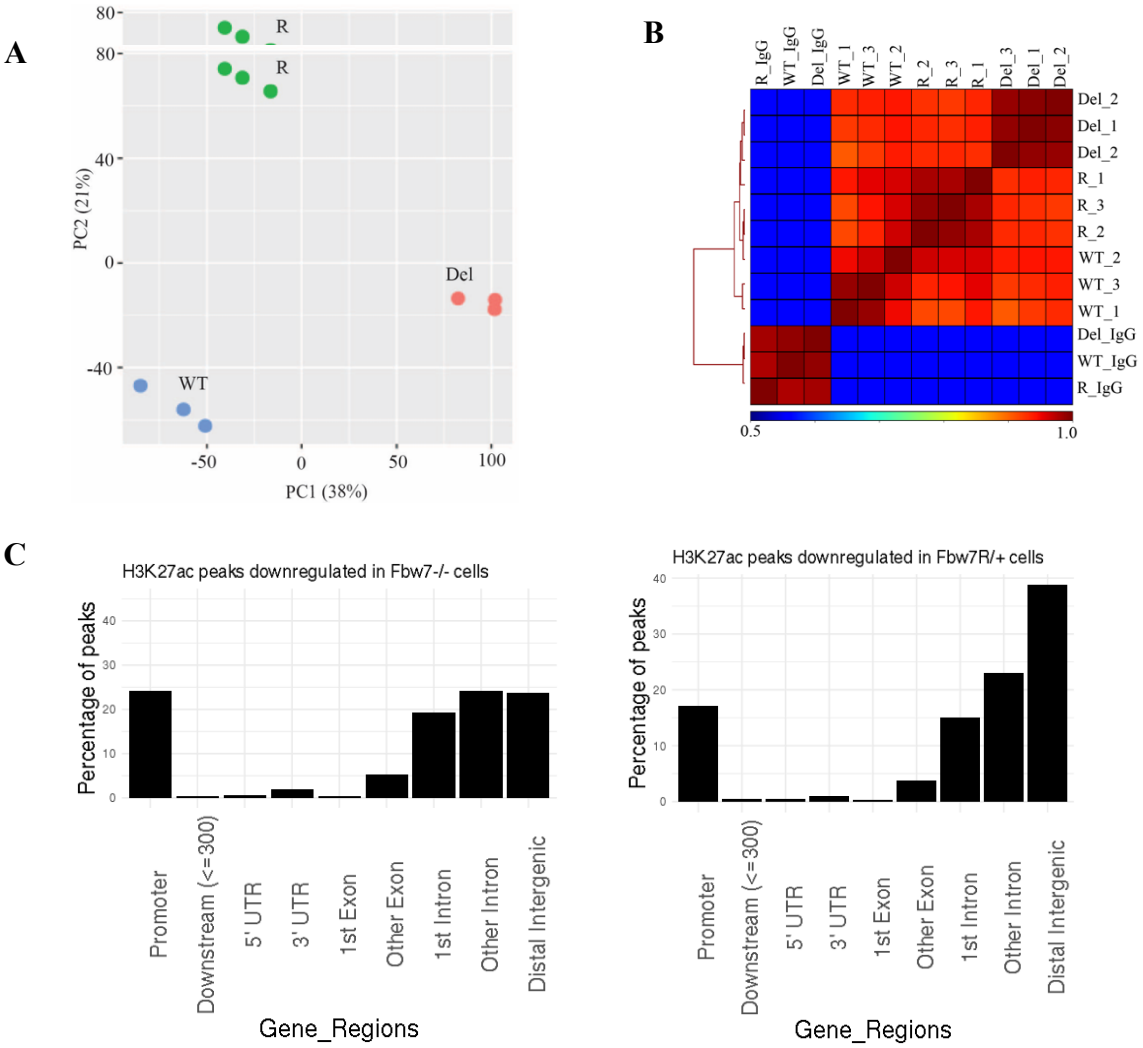

D

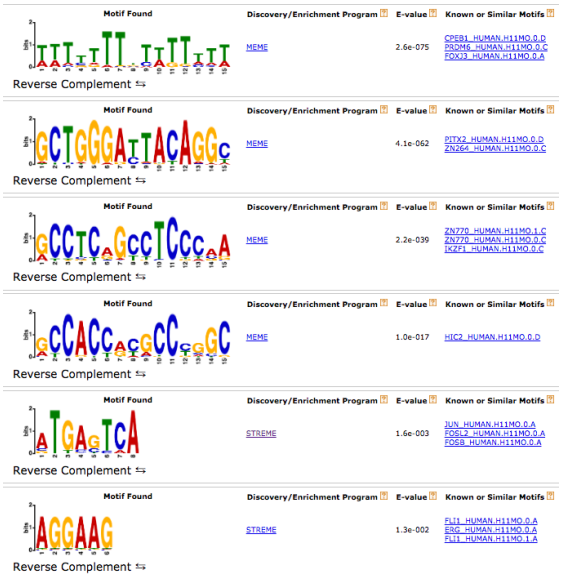

E

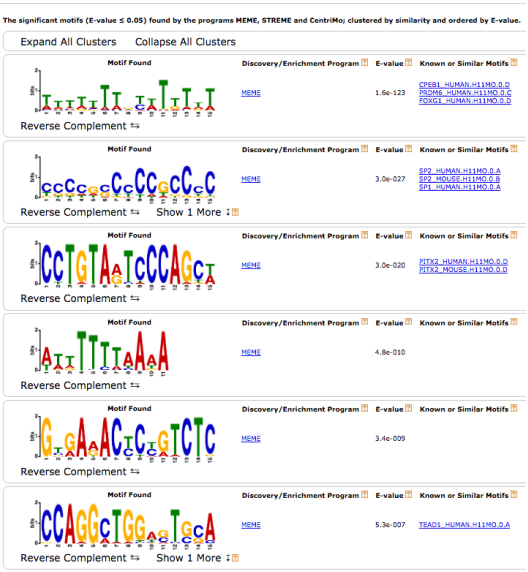

Supplemental Figure 1. (A) Principal Component Analysis (PCA) of RNA-Seq from Hct116 cells separates samples by genotype. Replicates from each condition are clustered together. (B) Hierarchically clustered correlation matrix of H3K27ac signal from Hct116 WT, Fbw7$^{-/-}$ (Del) and Fbw7$^{R/+}$ (R) cells (three replicate). IgG negative control for each cell type included. Peaks from the three cell types was merged to create a final peak-set. (C) Percentage of H3K27ac peaks located on different gene features. (D) Full output of the MEME-ChIP analysis on the sequences of H3K27ac upregulated sites in Fbw7$^{-/-}$ cells. (E) Output of the MEME-ChIP analysis on the sequences of non-differential H3K27ac sites in Fbw7-/- cells (negative control, 1409 sites). FIMO analysis on the non-differential sites (1409 sites) showed 17% of enrichment (p value =< 1.8e-5).

Supplemental Figure 2

A Hct116 WT cJun peaks Hct116 WT cMyc peaks

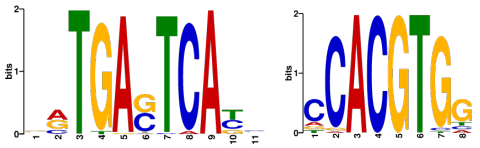

B

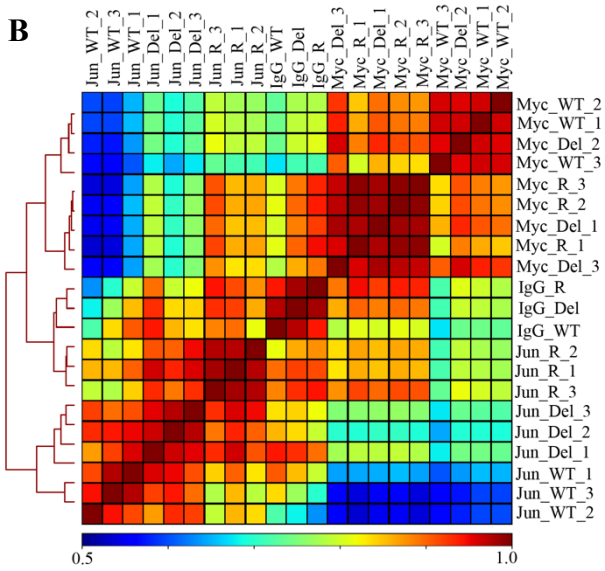

C

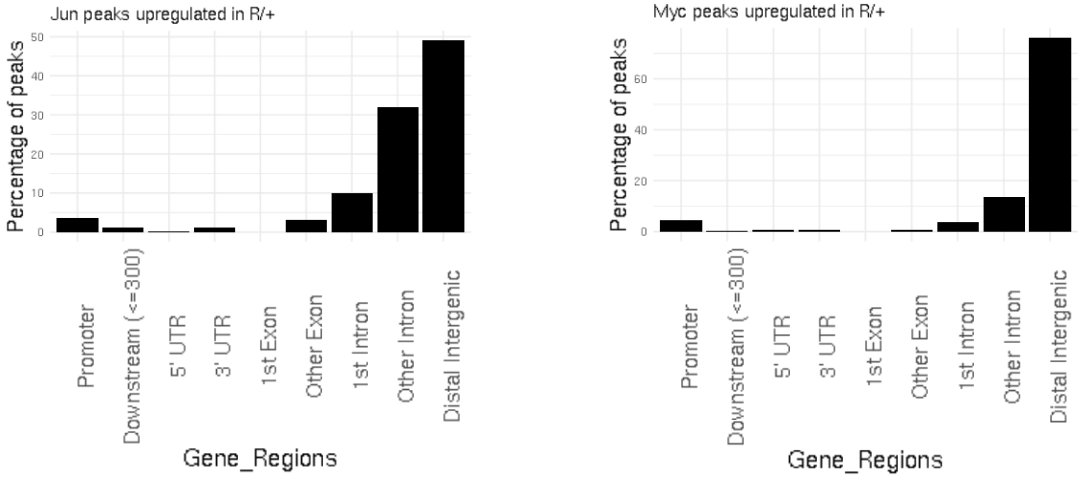

D

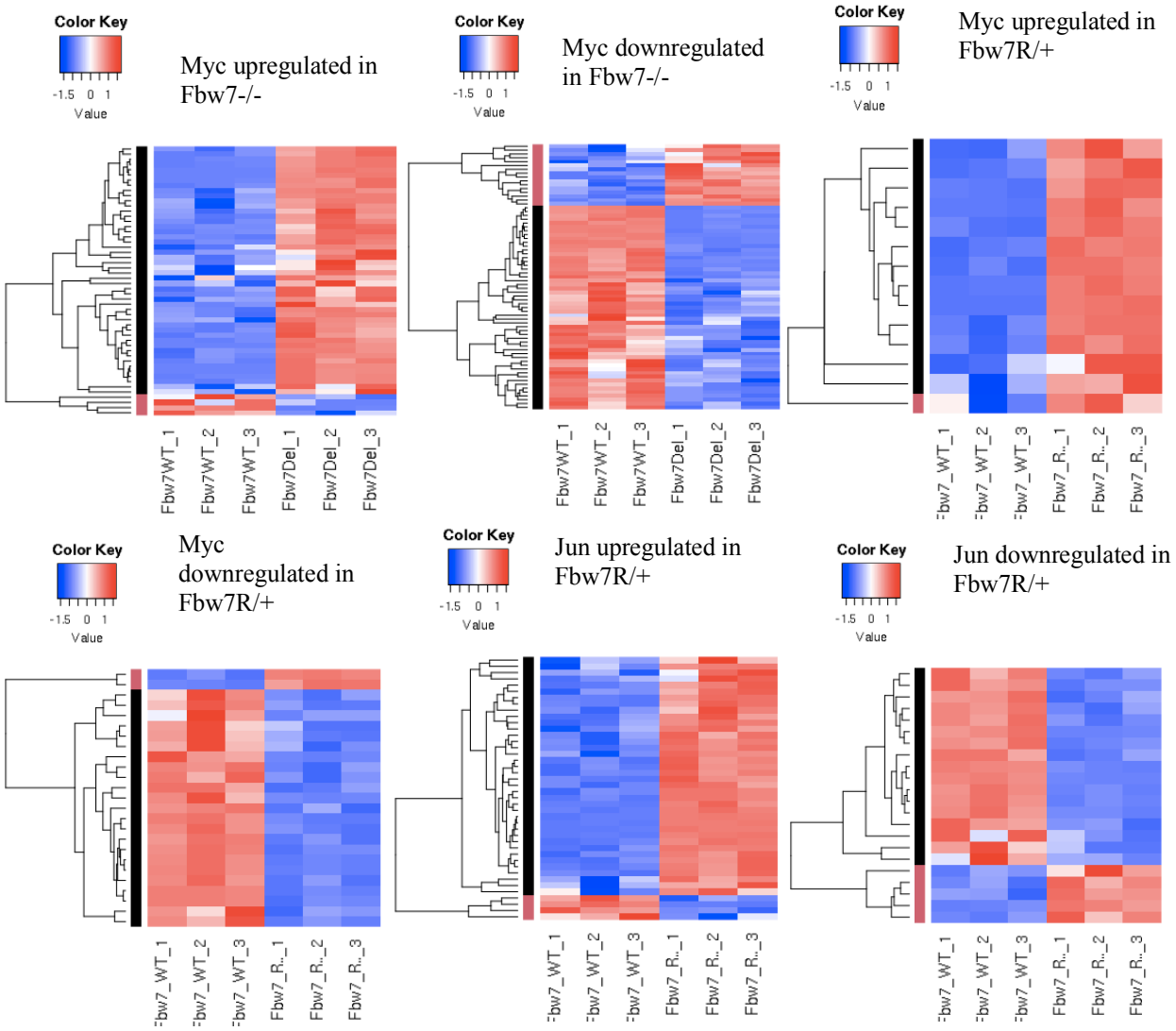

Supplemental Figure 2. (A) Sequence logo of the AP1 motif enriched in the center 100bp sequence of Jun peaks in Hct116 WT (E value 1.3e-53) and sequence logo of E-box motif enriched in the center 100bp sequence of Myc peaks in Hct116 WT (E value 1.7e-4). AP1 motif was input to FIMO to scan for the motif through the full sequence length of 25,527 cJun peaks in Hct116 WT. FIMO output showed that motifs with score between15.73 to 12.11 occurred 26,547 times (p value $\leq$ 6.46E-05). E-box motif was input to FIMO to scan for the motif through the full sequence length of 24,111 cMyc peaks in Hct116 WT. FIMO output showed that motifs with score between 15.32 – 9.24 occurred 9343 times (p value $\leq$ 0.00024). Motif score range was determined by the exact similarity to TGAG/CTCA (AP1 motif) or CACGTG (E box). (B) Hierarchically clustered correlation matrix of Jun and Myc signal mapped in Hct116 WT, Fbw7$^{-/-}$ (Del) and Fbw7$^{R/+}$ (R) cells. IgG negative control for each cell type included. Peaks from the three cell types were merged to create a final peak-set. (C) Percentage of Myc and Jun peaks located within each gene region. (D) Heatmap showing the transcription of genes that have upregulated and downregulated Myc and Jun in Fbw7$^{-/-}$ and Fbw7$^{R/+}$ cells at gene proximal sites.

Supplemental Figure 3

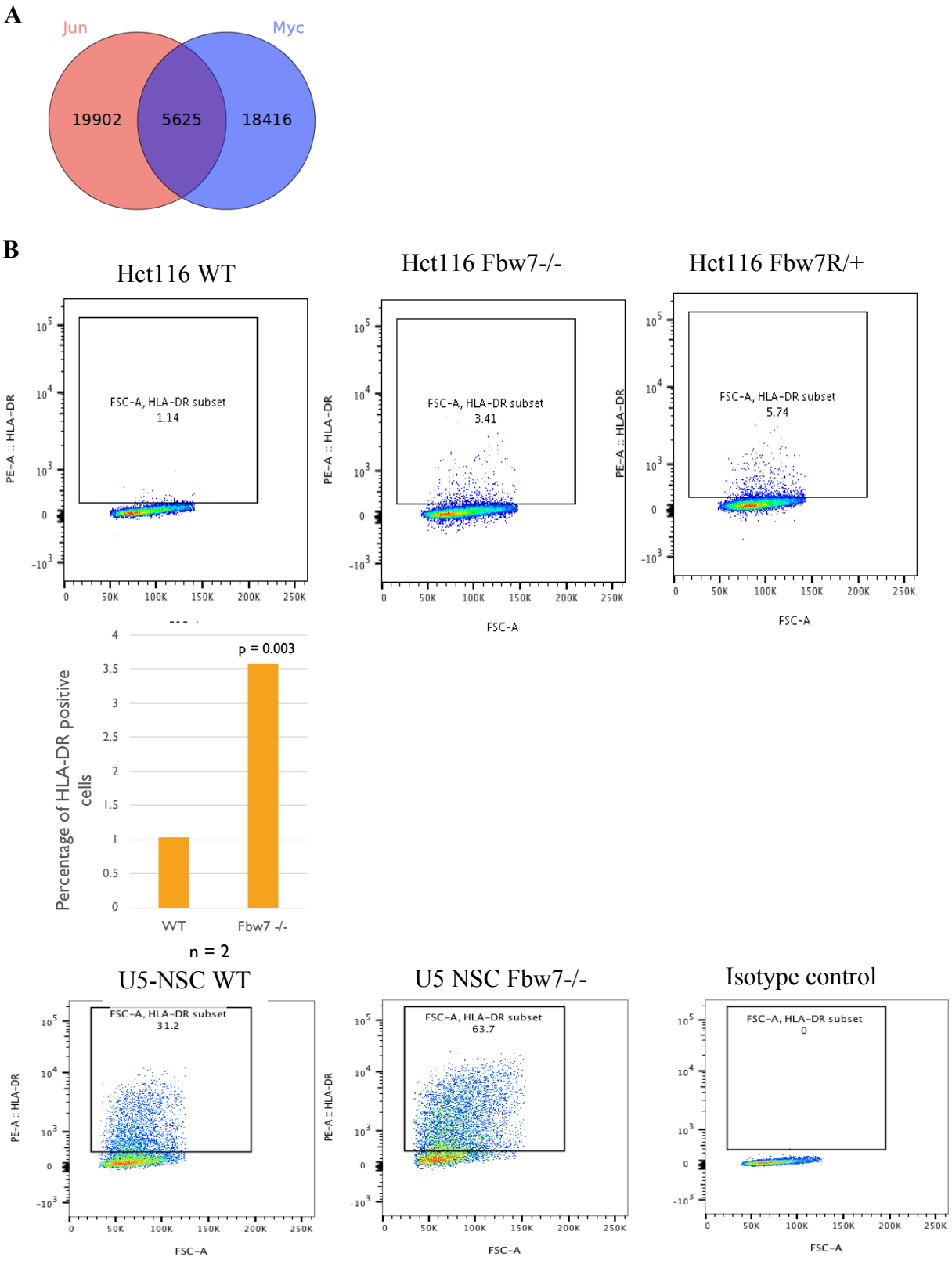

C

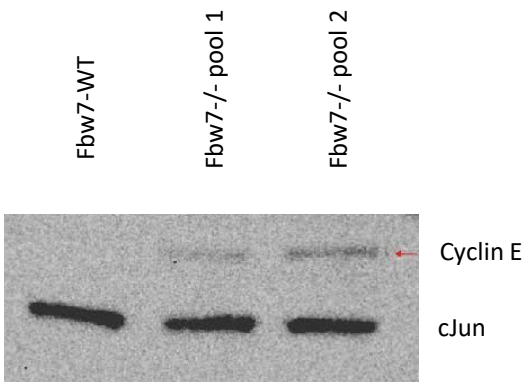

Supplemental Figure 3. (A) Venn diagram showing the overlap between Myc and Jun peaks in Hct116 WT cells (B) Flow cytometry detected HLA-DR protein expressed in Hct116 WT, $Fbw7^{-/-}$ and $Fbw7^{R/+}$, and U5-NSC WT and $Fbw7^{-/-}$ cells. (C) Western blot showing Cyclin E and cJun levels in whole cell lysates in U5-NSC WT and Fbw7-/- cells. Two different U5-NSC Fbw7 knockout pools are shown.

Supplemental Figure 4

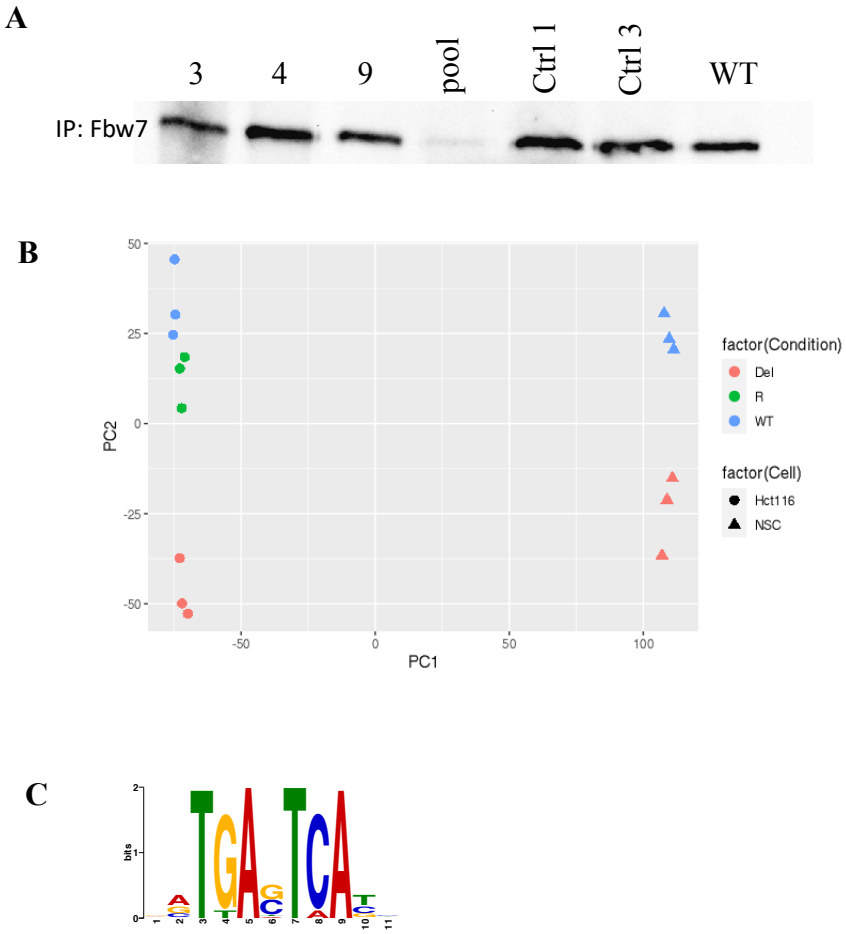

Supplemental Figure 4. (A) Western blot showing Fbw7 in samples 1-4: U5 NSCs with sgRNA targeting Fbw7 exon 3, 4, 9 and all three exons in one pool, samples 5-6 : U5 NSCs with control sgRNA 1x and 3x, and sample 7: Hct116 WT. (B) PCA performed on RNA-Seq data (normalized CPM) from Hct116 WT, Fbw7$^{-/-}$ (Del) and Fbw7$^{R/+}$ (R) and U5 NSCs (WT and Fbw7$^{-/-}$). (C) Sequence logo of AP1 motif enriched in Jun peaks in U5 NSCs (E value = 1.2e-146).

APPENDIX B

This Appendix provides the supplemental data for **Chapter 4**.

Table 1. Total number of peaks in control cells, number of differential sites in mutant cells for each TF and histone modification mark mapped in DLD1 cells.

A	**No. of differential sites (FDR < 0.01)**	**Total no. of H3K27ac peaks in WT**	**% of differential sites**
H3K27ac up in Fbw7-/- (spike-in normalized)	3389	8839	38%
H3K27ac down in Fbw7-/- (spike-in normalized)	115	8839	1.3%
H3K27ac up in Fbw7-/- (TMM normalized)	1250	8839	14.1%
H3K27ac down in Fbw7-/- (TMM normalized)	530	8839	6%
B	**No. of differential sites (FDR < 0.01)**	**Total no. of Jun peaks in WT**	**% of differential sites**
Jun up in Fbw7-/- (spike-in normalized)	6145	44055	14%
Jun down in Fbw7-/- (spike-in normalized)	2222	44055	5%
Jun up in Fbw7-/- (TMM normalized)	5160	44055	11.7%
Jun down in Fbw7-/- (TMM normalized)	4014	44055	9.1%
C	**No. of differential sites (FDR < 0.01)**	**Total no. of Myc peaks in WT**	**% of differential sites**
Myc up in Fbw7-/- (spike-in normalized)	21081	42260	50%
Myc down in Fbw7-/- (spike-in normalized)	593	42260	1.4%
Myc up in Fbw7-/- (TMM normalized)	2569	42260	6.1%
Myc down in Fbw7-/- (TMM normalized)	1816	42260	4.3%

Table 2. Number of reads mapped to hg19 and yeast genomes in DLD1 CUT&RUN samples.

	hg19 uniquely mapped reads	**Yeast uniquely mapped reads**
DLD Myc WT	6182013	21878
DLD Myc WT 2	6682277	25903
DLD Myc WT 3	6612895	24194
DLD Myc Del 1	6430705	10128
DLD Myc Del 2	6723328	10261
DLD Myc Del 3	5978496	7508
DLD Jun WT 1	6336158	10309
DLD Jun WT 2	6371006	8597
DLD Jun WT 3	5886203	9347
DLD Jun Del 1	6561581	6462
DLD Jun Del 2	6799728	8151
DLD Jun Del 3	5879502	11663
DLD H3K27ac WT 1	7077968	1603
DLD H3K27ac WT 2	7311280	1505
DLD H3K27ac Del 1	6681060	862
DLD H3K27ac Del 2	6290024	976

APPENDIX C

This Appendix provides experimental details of all the CUT&RUN samples used in this thesis.

Table 1. Experimental details of all the CUT&RUN experiments performed in this dissertation.

TF/histone	Cell Type	Fbw7 mutational status	Replicate	pA-Mnase Digestion Duration	Antibody	C&R Protocol	# of cells
H3K27ac	Hct116	WT	1	3 min	anti-H3K27ac	Manual CUT&RUN	1 million
H3K27ac	Hct116	WT	2	3 min	anti-H3K27ac	Manual CUT&RUN	1 million
H3K27ac	Hct116	WT	3	3 min	anti-H3K27ac	Manual CUT&RUN	1 million
H3K27ac	Hct116	Fbw7-/-	1	3 min	anti-H3K27ac	Manual CUT&RUN	1 million
H3K27ac	Hct116	Fbw7-/-	2	3 min	anti-H3K27ac	Manual CUT&RUN	1 million
H3K27ac	Hct116	Fbw7-/-	3	3 min	anti-H3K27ac	Manual CUT&RUN	1 million
H3K27ac	Hct116	Fbw7R/+	1	3 min	anti-H3K27ac	Manual CUT&RUN	1 million
H3K27ac	Hct116	Fbw7R/+	2	3 min	anti-H3K27ac	Manual CUT&RUN	1 million
H3K27ac	Hct116	Fbw7R/+	3	3 min	anti-H3K27ac	Manual CUT&RUN	1 million
Negative Control for H3K27ac	Hct116	WT		3 min	IgG	Manual CUT&RUN	1 million
Negative Control for H3K27ac	Hct116	Fbw7-/-		3 min	IgG	Manual CUT&RUN	1 million
Negative Control for H3K27ac	Hct116	Fbw7R/+		3 min	IgG	Manual CUT&RUN	1 million
H3K27me3	Hct116	WT	1	30 min	anti-H3K27me3	Auto CUT&RUN	0.1 million
H3K27me3	Hct116	WT	2	30 min	anti-H3K27me3	Auto CUT&RUN	0.1 million
H3K27me3	Hct116	WT	3	30 min	anti-H3K27me3	Auto CUT&RUN	0.1 million
Negative Control for H3K27me3	Hct116	WT		30 min	IgG	Auto CUT&RUN	0.1 million
H3K4me1	Hct116	WT	1	30 min	anti-H3K4me1	CUT&RUN with nuclei	5 million
H3K4me1	Hct116	Fbw7-/-	1	30 min	anti-H3K4me1	CUT&RUN with nuclei	5 million
Negative Control for H3K4me1	Hct116	Fbw7-/-		30 min	IgG	CUT&RUN with nuclei	5 million
cJun	Hct116	WT	1	30 min	anti-cJun	Auto CUT&RUN	1 million
cJun	Hct116	WT	2	30 min	anti-cJun	Auto CUT&RUN	1 million
cJun	Hct116	WT	3	30 min	anti-cJun	Auto CUT&RUN	1 million
cJun	Hct116	Fbw7-/-	1	30 min	anti-cJun	Auto CUT&RUN	1 million
cJun	Hct116	Fbw7-/-	2	30 min	anti-cJun	Auto CUT&RUN	1 million
cJun	Hct116	Fbw7-/-	3	30 min	anti-cJun	Auto CUT&RUN	1 million
cJun	Hct116	Fbw7R/+	1	30 min	anti-cJun	Auto CUT&RUN	1 million
cJun	Hct116	Fbw7R/+	2	30 min	anti-cJun	Auto CUT&RUN	1 million
cJun	Hct116	Fbw7R/+	3	30 min	anti-cJun	Auto CUT&RUN	1 million
cMyc	Hct116	WT	1	30 min	anti-cMyc	Auto CUT&RUN	1 million
cMyc	Hct116	WT	2	30 min	anti-cMyc	Auto CUT&RUN	1 million

cMyc	Hct116	WT	3	30 min	anti-cMyc	Auto CUT&RUN	1 million
cMyc	Hct116	Fbw7-/-	1	30 min	anti-cMyc	Auto CUT&RUN	1 million
cMyc	Hct116	Fbw7-/-	2	30 min	anti-cMyc	Auto CUT&RUN	1 million
cMyc	Hct116	Fbw7-/-	3	30 min	anti-cMyc	Auto CUT&RUN	1 million
cMyc	Hct116	Fbw7R/+	1	30 min	anti-cMyc	Auto CUT&RUN	1 million
cMyc	Hct116	Fbw7R/+	2	30 min	anti-cMyc	Auto CUT&RUN	1 million
cMyc	Hct116	Fbw7R/+	3	30 min	anti-cMyc	Auto CUT&RUN	1 million
Negative Control for cJun and cMyc	Hct116	WT		30 min	IgG	Auto CUT&RUN	1 million
Negative Control for cJun and cMyc	Hct116	Fbw7-/-		30 min	IgG	Auto CUT&RUN	1 million
Negative Control for cJun and cMyc	Hct116	Fbw7R/+		30 min	IgG	Auto CUT&RUN	1 million
cJun	U5-NSC	WT	1	30 min	anti-cJun	Auto CUT&RUN	0.5 million
cJun	U5-NSC	WT	2	30 min	anti-cJun	Auto CUT&RUN	0.5 million
cJun	U5-NSC	WT	3	30 min	anti-cJun	Auto CUT&RUN	0.5 million
cJun	U5-NSC	Fbw7-/-	1	30 min	anti-cJun	Auto CUT&RUN	0.5 million
cJun	U5-NSC	Fbw7-/-	2	30 min	anti-cJun	Auto CUT&RUN	0.5 million
cJun	U5-NSC	Fbw7-/-	3	30 min	anti-cJun	Auto CUT&RUN	0.5 million
Negative Control for cJun and cMyc	U5-NSC	WT		30 min	IgG	Auto CUT&RUN	0.5 million
Negative Control for cJun and cMyc	U5-NSC	Fbw7-/-		30 min	IgG	Auto CUT&RUN	0.5 million
cMyc	U5-NSC	WT	1	30 min	anti-cMyc	Auto CUT&RUN	1 million
cMyc	U5-NSC	WT	2	30 min	anti-cMyc	Auto CUT&RUN	1 million
cMyc	U5-NSC	WT	3	30 min	anti-cMyc	Auto CUT&RUN	1 million
cMyc	U5-NSC	Fbw7-/-	1	30 min	anti-cMyc	Auto CUT&RUN	1 million
cMyc	U5-NSC	Fbw7-/-	2	30 min	anti-cMyc	Auto CUT&RUN	1 million
cMyc	U5-NSC	Fbw7-/-	3	30 min	anti-cMyc	Auto CUT&RUN	1 million
cJun	DLD1	WT	1	30 min	anti-cJun	Auto CUT&RUN	0.5 million
cJun	DLD1	WT	2	30 min	anti-cJun	Auto CUT&RUN	0.5 million
cJun	DLD1	WT	3	30 min	anti-cJun	Auto CUT&RUN	0.5 million
cJun	DLD1	Fbw7-/-	1	30 min	anti-cJun	Auto CUT&RUN	0.5 million
cJun	DLD1	Fbw7-/-	2	30 min	anti-cJun	Auto CUT&RUN	0.5 million
cJun	DLD1	Fbw7-/-	3	30 min	anti-cJun	Auto CUT&RUN	0.5 million
cMyc	DLD1	WT	1	30 min	anti-cMyc	Auto CUT&RUN	0.5 million
cMyc	DLD1	WT	2	30 min	anti-cMyc	Auto CUT&RUN	0.5 million
cMyc	DLD1	WT	3	30 min	anti-cMyc	Auto CUT&RUN	0.5 million
cMyc	DLD1	Fbw7-/-	1	30 min	anti-cMyc	Auto CUT&RUN	0.5 million
cMyc	DLD1	Fbw7-/-	2	30 min	anti-cMyc	Auto CUT&RUN	0.5 million
cMyc	DLD1	Fbw7-/-	3	30 min	anti-cMyc	Auto CUT&RUN	0.5 million
Negative Control for cJun and cMyc	DLD1	WT		30 min	IgG	Auto CUT&RUN	0.5 million
Negative Control for cJun and cMyc	DLD1	Fbw7-/-		30 min	IgG	Auto CUT&RUN	0.5 million

H3K27ac	DLD1	WT	1	30 min	anti-H3K27ac	Auto CUT&RUN	0.5 million
H3K27ac	DLD1	WT	2	30 min	anti-H3K27ac	Auto CUT&RUN	0.5 million
H3K27ac	DLD1	Fbw7-/-	1	30 min	anti-H3K27ac	Auto CUT&RUN	0.5 million
H3K27ac	DLD1	Fbw7-/-	2	30 min	anti-H3K27ac	Auto CUT&RUN	0.5 million